Pliocene-Pleistocene Stratigraphy

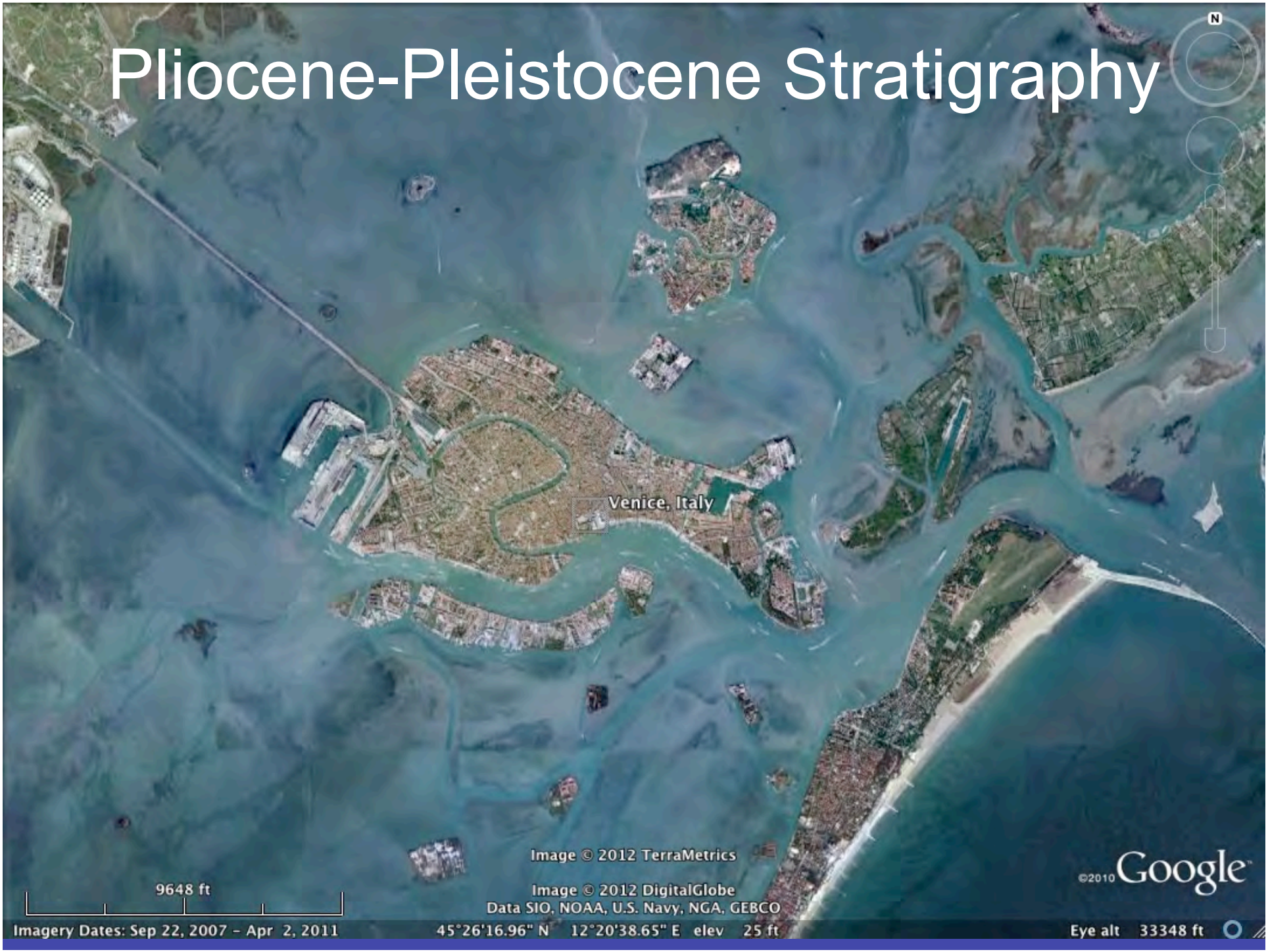

SEDIMENTARY ROCKS

Late and post-Alpine Orogeny marine and continental deposits, Plio-Quaternary continental deposits

Continental and paralic deposits

1 — Deltaic, alluvial and coastal plain deposits; aeolian deposits
Holocene

2 — Terraced alluvial deposits; aeolian deposits; travertines
Pleistocene, locally up to Holocene

3 — Glacial deposits
Pleistocene

4 — Pelites, sands and conglomerates
Pliocene-Pleistocene

5 — Pelites, sands, conglomerates and limestones
Middle Eocene-Miocene

Marine deposits

6 — Detrital and organogenic limestones, pelites, sands and conglomerates, locally terraced
Pliocene-Pleistocene, locally since Middle Miocene

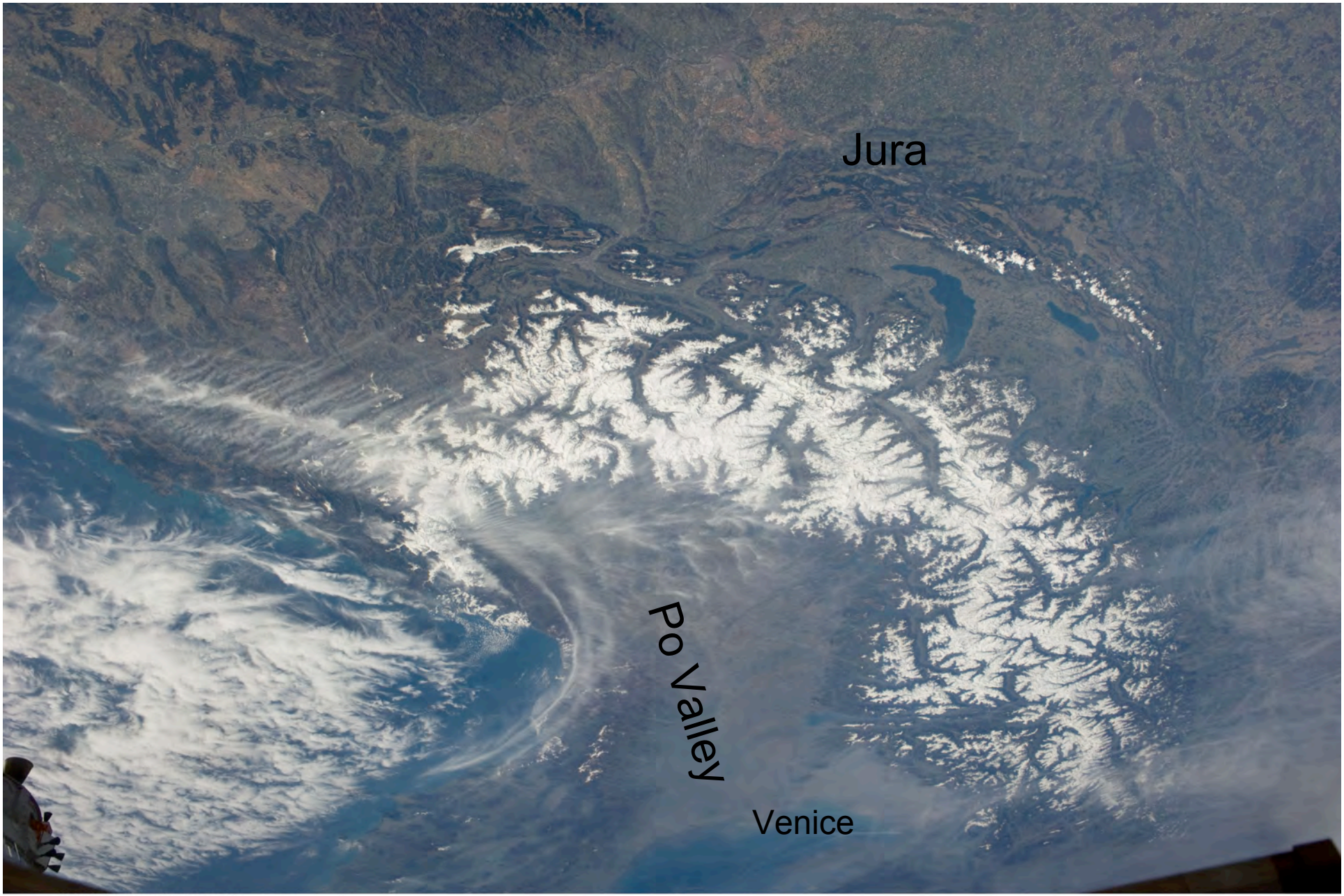

ISS027E007723

Alps, Lake Geneva, Adriatic

http://eol.jsc.nasa.gov/

The Siena Basin

View sotheast from San Gimignano

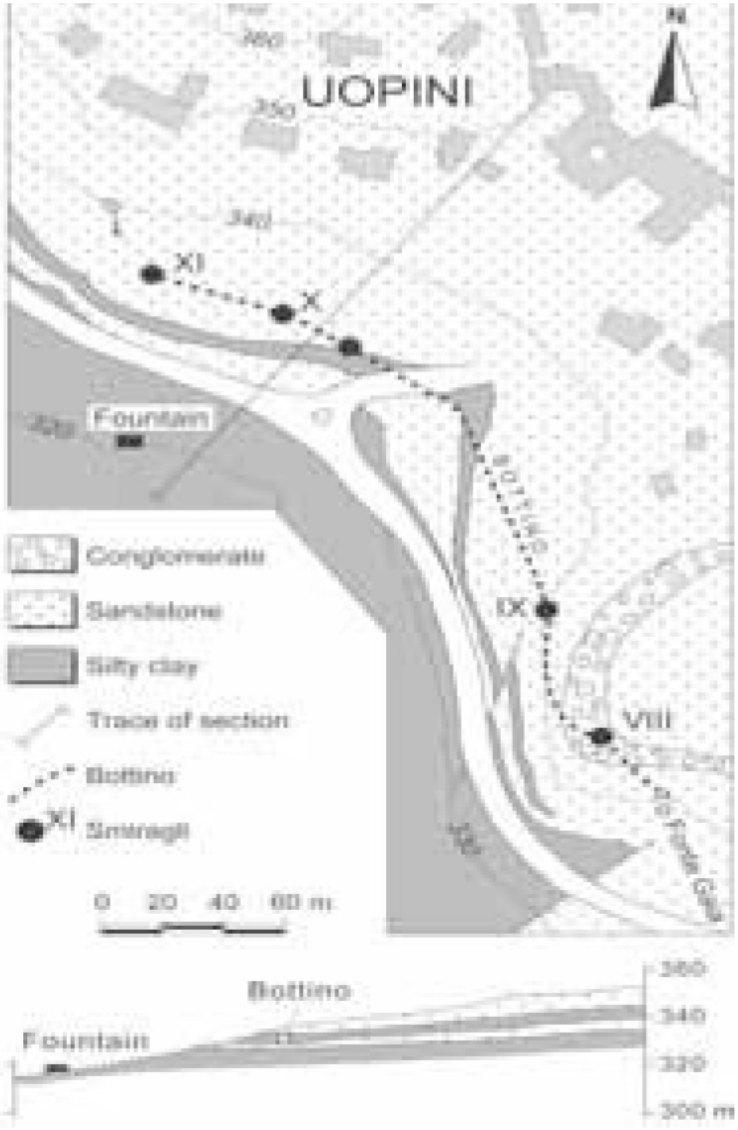

Figure 5 - Uopini area: A. Schematic geological map with trace of the Bottino and location of the smiragli; B. Schematic cross-section with location of the Bottino intercepting the groundwater flow of the largest topmost aquifer. Note optimum position of Bottino in respect to surface morphology and dip of the strata.

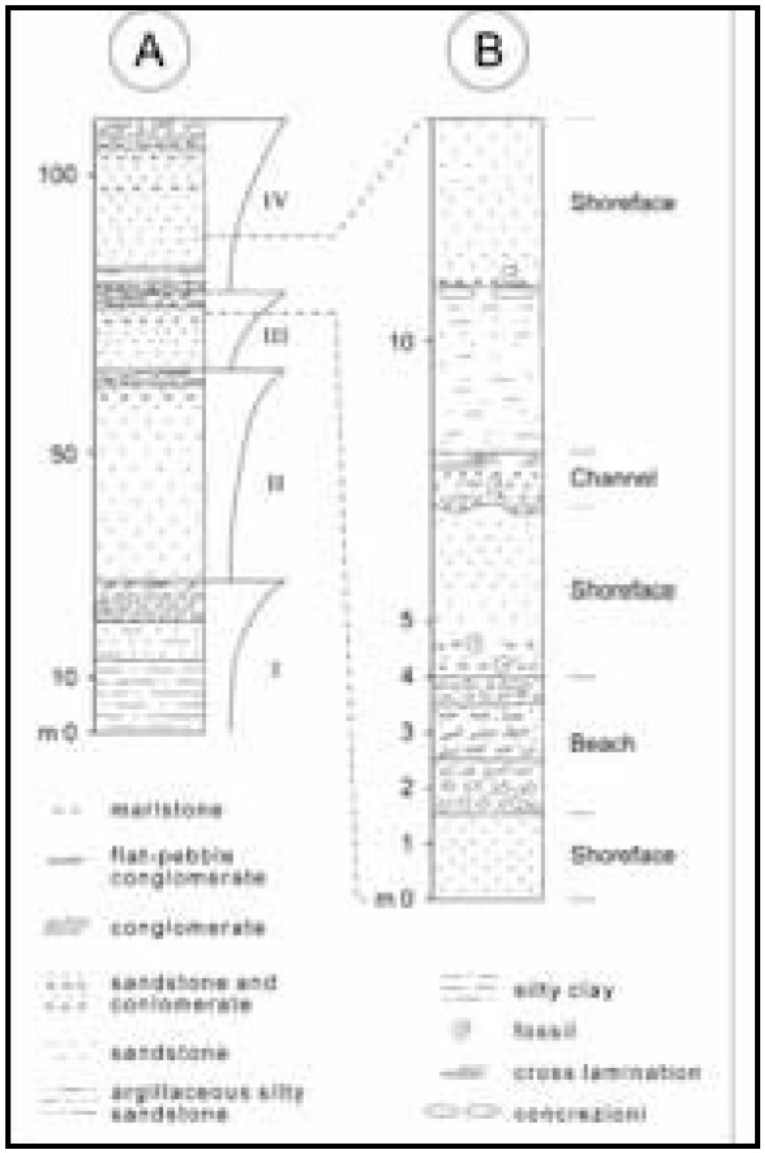

Figure 3 - Generalized stratigraphy of the Siena area: A. Four coarsening-upward sequences (I - IV) recognized in the western part of the city area (after Terzuoli, 1997); B. Enlarged portions of the two topmost sequences exposed on the walls of the Bottini visited during stop 4. Paleoenvironment interpretation is indicated on the right column

IGC

Simplified Geological Map Siena Basin

Martini et al 2011

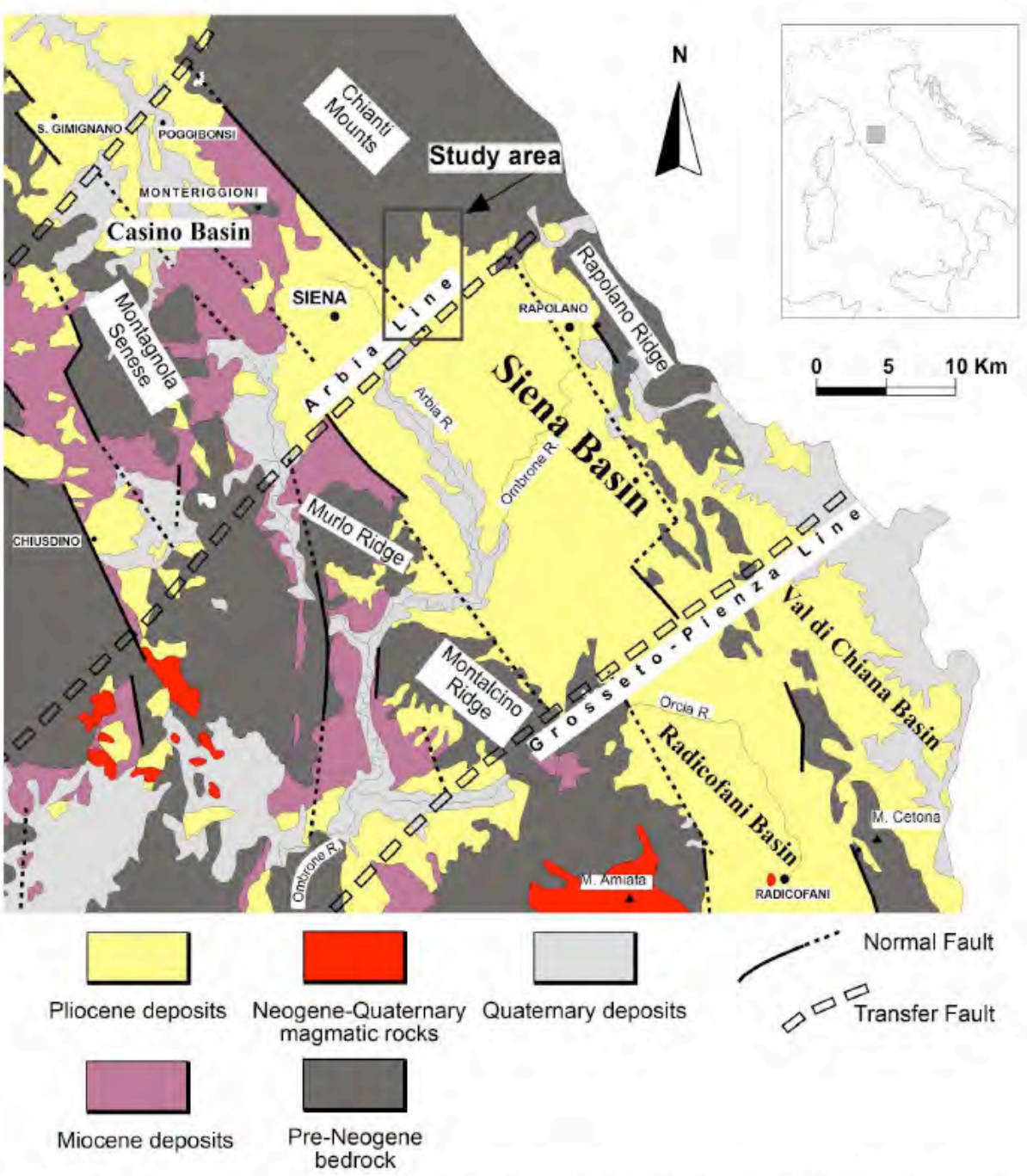

Figure 1. Simplified geological sketch of southern Tuscany with location of the study area and the Siena Basin.

Martini et al 2011

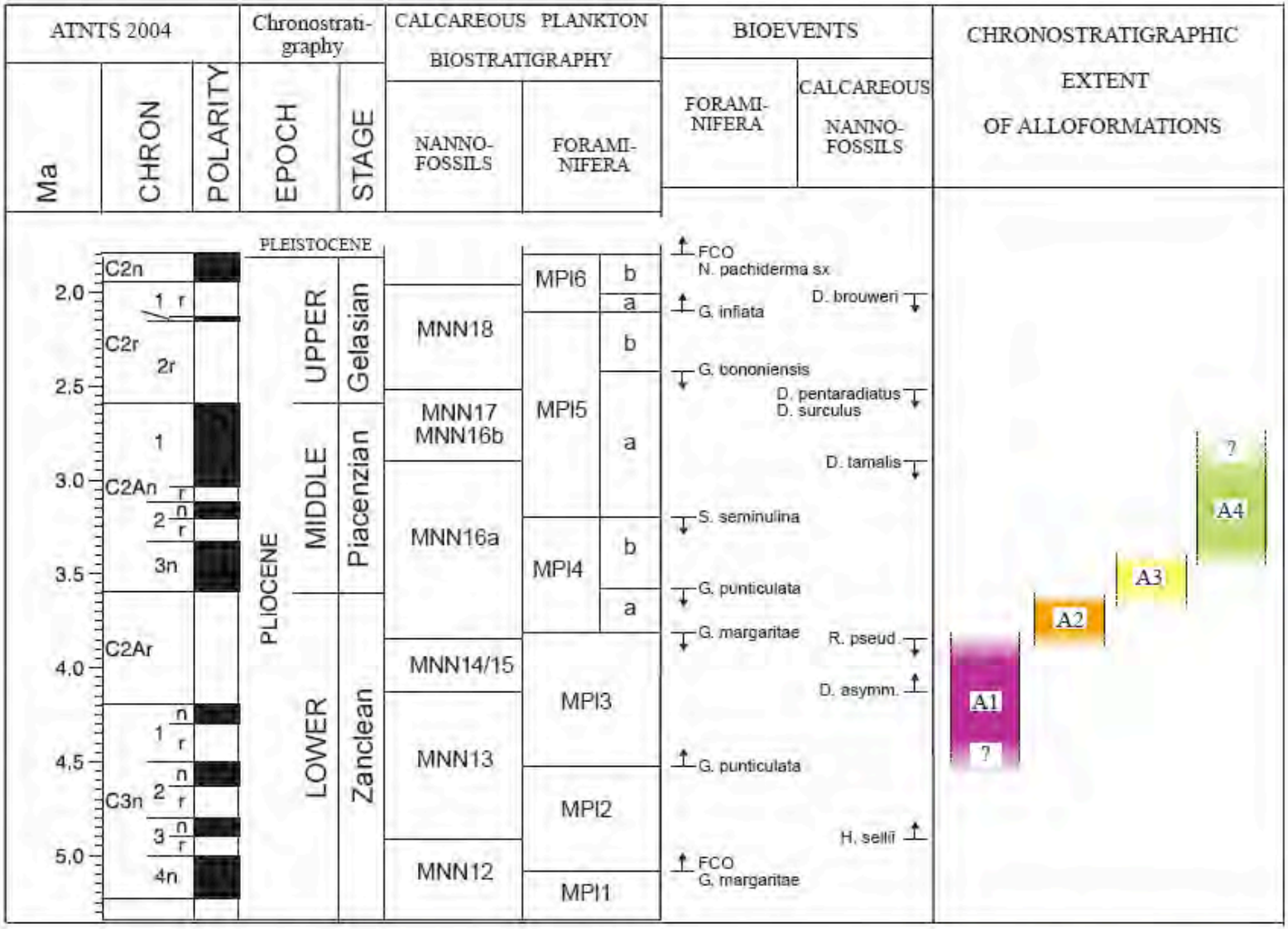

Figure 2. Estimated bio-chronostratigraphic extent of the Pliocene allostratigraphic units of the northern Siena Basin. Calcareous plankton bio-magnetostratigraphy derived from the original scheme of Cita (1975), Raffi and Rio (1979), Rio et al. (1990) and Foresi et al. (2001) integrated and chronologically calibrated by various authors (Lourens et al., 2004; Iaccarino et al., 2007). The Astronomical Tuned Neogene Time Scale (ATNTS) is after Lourens et al. (2004).

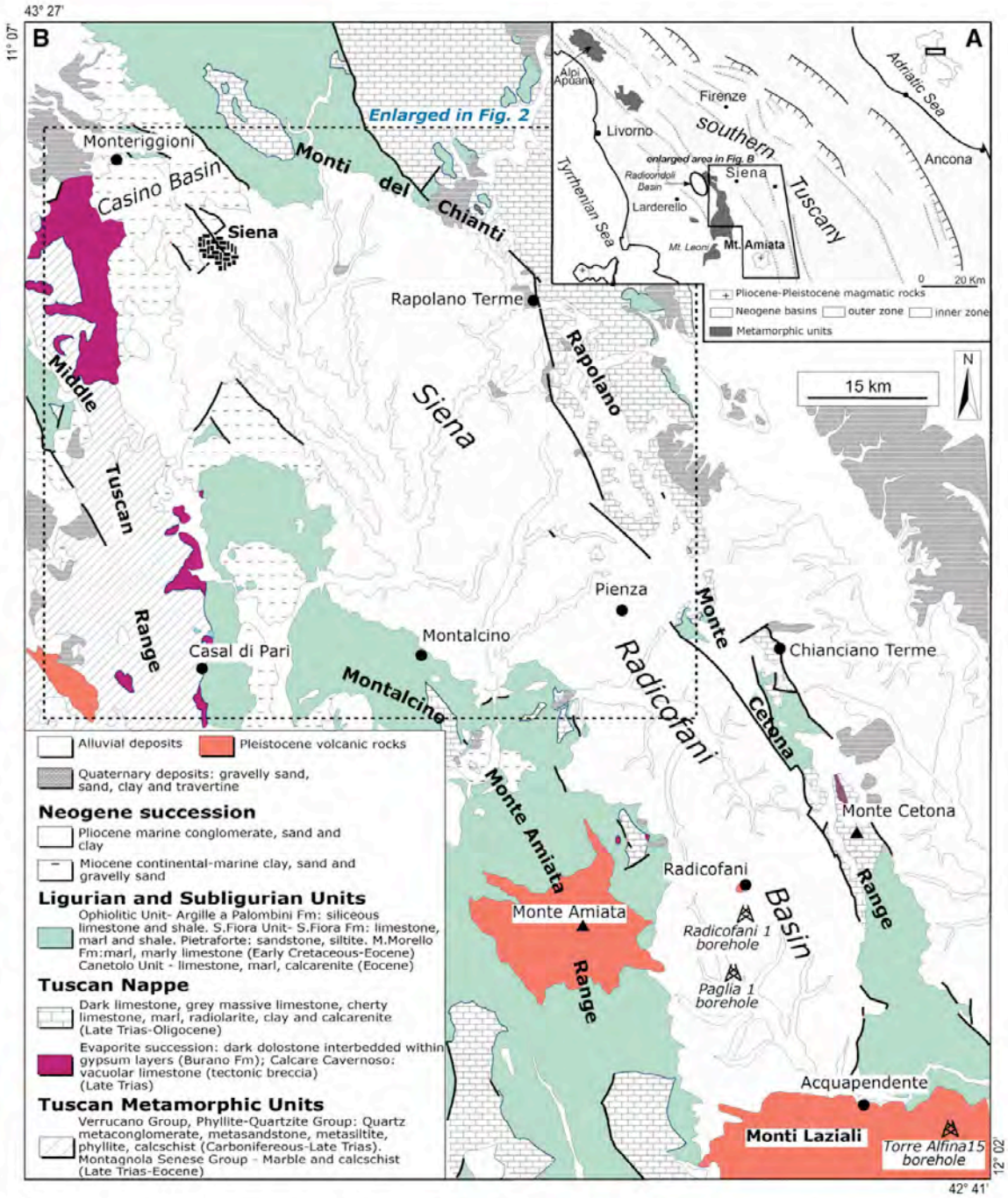

Fig. 1. A) Tectonic sketch of the inner and outer zones of the Northern Apennines; southern Tuscany is mainly located in the inner part. B) Geological sketch-map of the Neogene Siena–Radicofani structural depression; the Casino (sub-)Basin corresponds to the northern part of the Siena–Radicofani basin.

Brogi et al 2011

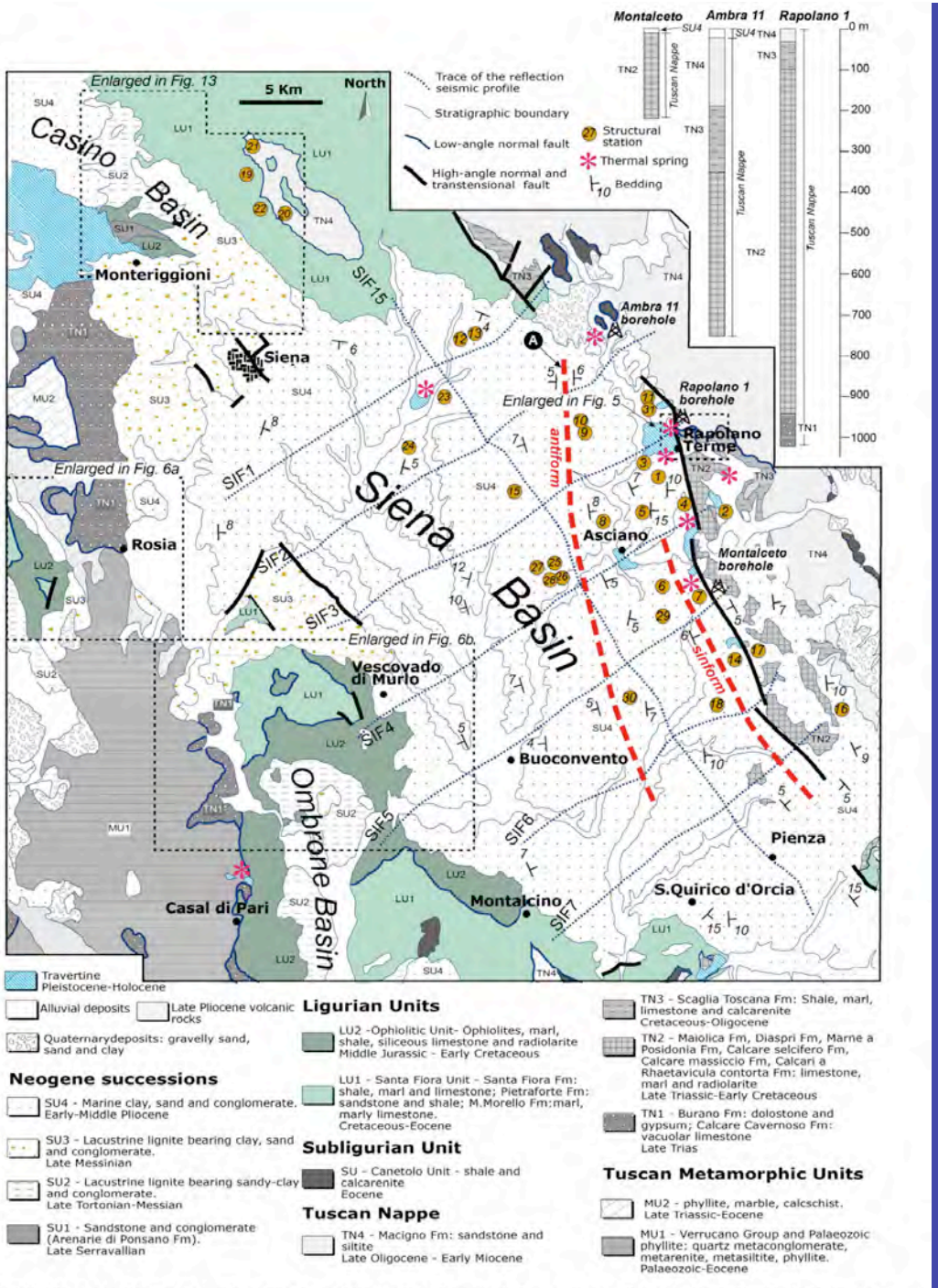

Fig. 2. Geological sketch-map of the Siena basin and stratigraphic logs of deep boreholes; the traces of reflection seismic profiles acquired by AGIP-FINA in the 80s are also indicated.

Brogi et al 2011

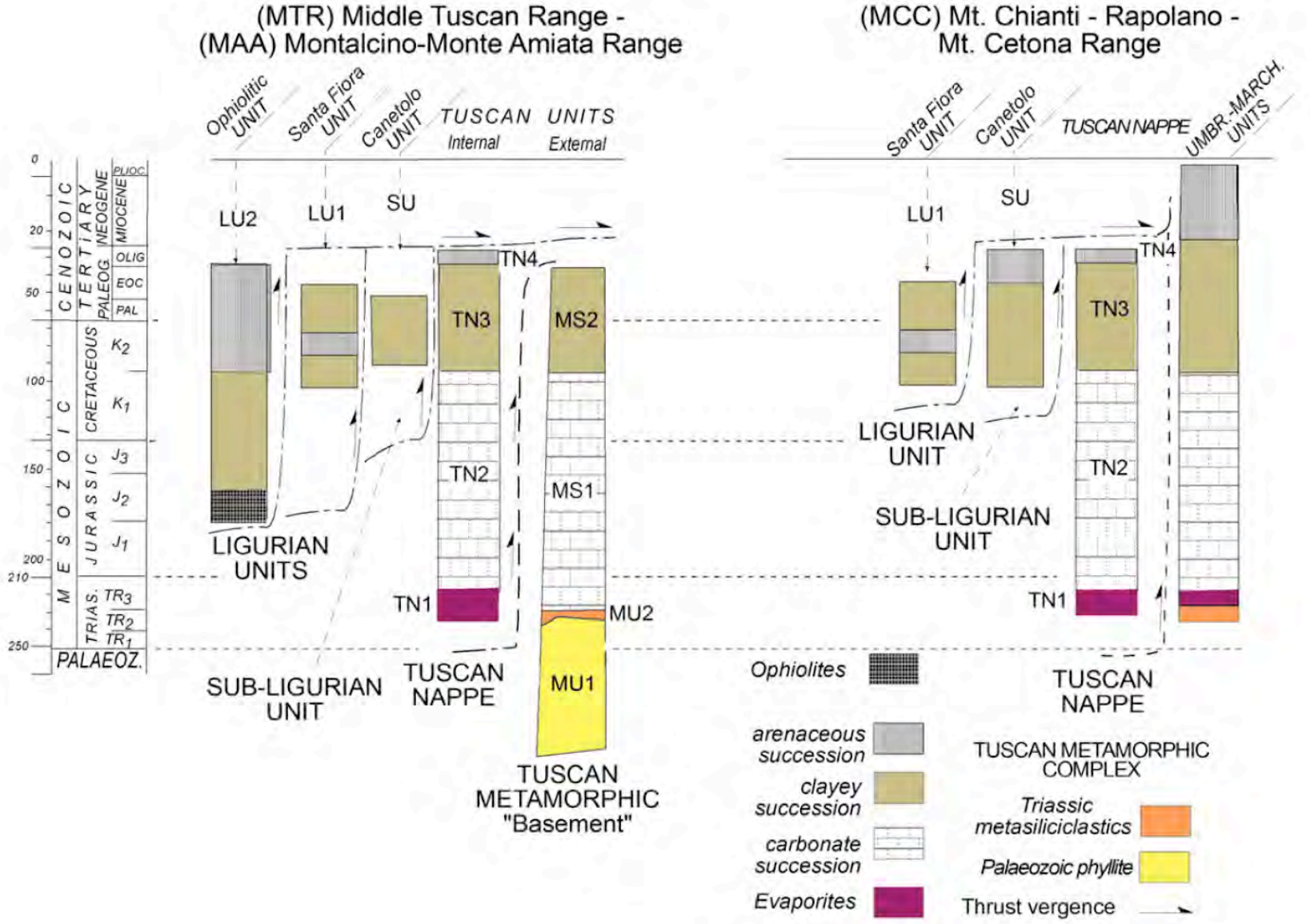

Fig. 3. Relations among the different tectonic units of the Northern Apennines exposed in the indicated margins of the Siena basin. Symbols: LU — Ligurian Units: LU1 — Ophiolitic Unit; LU2 — S.Fiora Unit; SU — Subligurian Unit: Canetolo Unit; TN — Tuscan Nappe; TN1 — Late Triassic evaporites; TN2 — Late Triassic–Cretaceous carbonate and siliceous succession; TN3 — Late Cretaceous–Oligocene clayey (Scaglia Toscana) succession; TN4 — Oligocene–Early Miocene arenaceous (Macigno) succession; MU — Metamorphic Units: MU1 — Carboniferous–Permian phyllites and metasandstones; MU2 — Triassic metasiliciclastics; MS — Metamorphic Tuscan Nappe (Montagnola Senese Group): MS1 — Late Triassic–Cretaceous metacarbonate and metasiliceous succession; MS2 — Late Cretaceous–Eocene phyllite and matacarbonate succession.

Brogi et al 2011

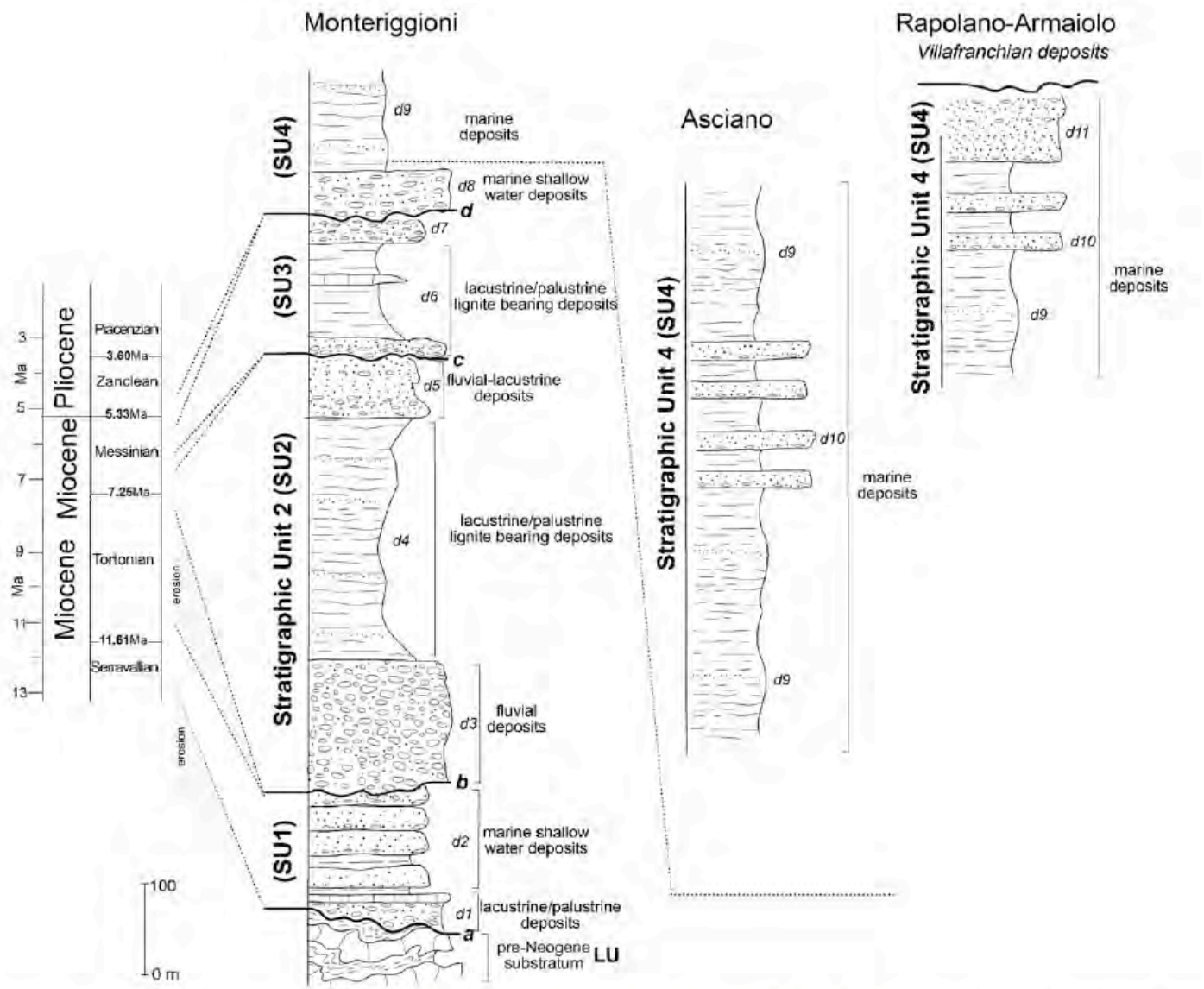

Fig. 4. Stratigraphic columns of the filling sediments exposed in the Siena Basin and its northern prolongation (Casino Basin) as reconstructed in the indicated localities through fieldwork data integrated with information from Lazzarotto and Sandrelli (1977), Gandin and Sandrelli (1992), Bonini and Sani (2002). a, b, c and d are the main unconformities that separate the indicated stratigraphic units (SU1–4). Key: d1 — conglomerate composed of carbonate and sandstone clasts deriving from the Ligurian Units, mainly; d2 — marly-limestone and marl; d3 — sandstone and pebbly-sandstone; d4 — grey clay and sandy-clay; d5 — red conglomerates; d6 — lignite-bearing clay and sandy-clay; d7 — fluvio-lacustrine polygenic conglomerate; d8 — polygenic conglomerate, gravel and sandstone; d9 — marine clay and sandy-clay; d10 — marine sand interbedded within clay; d11 — marine gravel, sand and conglomerate.

Brogi et al 2011

Digression 1: clastic sedimentary rocks

Breccia

Conglomerate

Sandstone

Siltstone

Claystone

http://geology.com/rocks/sedimentary-rocks.shtml

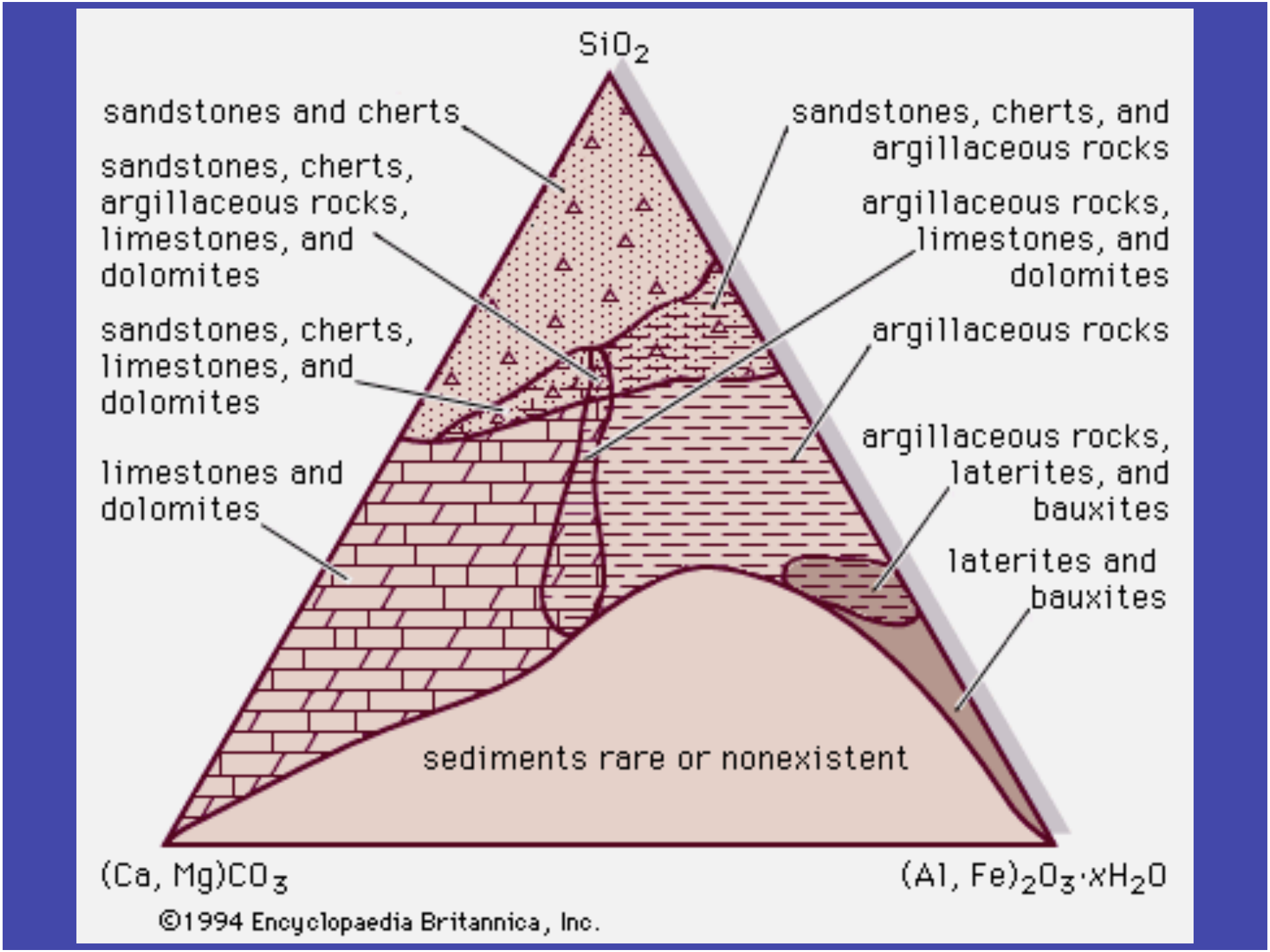
SiO_2
sandstones and cherts
sandstones, cherts, argillaceous rocks, limestones, and dolomites
sandstones, cherts, limestones, and dolomites
limestones and dolomites
sandstones, cherts, and argillaceous rocks
argillaceous rocks, limestones, and dolomites
argillaceous rocks
argillaceous rocks, laterites, and bauxites
laterites and bauxites
sediments rare or nonexistent
$(Ca, Mg)CO_3$
$(Al, Fe)_2O_3 \cdot xH_2O$
©1994 Encyclopaedia Britannica, Inc.

Digression 2: clastic depositional environments

The beginning: How and where do we make sedimentary rocks?

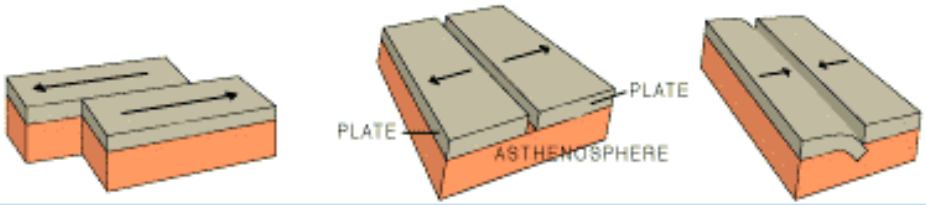

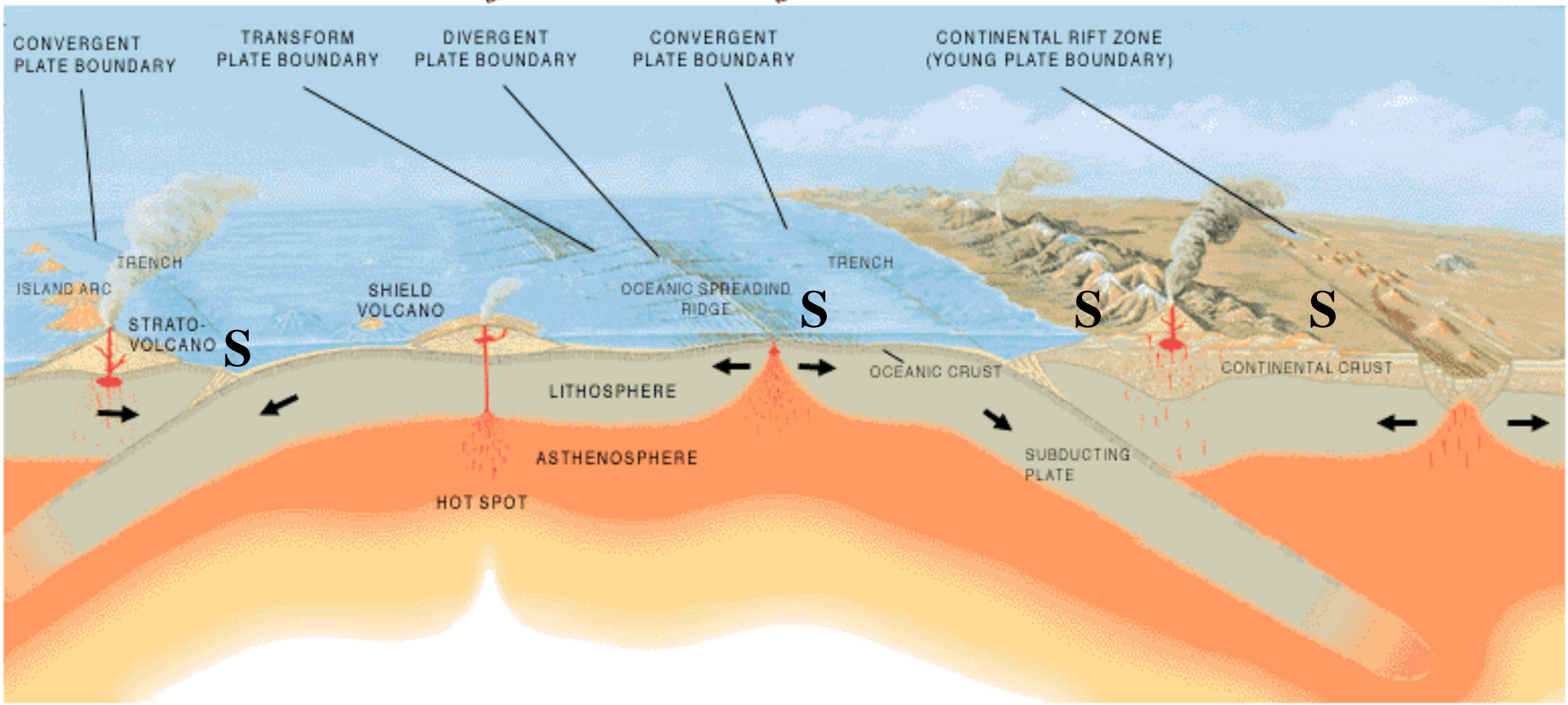

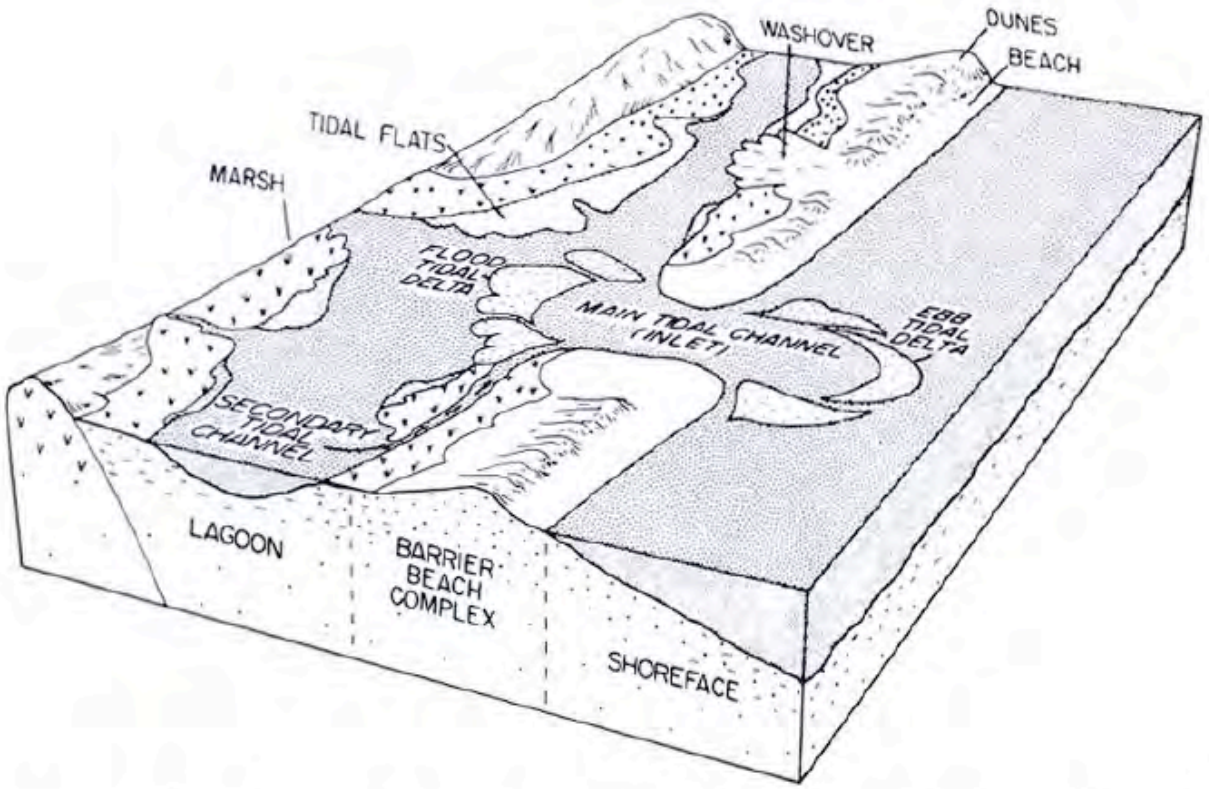

FIG. 15.—Block diagram of a barrier-island and lagoonal depositional environment, from Reinson (1992). Note that this is a "snapshot in time" and that the various environments shown in the diagram may not be preserved if the barrier progrades or is transgressed. For the transgressive setting, see Figure 16.

Walker 2006 in Posamentier and Walker (Eds) 2006

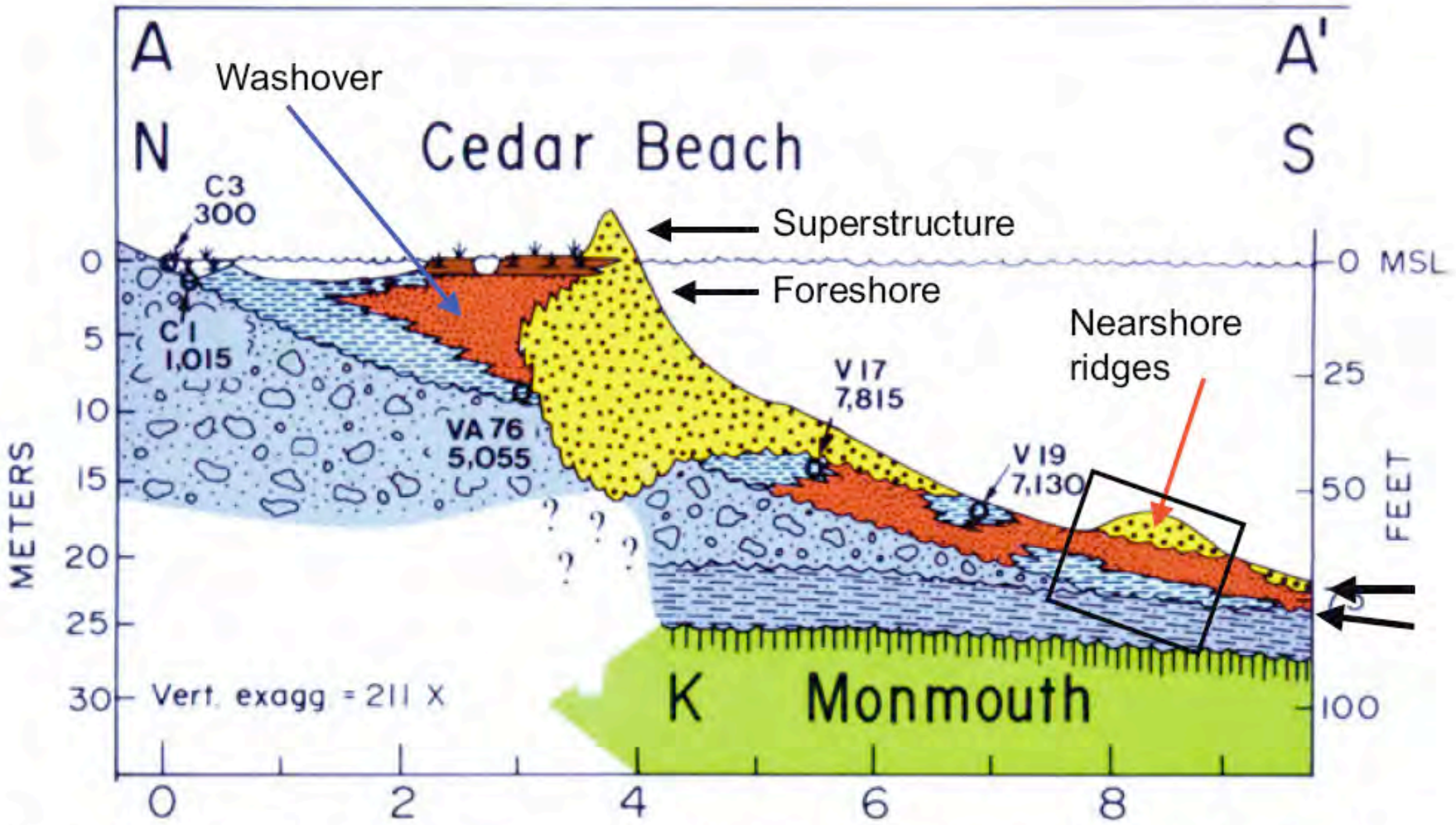

FIG. 16.—Cross section of Cedar Beach, Long Island, New York. Barrier–lagoon system rests disconformably on Pleistocene diamictite (blue, conglomerate–breccia symbols). The barrier cuts down into the Pleistocene at a tidal inlet. Note the age dates of lagoonal deposits, 7815 and 7130 years BP south of the barrier, 5055 years BP at Cedar beach, and 1015 and 300 years BP at the northern edge of the lagoon. The sand of the barrier superstructure is not preserved during transgression—it is washed into the lagoon (dark red) during storms (blue arrow) and is also moved offshore to form small ridges (red arrow—southern end of cross section). The record of barrier transgression is shown in the black rectangle, and consists of a thin sheet of lagoonal and washover facies (blue, dark red, seaward of barrier) overlain disconformably by modern storm sands. The two black arrows at the right show two erosion surfaces, one separating Pleistocene from Holocene sediments and one separating 7000+ year-old lagoonal and washover facies from offshore sands forming today. From Rampino and Sanders (1970).

Walker 2006 in Posamentier and Walker (Eds) 2006

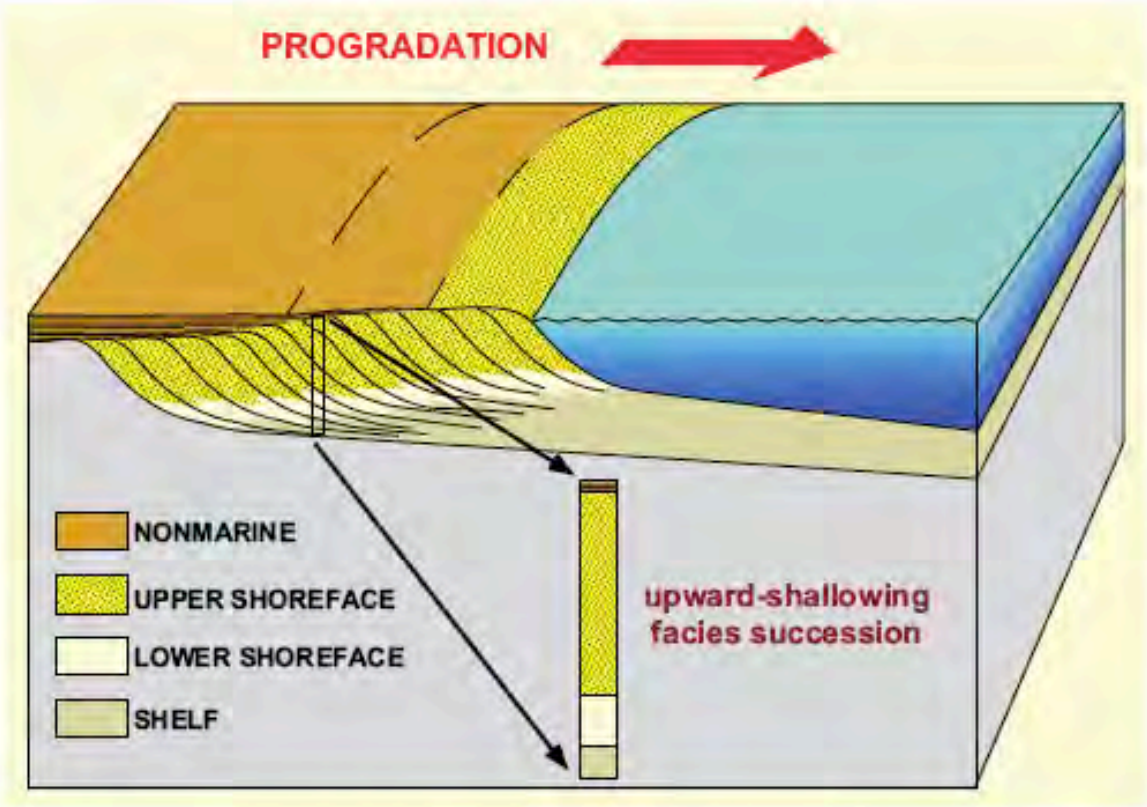

FIG. 1.—Characteristic mode of accumulation of shoreline deposits through progradation (shown here with a slight rise of relative sea level during progradation), whereby shallow-water facies build laterally over deeper-water counterparts, generating an upward-shallowing succession or, if sandwiched between transgressive episodes, a parasequence (see Harms et al., 1982).

Clifton 2006 in Posamentier and Walker (Eds) 2006

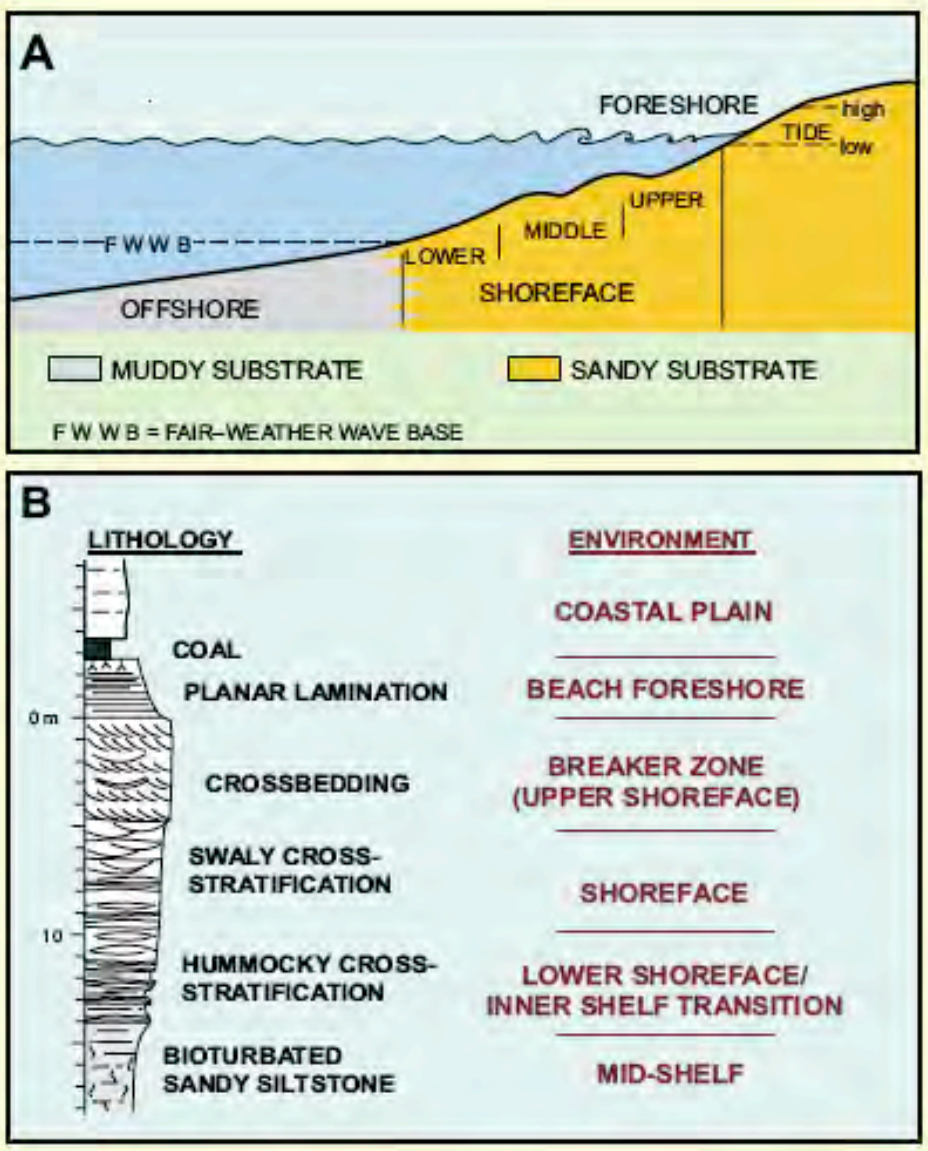

FIG. 2.—A) Beach-to-offshore profile in facies model of Walker and Plint (1992). Fair-weather wave base at base of shoreface. B) Shallowing-up facies succession in facies model of Walker and Plint (1992).

Clifton 2006 in Posamentier and Walker (Eds) 2006

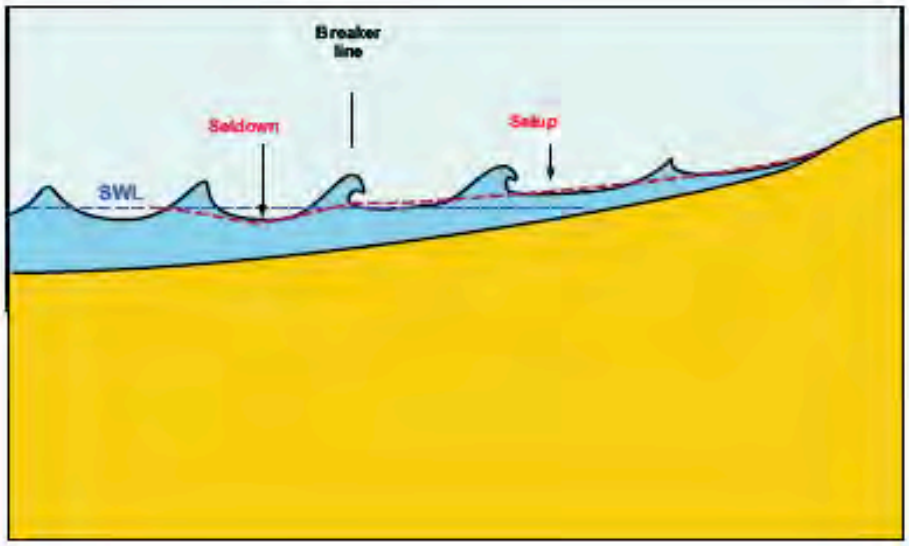

FIG. 10.—Setup and setdown of the sea surface (departure from the still-water line (SWL)) owing to the landward transport of water within the surf zone. Depression of the sea surface (setdown) just outside the breaker line and elevation of the sea surface adjacent to the beach provides the hydraulic head for nearshore circulation cells.

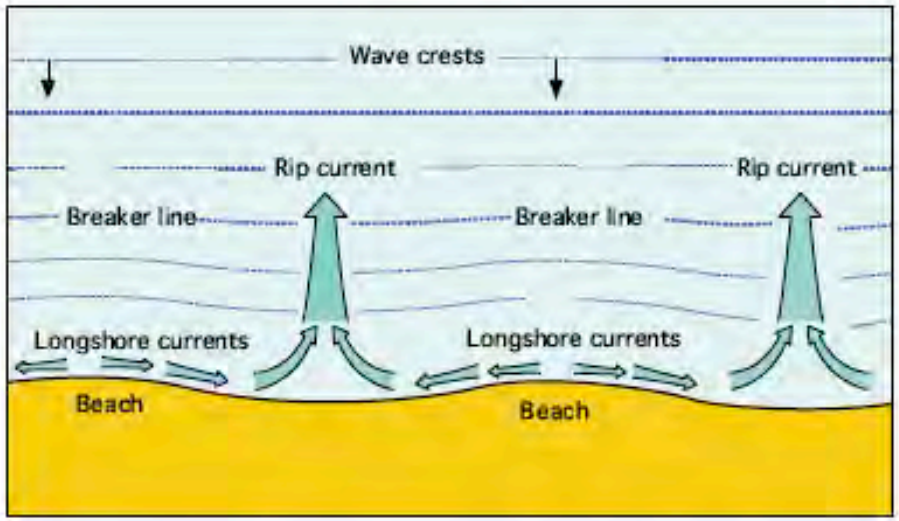

FIG. 11.—Nearshore circulation cells where wave incidence is parallel to coast. Circulation consists of unidirectional rip and longshore currents generated by the hydraulic head caused by setup and setdown of the sea surface in and near the breaker zone.

Clifton 2006 in Posamentier and Walker (Eds) 2006

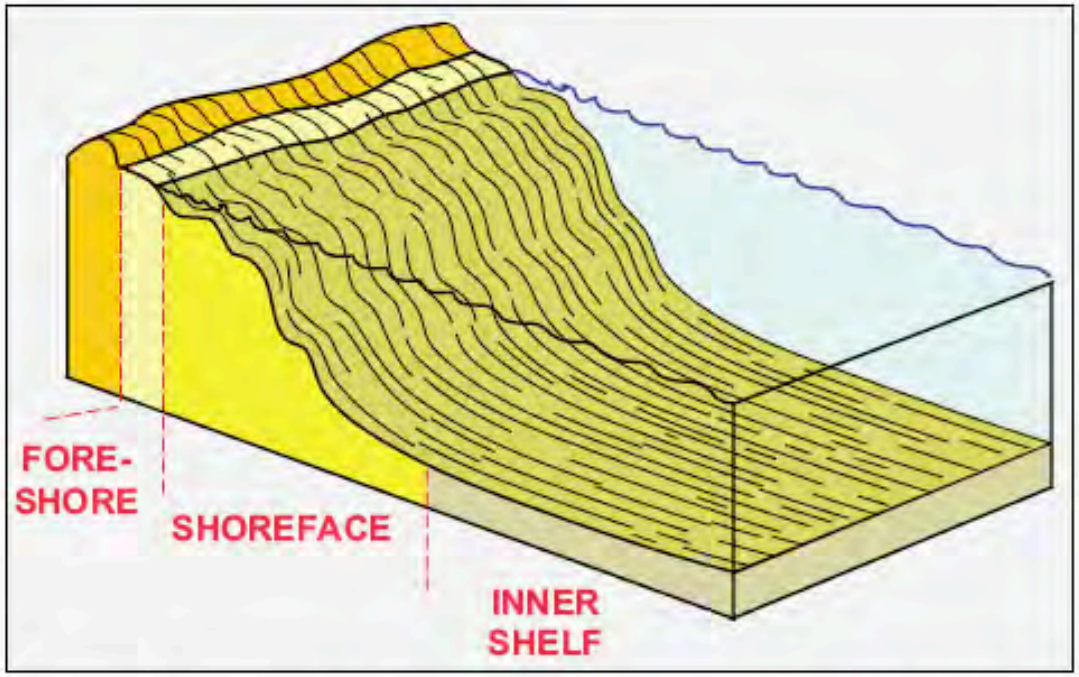

FIG. 12.—The shoreface is best defined as a morphologic feature that attends nearly all clastic shorelines. It has a relatively steep concave-up surface that extends seaward from the beach foreshore and merges with the much flatter shelf or basin platform. Breaker bars, as shown, may cover the upper part of the shoreface here.

Clifton 2006 in Posamentier and Walker (Eds) 2006

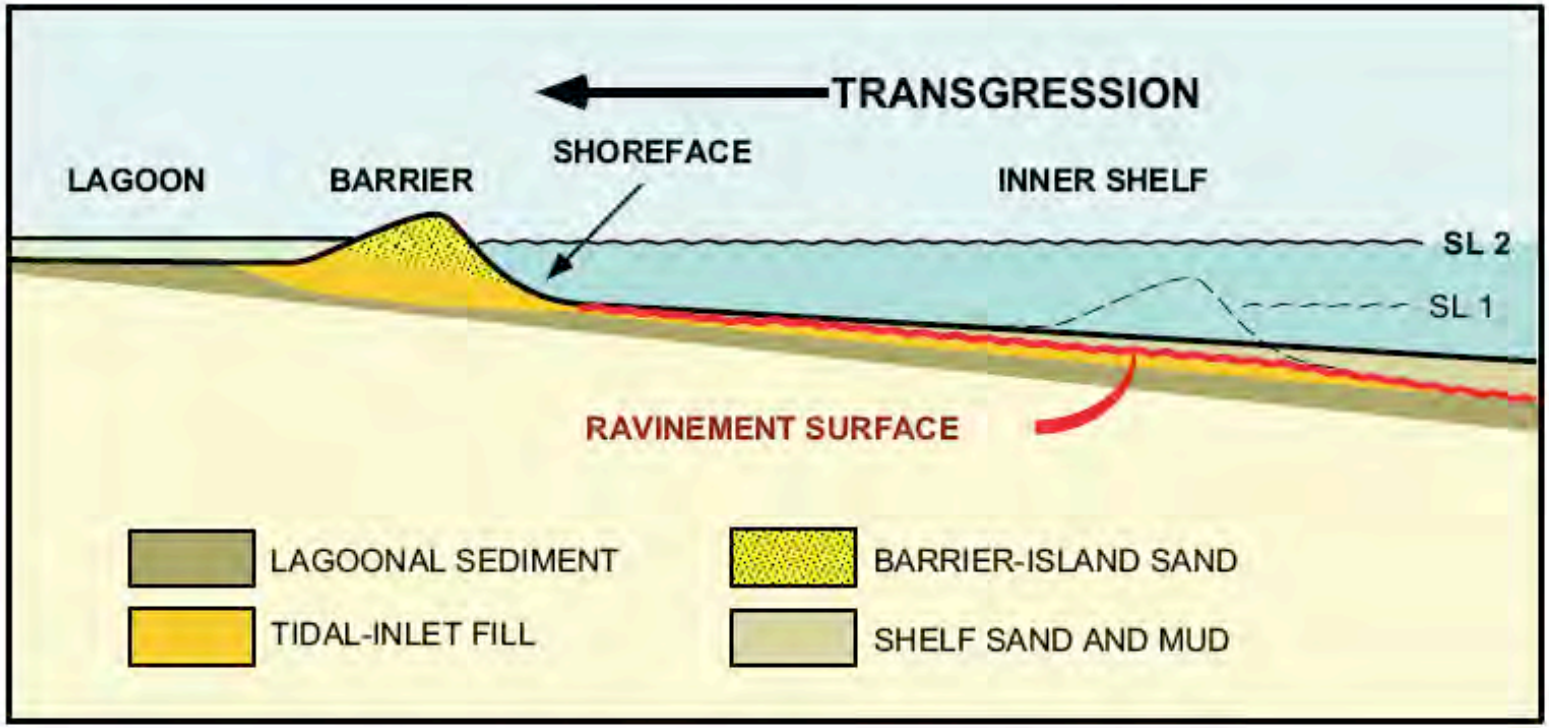

FIG. 14.—Process of marine transgression is commonly associated with the landward migration of a barrier island or barrier spit. Landward translation of the shoreface profile as sea level rises (here from SL 1 to SL 2) creates an erosional surface (surface of ravinement or transgressive surface of erosion) cut into previously deposited sediment. Because deeper-water sediments (here inner-shelf sand / mud) accumulate on the ravinement surface, it marks an abrupt upward change to deeper-water deposits.

Clifton 2006 in Posamentier and Walker (Eds) 2006

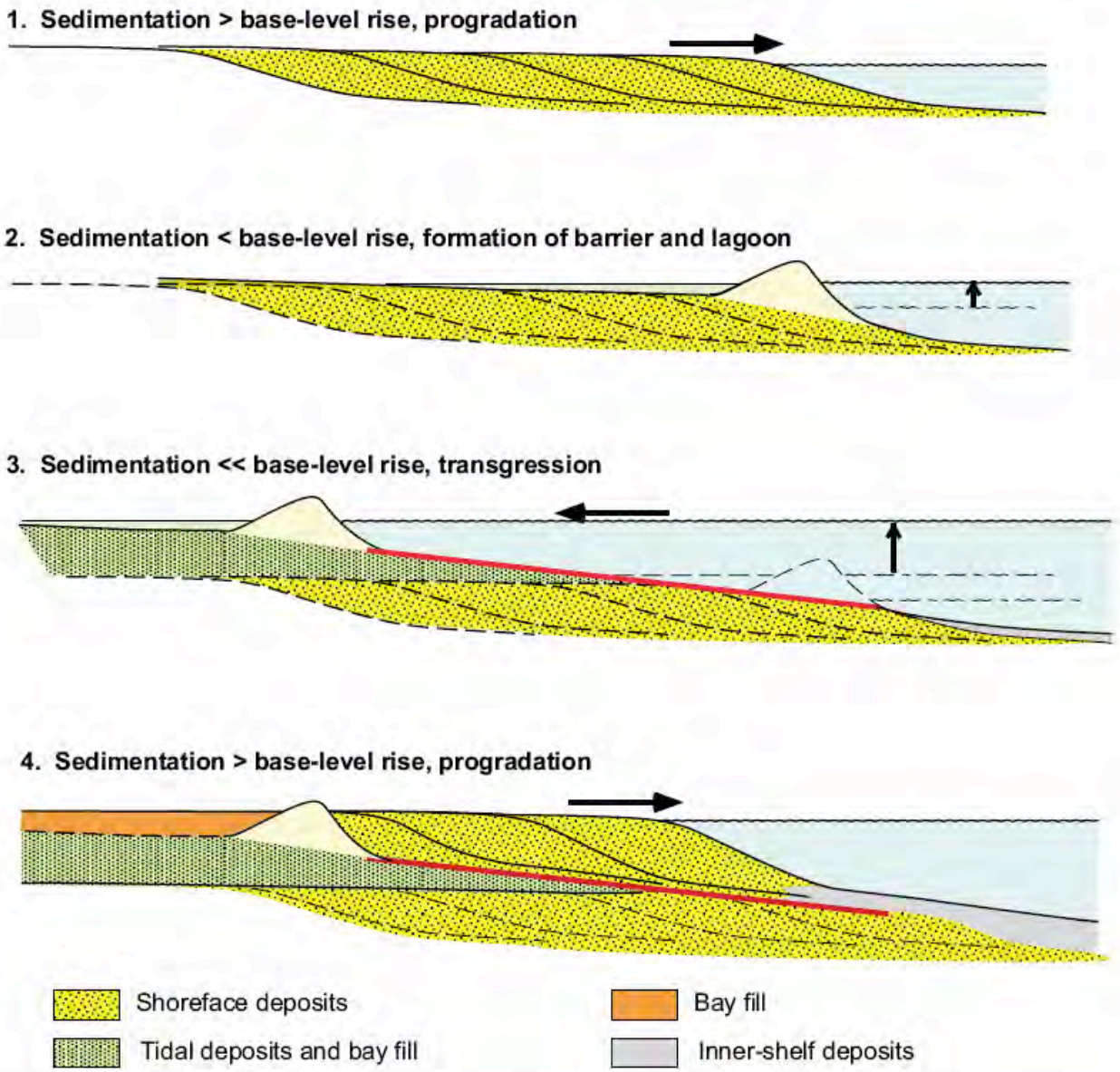

FIG. 21. Schematic diagram showing the development, landward migration, and stranding of a barrier in response to changes in the balance of sedimentation and relative sea-level fluctuation. During progradation in step 4, barrier maintains its identity until the embayment created by the barrier is filled, at which time the coast converts to a strand plain.

Clifton 2006 in Posamentier and Walker (Eds) 2006

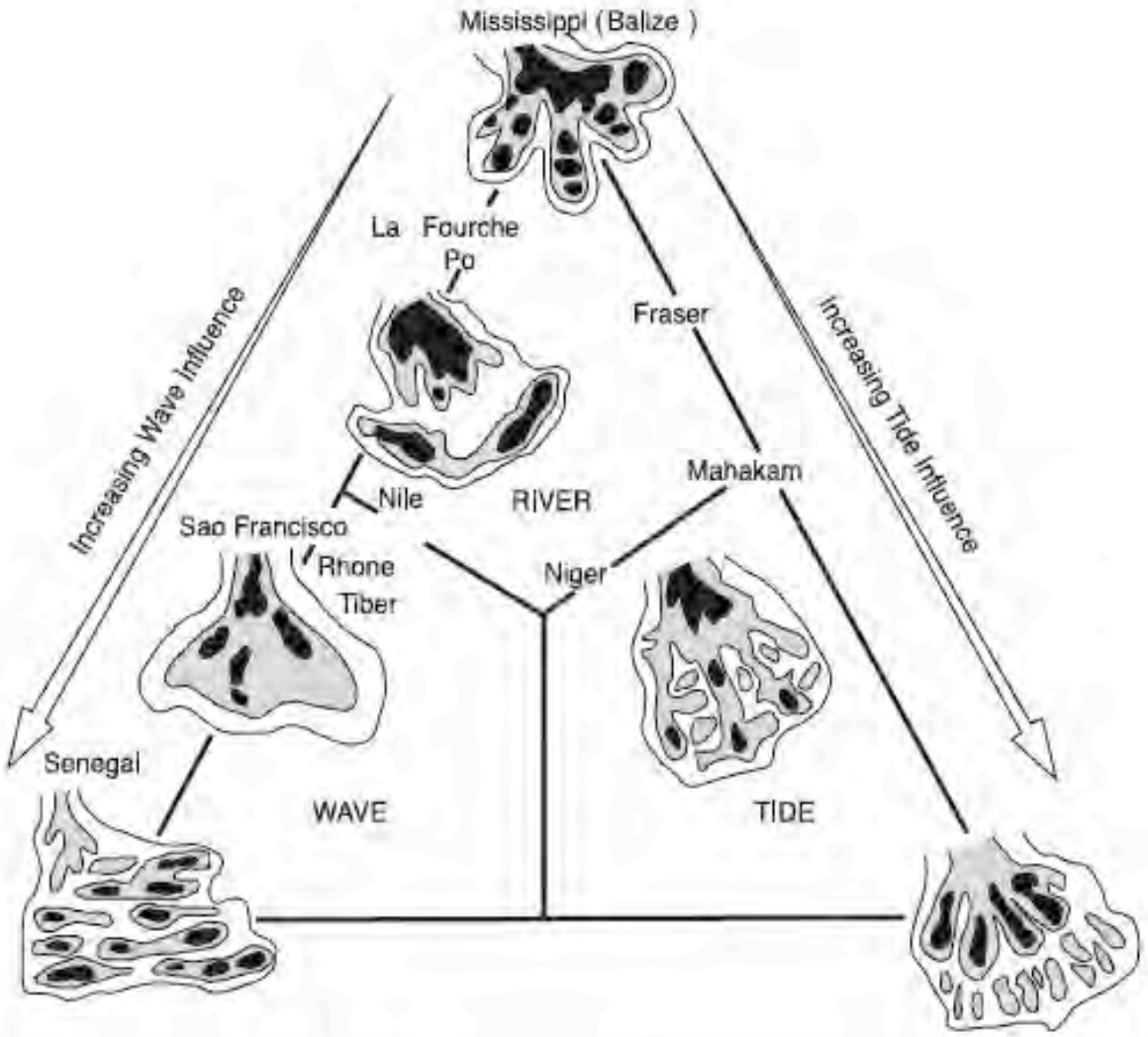

FIG. 4.—Sandbody geometries of the six delta types of Coleman and Wright (1975) plotted on the river-, wave-, and tide-dominated tripartite classification of Galloway (1975), from Bhattacharya and Walker (1992). Note that all sand bodies narrow and thicken towards a point (fluvial) source. Also note similarity of tide-dominated isolith to river-dominated end member.

Bhattacharya 2006 in Posamentier and Walker (Eds) 2006

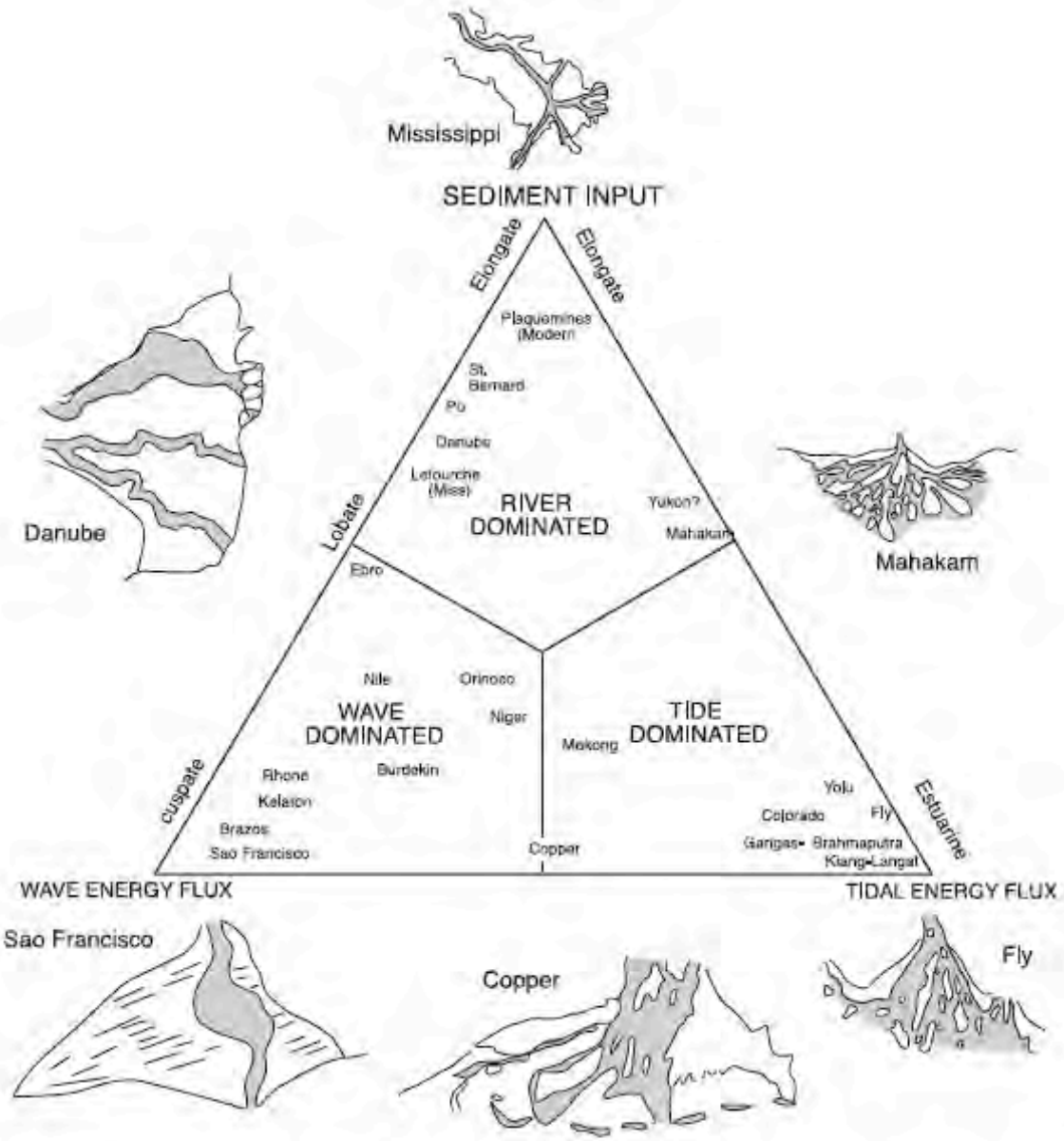

FIG. 5.—Tripartite classification of deltas, into river-, wave-, and tide- dominated end members (Galloway, 1975). Tide-dominated end members are noted as being "estuarine". This prompted Walker (1992) to abandon the concept of a tide-influenced delta. Also note that the São Francisco and Brazos deltas are considered as type examples of wave-dominated end members.

Bhattacharya 2006 in Posamentier and Walker (Eds) 2006

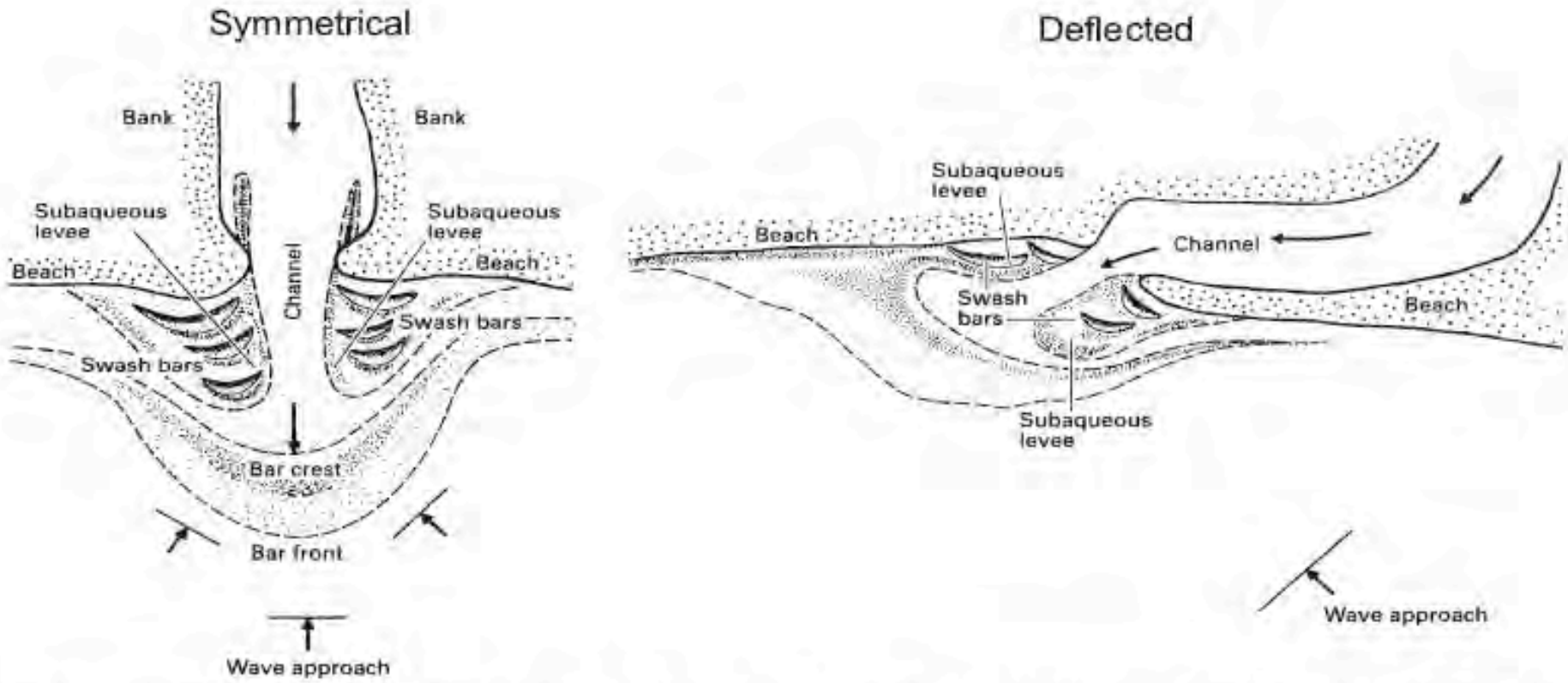

FIG. 12.—A) Symmetrical mouth bars, versus B) deflected mouth bars. As a result of oblique wave approach (compare with Figure 6). From Reading and Collinson (1996), after Wright (1977).

Bhattacharya 2006 in Posamentier and Walker (Eds) 2006

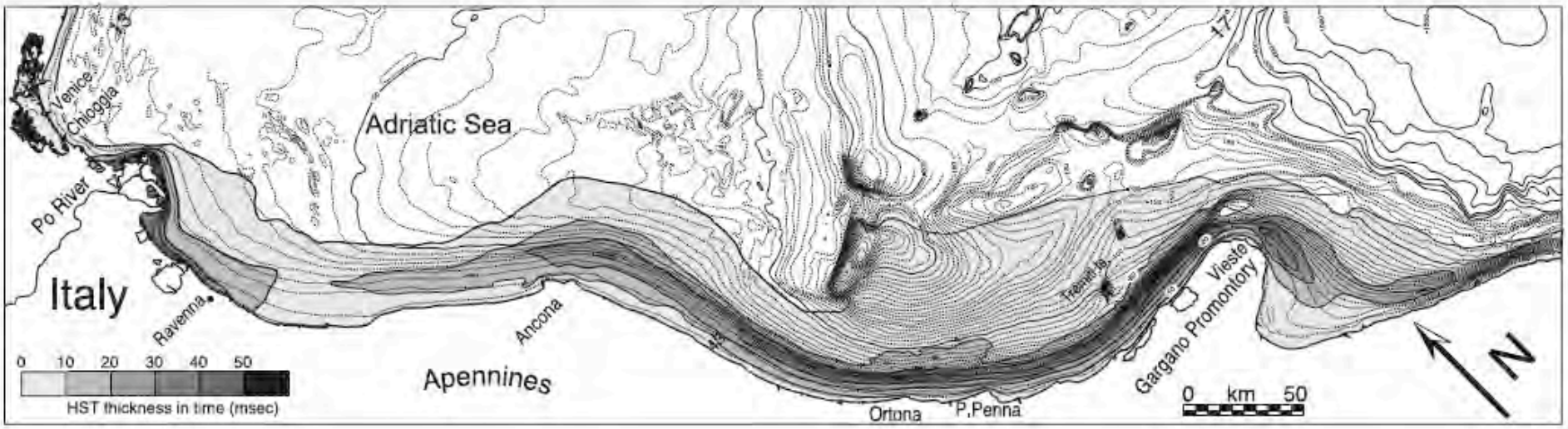

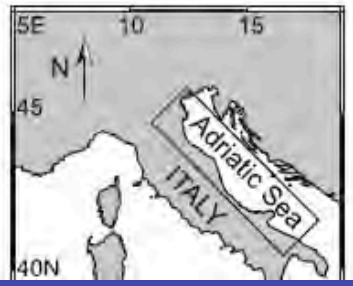

FIG. 13.—Mud from the Po delta, deposited during the Holocene highstand (HST) is carried several hundred kilometers along the Adriatic coast by geostrophic currents (from Correggiari et al., 2001).

Bhattacharya 2006 in Posamentier and Walker (Eds) 2006

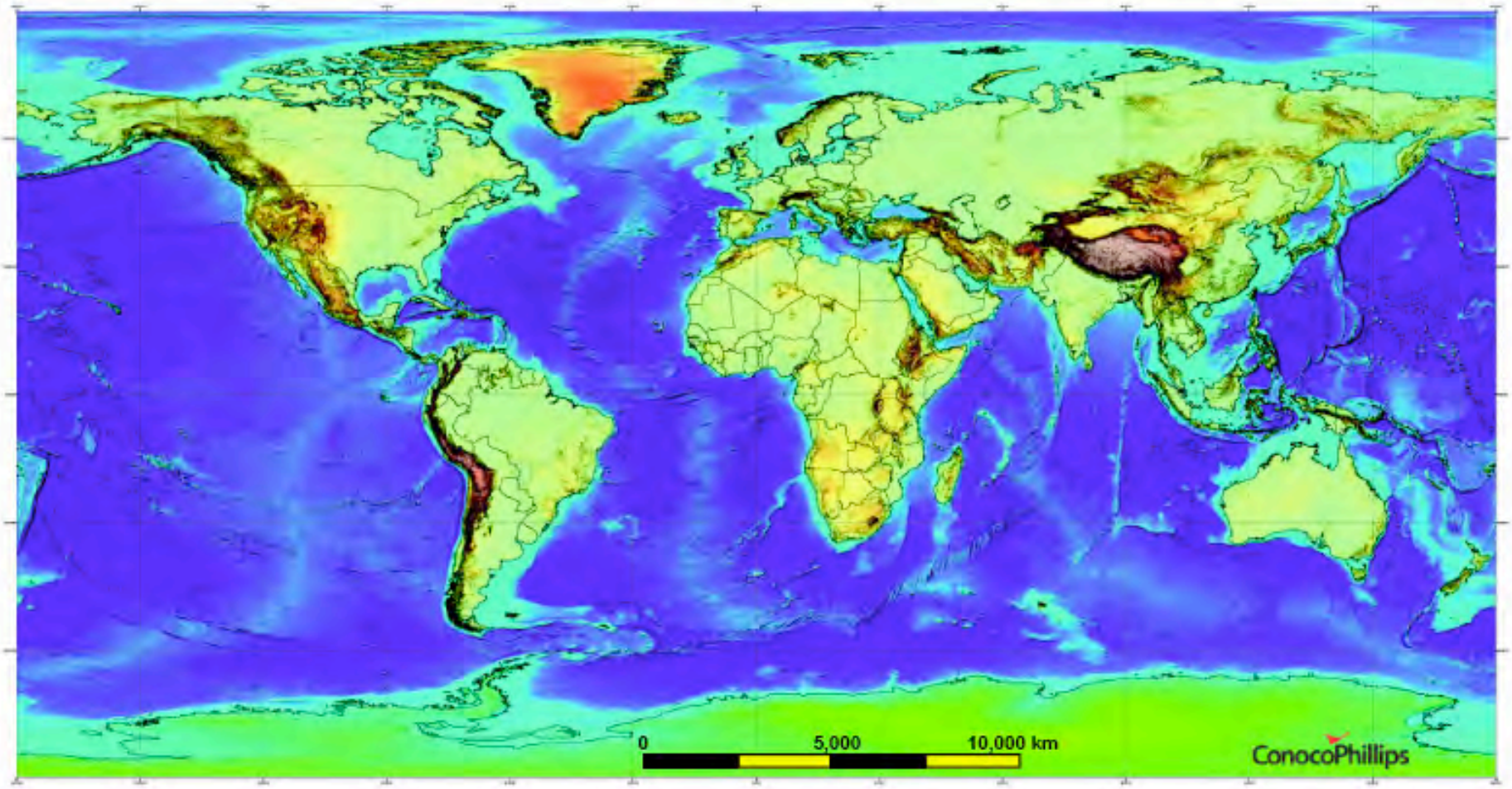

FIG. 1.—Satellite topographic–bathymetric image of the world (image courtesy of K. Soofi, ConocoPhillips, 2004). Continental shelves are those portions of the ocean basins shown in light blue, comprising depths between 10 and 200 m. This designation represents about 6% of the total area of the globe. Slopes on the continental shelves range from about 0.001° to ~ 1°, and widths vary from less than 10 km to greater than 200 km.

Suter 2006 in Posamentier and Walker (Eds) 2006

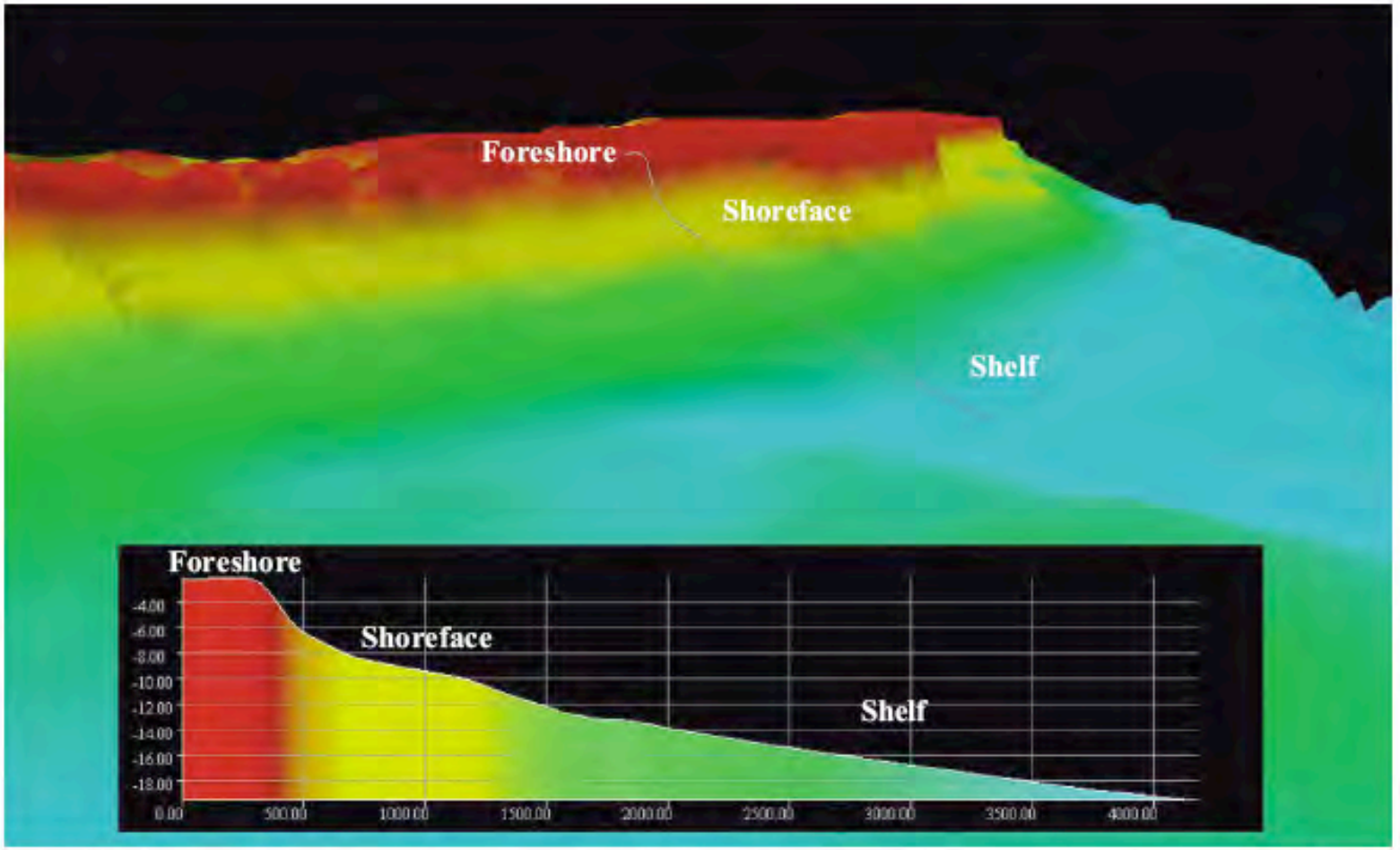

FIG. 2.—Digital bathymetry and profile of a modern shoreface–shelf transition, from offshore of Fraser Island in northeastern Australia (image courtesy of R. Boyd, 2004). The continental shelf begins at the change in slope at the toe of the lower shoreface. The depth at which this occurs is highly variable and ranges from about 2 m to as much as 25 m in different parts of the world (Clifton, this volume).

Suter 2006 in Posamentier and Walker (Eds) 2006

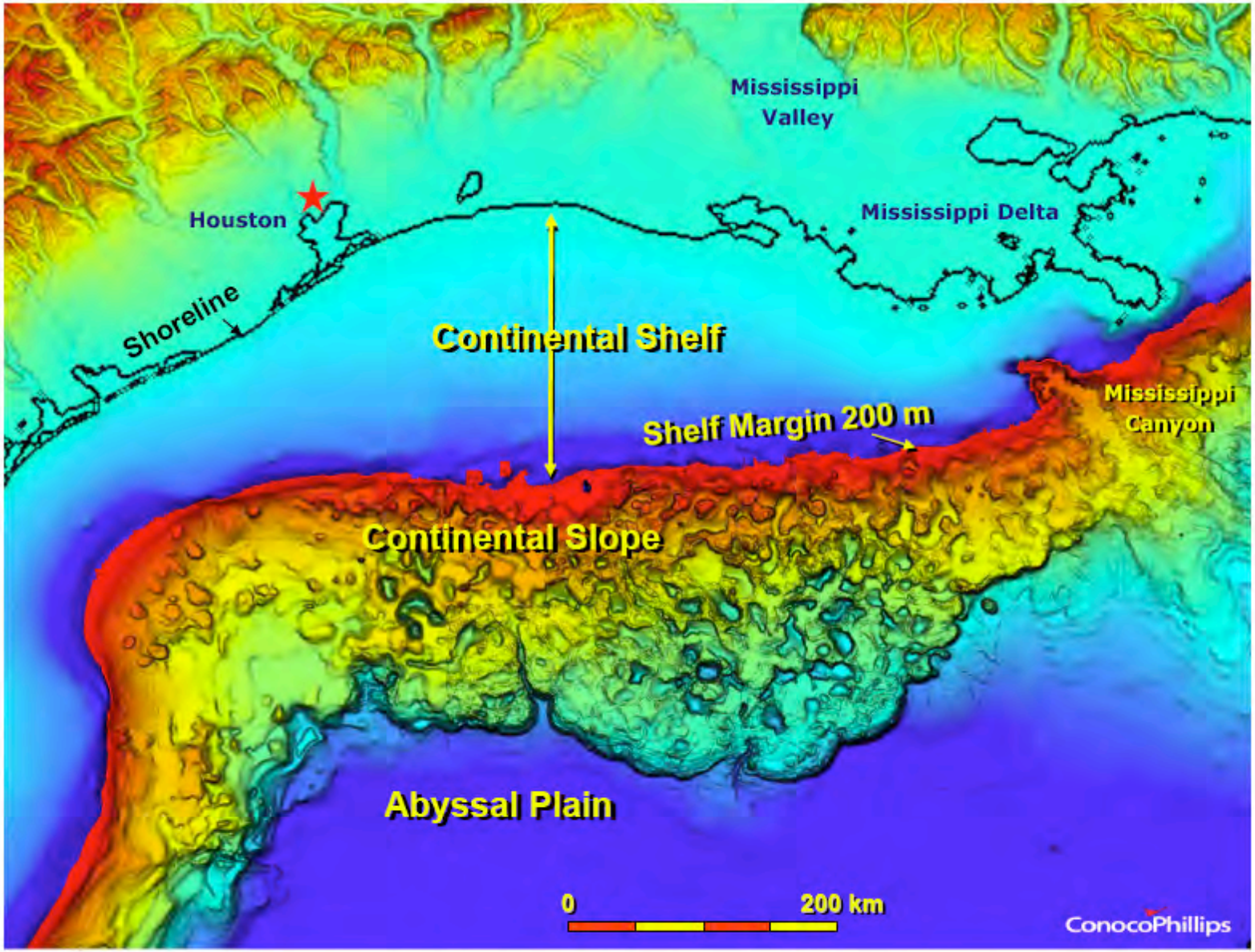

FIG. 3.—The Gulf of Mexico is an excellent example of a submerged continental margin, or pericontinental clastic shelf. Shelves of this kind are the most common today. The continental shelf extends from just seaward of the shoreline to the shelf margin, which lies just landward of the 200 m contour indicated. The rugose topography of the continental slope in this area is the result of extensive salt tectonics. (Satellite topography–bathymetry image courtesy of K. Soofi, ConocoPhillips).

Suter 2006 in Posamentier and Walker (Eds) 2006

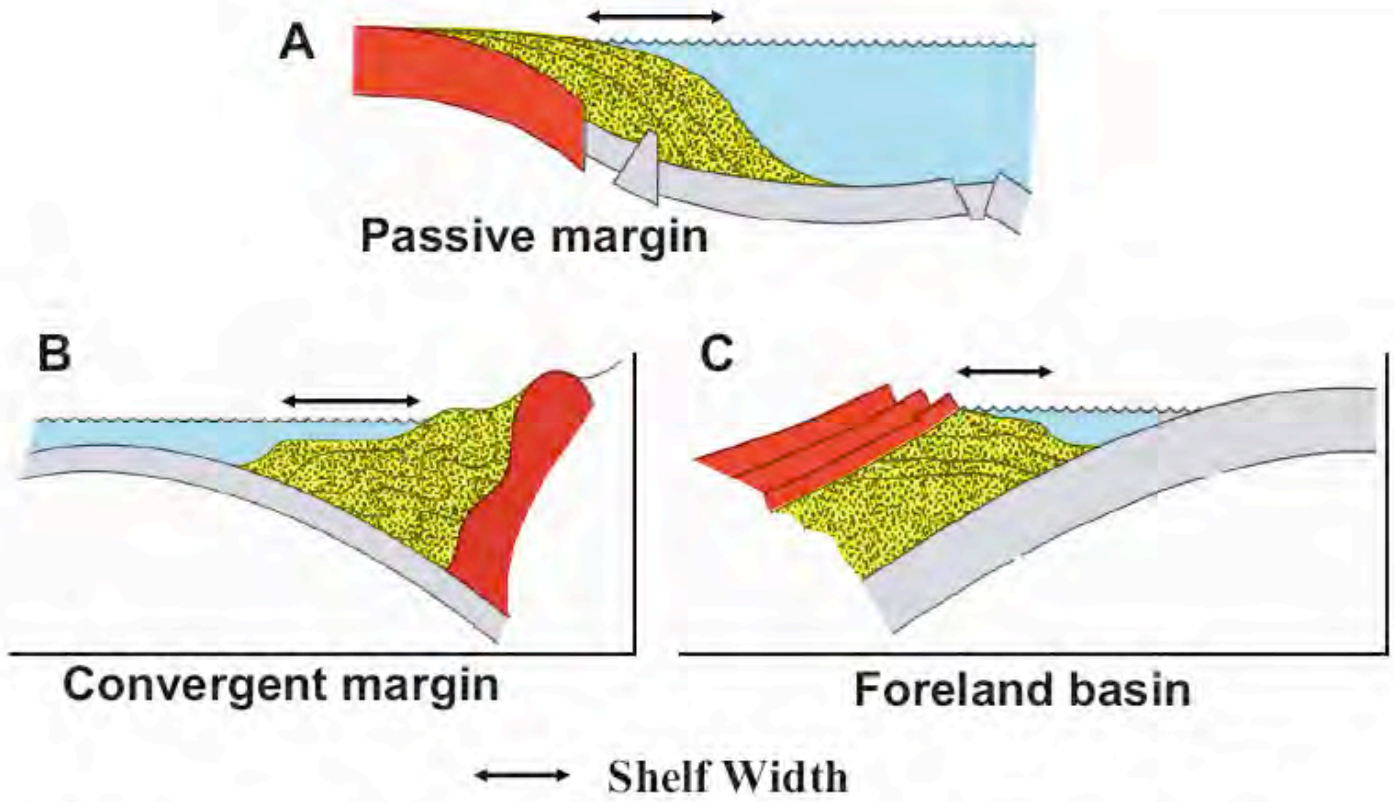

FIG. 5.—Variations in the tectonic setting of continental shelves (redrawn from Swift and Thorne, 1991). A) Passive margins, or trailing margins, are pericontinental shelves (Fig. 3), with increasing rates of subsidence seaward, and consequent seaward-thickening sedimentary deposits. B) Convergent margins form around subduction zones. Subsidence rates are greatest in the area of subduction. Shelf areas are typically narrow, wave-cut platforms, but they may also be aggradational accretionary prisms. C) Foreland basins also occur at convergent margins, with maximum rates of subsidence and deposition adjacent to the thrust belt. Extensive shelf areas commonly develop.

Suter 2006 in Posamentier and Walker (Eds) 2006

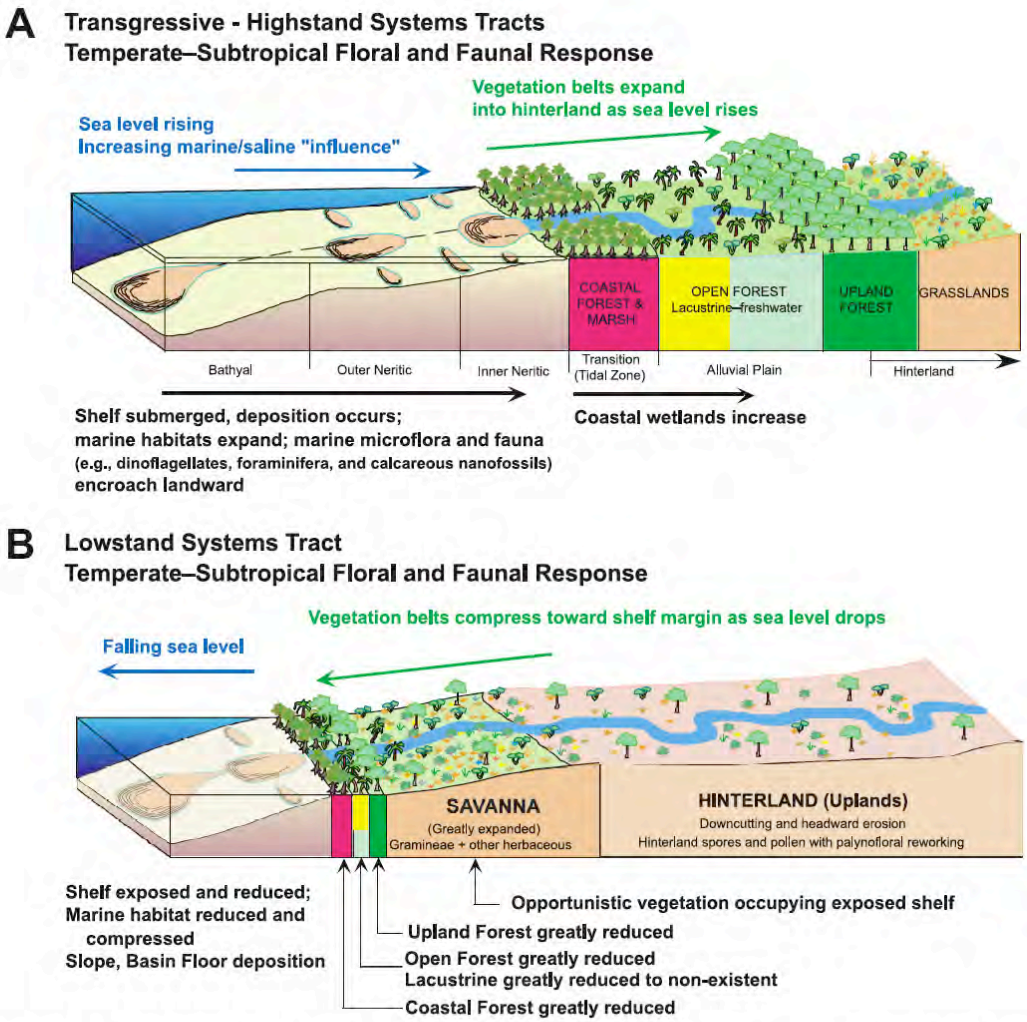

FIG. 26.—Vegetative and palynological response to base-level fluctuations. **A)** During conditions of a relatively high base level in a transgressive and highstand setting, the influence of marine waters encroaches a significant distance landward, increasing the suitable habitat for salt-water-tolerant species, predominantly mangrove. Thus, mangrove pollen as well as marine dinoflagellates should be abundant and characteristic of these systems tracts. Terrestrial spore and pollen habitat is pushed back well into the hinterland and may constitute a small percentage of the overall palynofloral assemblage. Fluvial drainage can take these terrestrial palynoflora out onto the extensive continental shelves, mixing with the marine indicators mentioned above as well as marine microfossils. **B)** In an idealized lowstand setting, opportunistic species of the savanna and hinterland occupy the exposed shelf. Accordingly, the terrestrial pollen/spore habitat is abundant and their palynoflora can be transported significant distances offshore, giving a more terrestrial signal. Mangrove areas are less extensive, and marine dinoflagellates are rarer owing to reduced habitat. (Redrawn from Demchuk et al., 2004; based therein on Poumot, 1989).

Suter 2006 in Posamentier and Walker (Eds) 2006

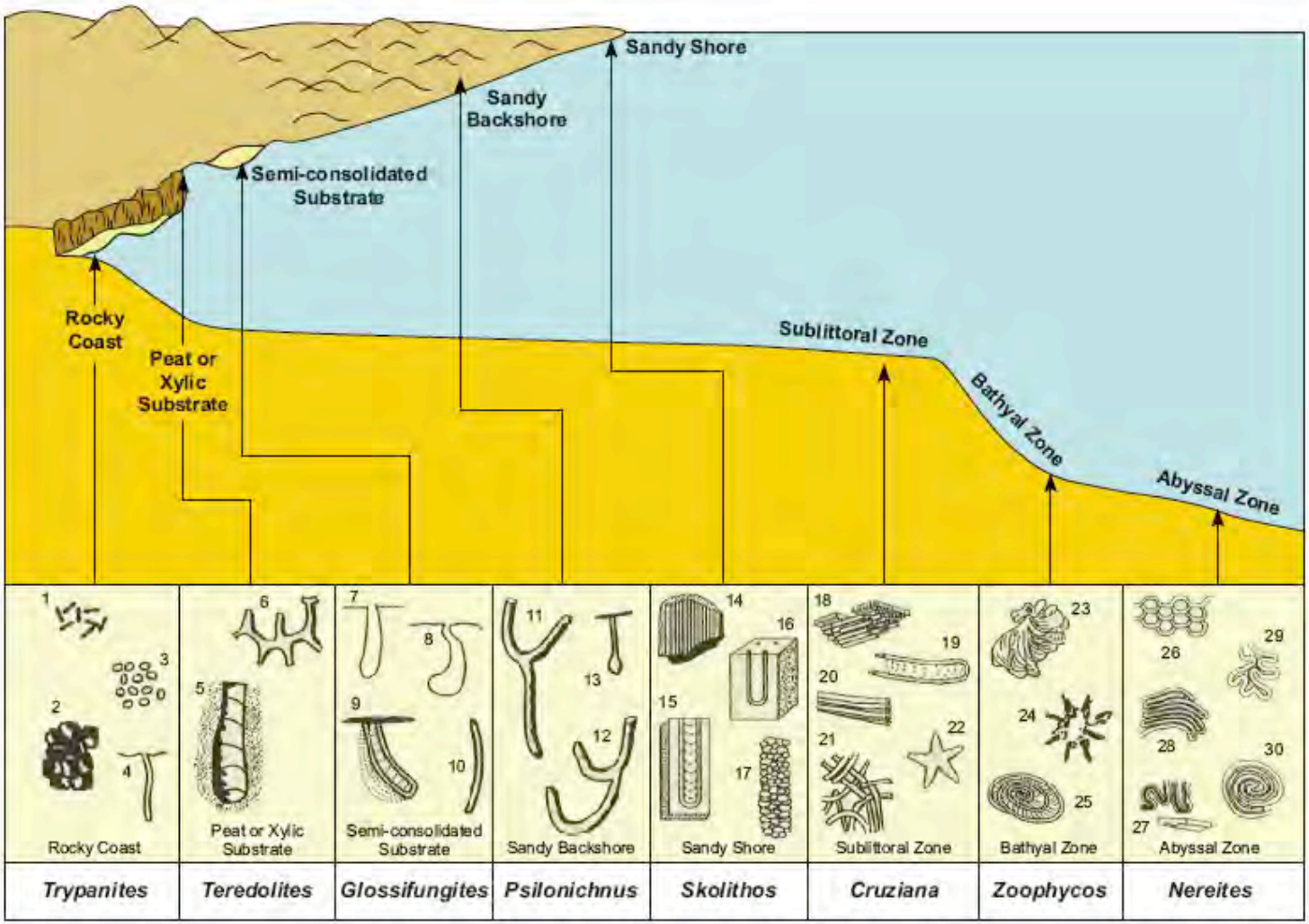

FIG. 44.—Seilacher's (1967) model of ichnofacies distribution, based on a number of environmental parameters, was originally developed for a normal "beach to offshore" trend. The main parameters of the ichnofacies concept include substrate consistency, hydrodynamic energy, food supply, food type, salinity, temperature, oxygen levels, sedimentation rate, etc., which tend to change progressively with increasing water depth. However, the relation to water depth is passive, inasmuch as ichnofacies distribution is rarely directly controlled only by bathymetry (Frey et al., 1990). Consequently, ichnofacies commonly occur outside the zone specified in the original paradigm. Continental-shelf ichnofacies are no exception to this observation. (Redrawn from Pemberton et al., 2001.)

Suter 2006 in Posamentier and Walker (Eds) 2006

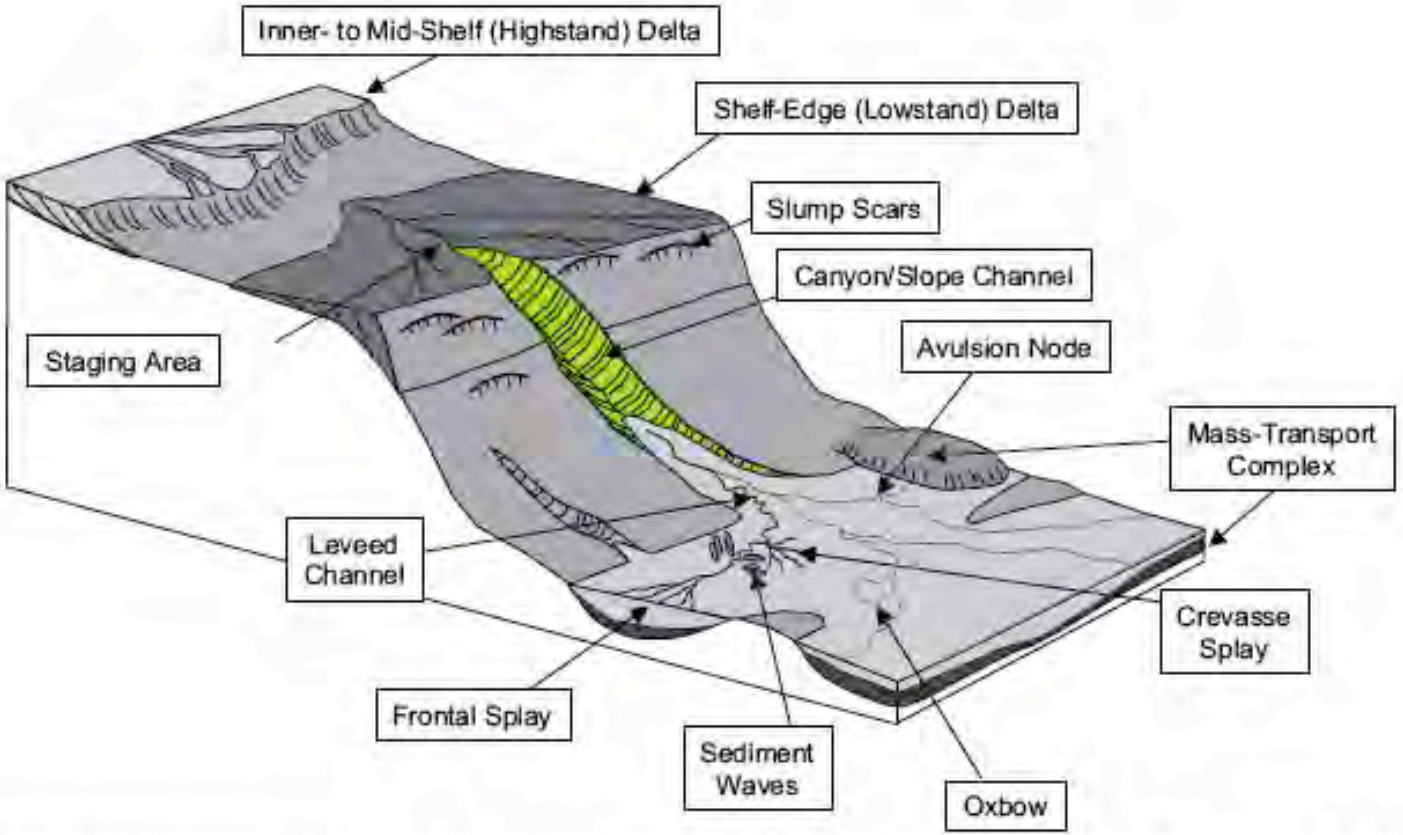

FIG. 1.—Schematic representation of shelf to deep-water physiography. The shelf staging area is connected to the deep-water environment through slope channels and/or canyons. Depositional elements in the deep water include leveed channels, crevasse splays, sediment waves, and frontal splays or lobes. (modified after Posamentier and Kolla, 2003a).

Posamentier and Walker 2006 in Posamentier and Walker (Eds) 2006

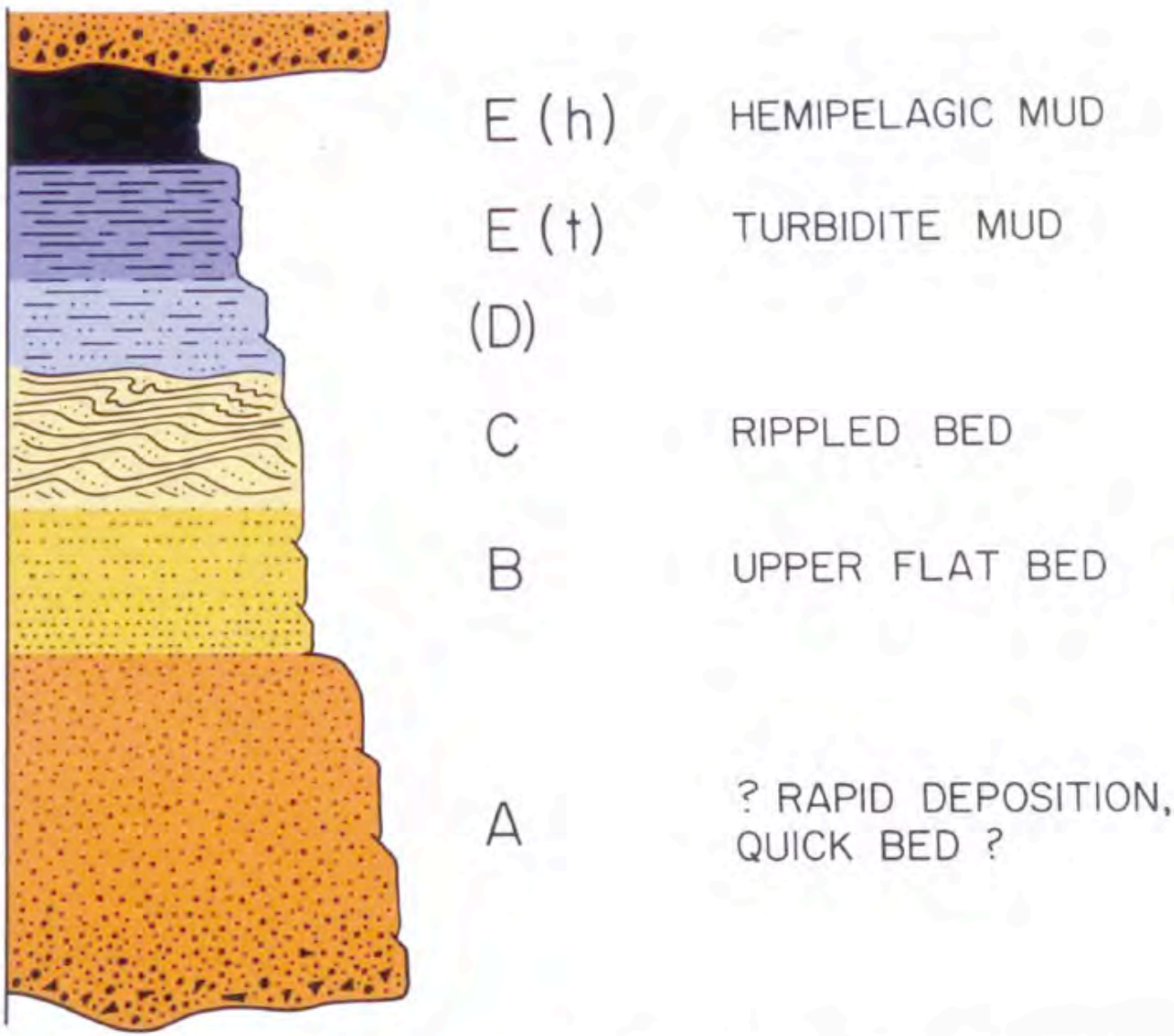

FIG. 2.—The Bouma (1962) sequence for classical turbidites. Division D is placed in brackets because it is difficult to identify in weathered or tectonized outcrops. Division E can be subdivided into two parts: turbidite mud E(t) and hemipelagic mud E(h). In most beds, the turbidite mud predominates.

Posamentier and Walker 2006 in Posamentier and Walker (Eds) 2006

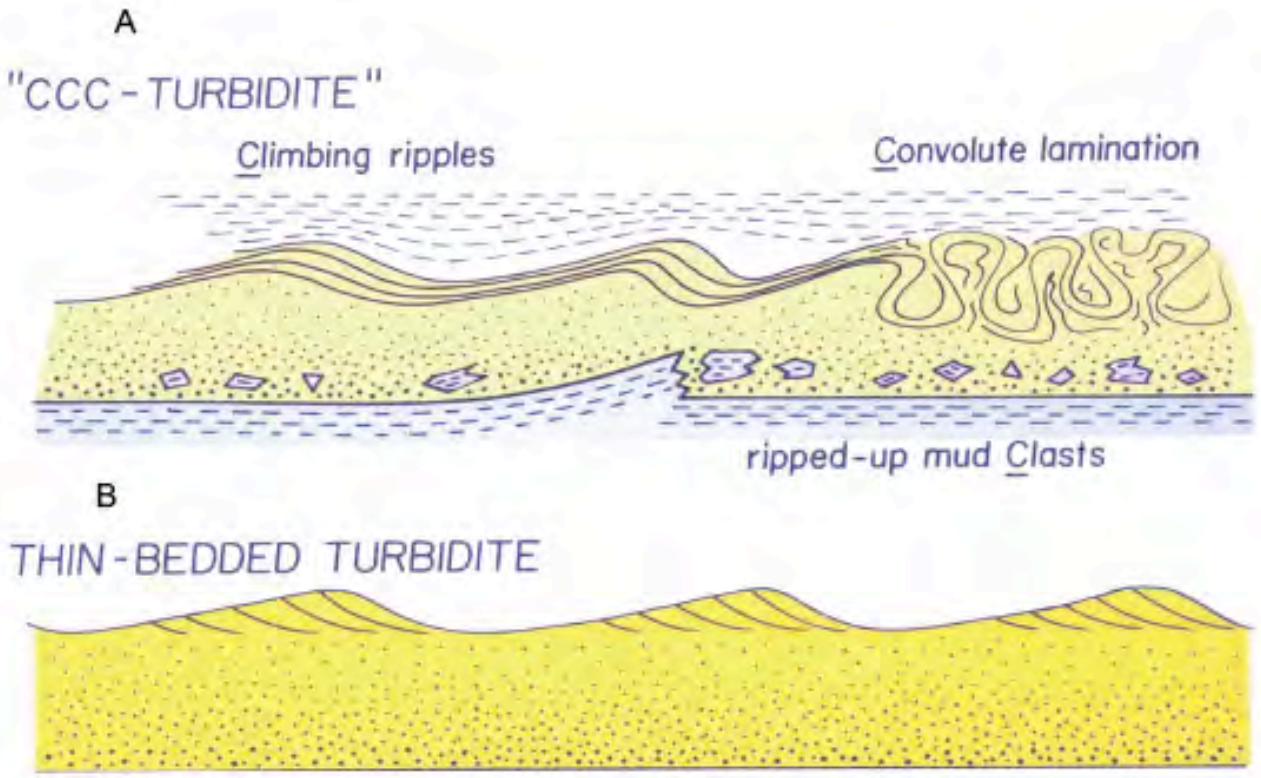

FIG. 8.—Diagram showing two types of thin-bedded turbidites. One is characterized by single rows of ripple cross lamination without climbing, and the other is characterized by climbing ripples, convolute lamination, and ripped-up mudstone clasts A). The "CCC turbidites" are interpreted as levee deposits (see text), and the others as distal basin plain deposits B) (From Walker, 1985).

Posamentier and Walker 2006 in Posamentier and Walker (Eds) 2006

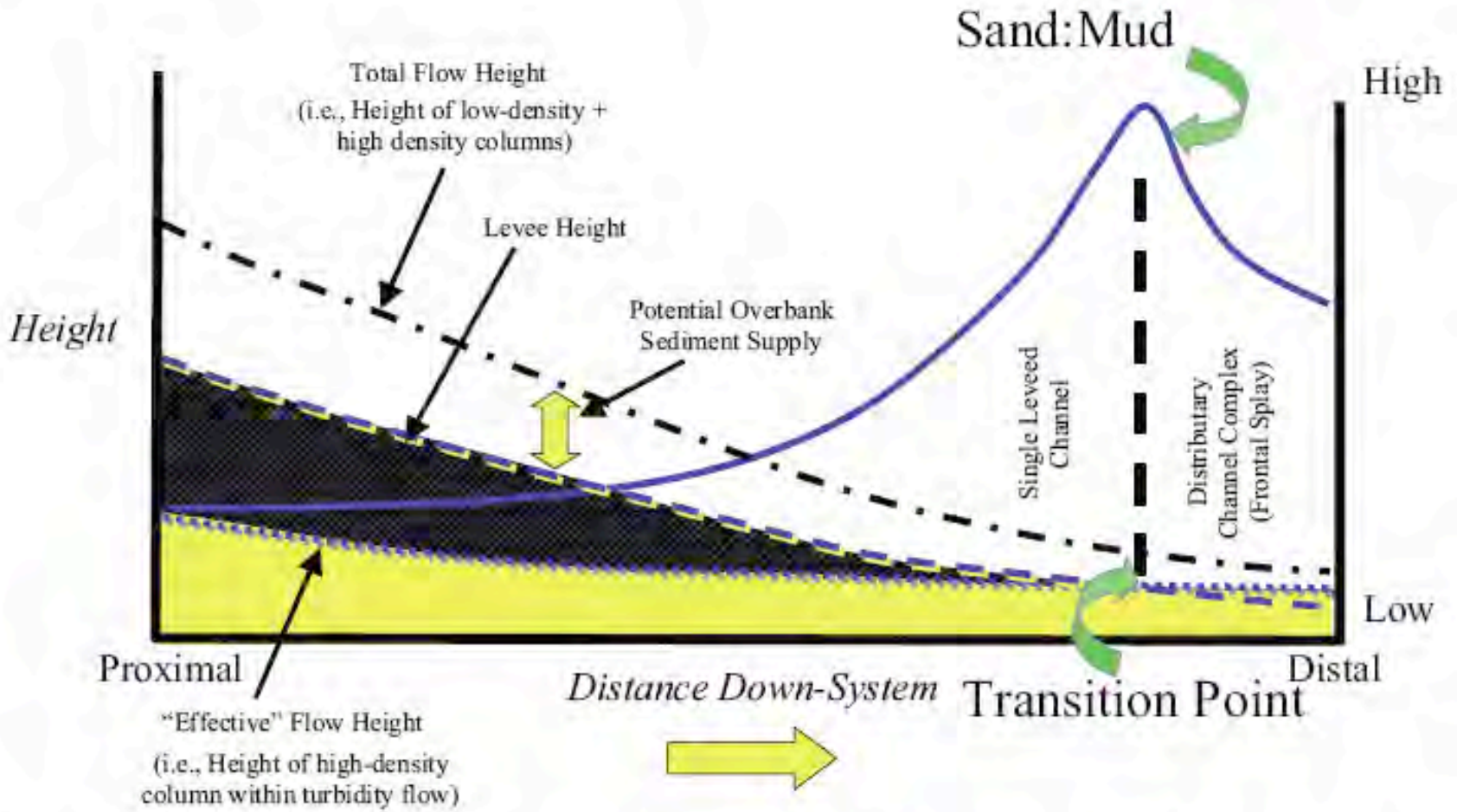

FIG. 26.—Schematic depiction of the interplay between sediment gravity flows, net sand, and levee height with distance down-system. Note that the high-density part of the gravity flow is located progressively more closely to the levee crest with distance seaward. A transition from leveed channel to frontal splay/lobe occurs when the high-density part of the flow (i.e., the sand-rich part of the flow) reaches bankfull stage. Note also that the highest sand-to-mud ratio occurs there as well (modified from Posamentier and Kolla, 2003a).

Posamentier and Walker 2006 in Posamentier and Walker (Eds) 2006

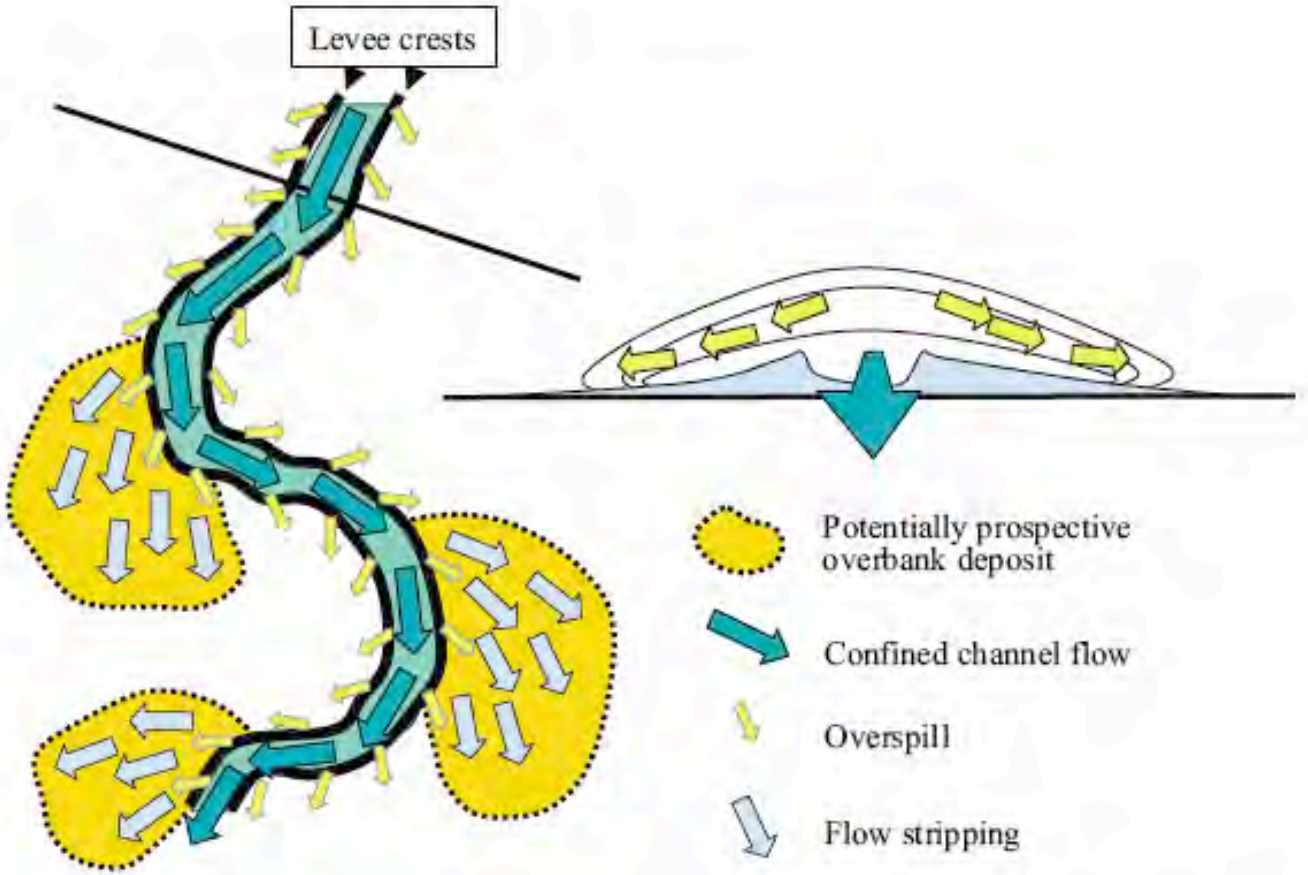

FIG. 27.—Schematic illustration of sediment gravity flow through a leveed channel (compare with Fig. 77). The cross-sectional view illustrates that the flow top lies well above the levee crest. The part of the flow between the flow top and levee crest is unconfined and systematically spills out of the channel. Enhanced spillover occurs at outer bends (by the process of flowstripping). These locations constitute areas of preferred sand deposition in the levee environment.

Posamentier and Walker 2006 in Posamentier and Walker (Eds) 2006

End of digression

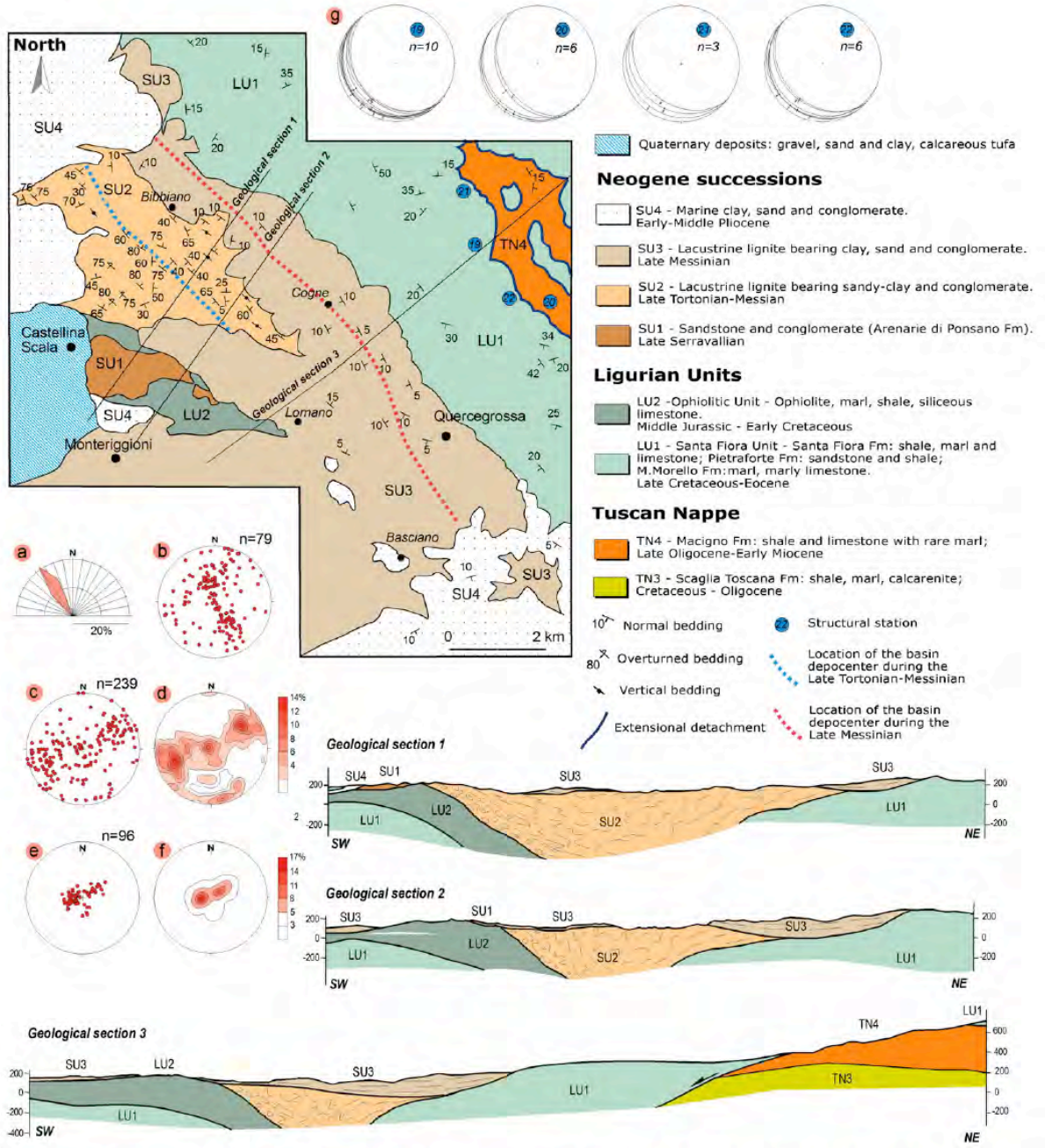

Fig. 13. Geological sketch-map of the Casino Basin and surroundings. The rose and stereographic diagrams (Schmidt diagram, lower hemisphere) show structural data discussed in the text: a) rose diagram illustrating the axial trend of the folds as reconstructed by the bedding attitude in the whole basin; b) the axial lines of mesoscopic folds measured in several outcrops; c) and d) poles of the bedding and contouring for the SU2 sediments; e) and f) poles of the bedding and contouring for the SU3 sediments; g) minor faults and striae collected in the indicated structural stations (see also the Fig. 2) consisting of minor structures related to the main west dipping extensional detachment separating the S.Fiora Unit from the Macigno Fm.

Brogi et al 2011

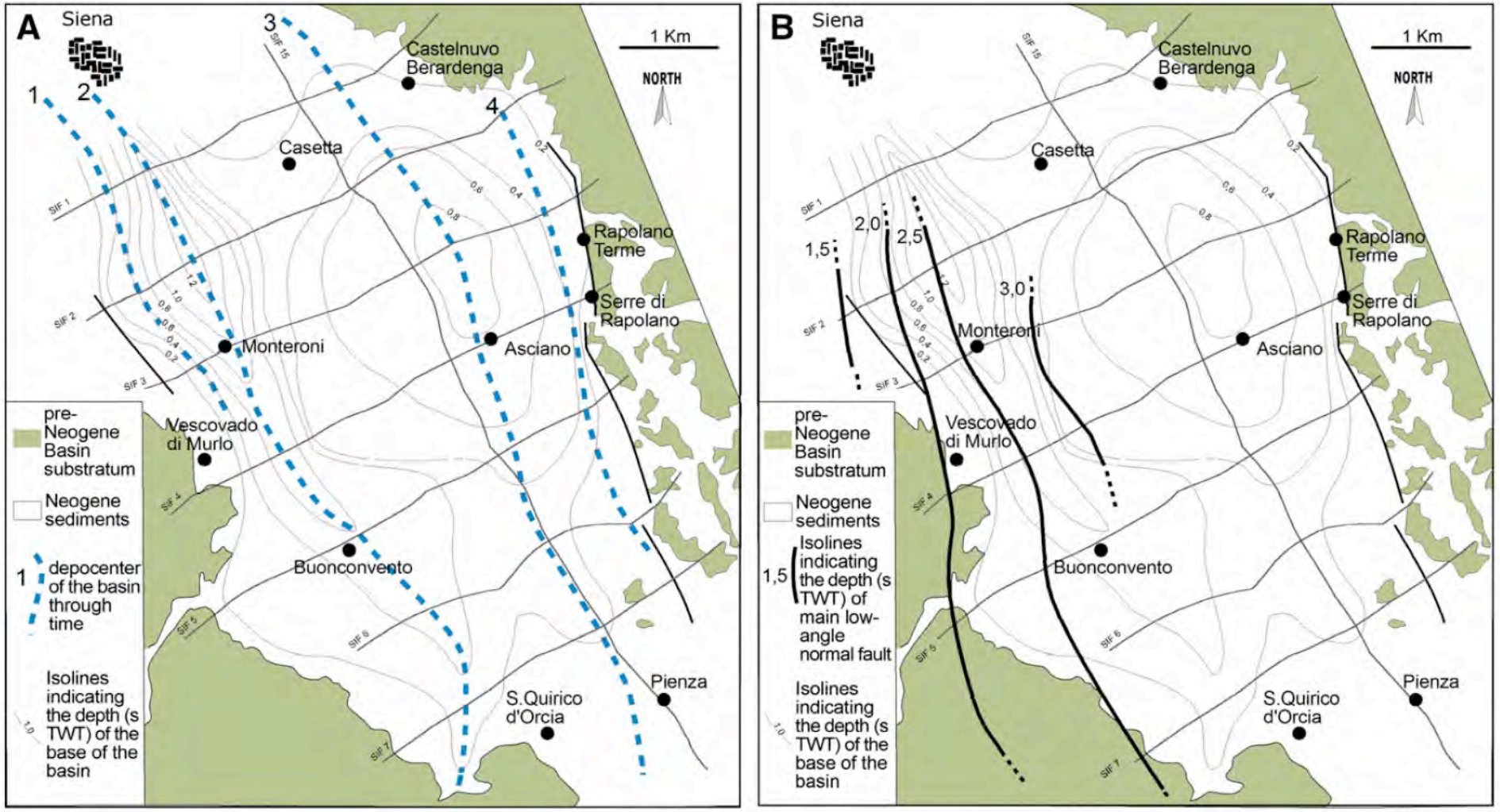

Fig. 17. Cartoon showing: A) isobaths (TWTs) of the basin substratum as obtained through the interpretation of the indicated seismic profiles and location of the basin depocenter through time: 1) Tortonian; 2) Messinian; 3) Early–Middle Pliocene; 4) Middle Pliocene; B) isobaths (TWTs) of the east-dipping extensional detachment as inferred through seismic profiles, and exposed in the eastern margin of the Middle Tuscan Range (see Fig. 6).

Brogi et al 2011

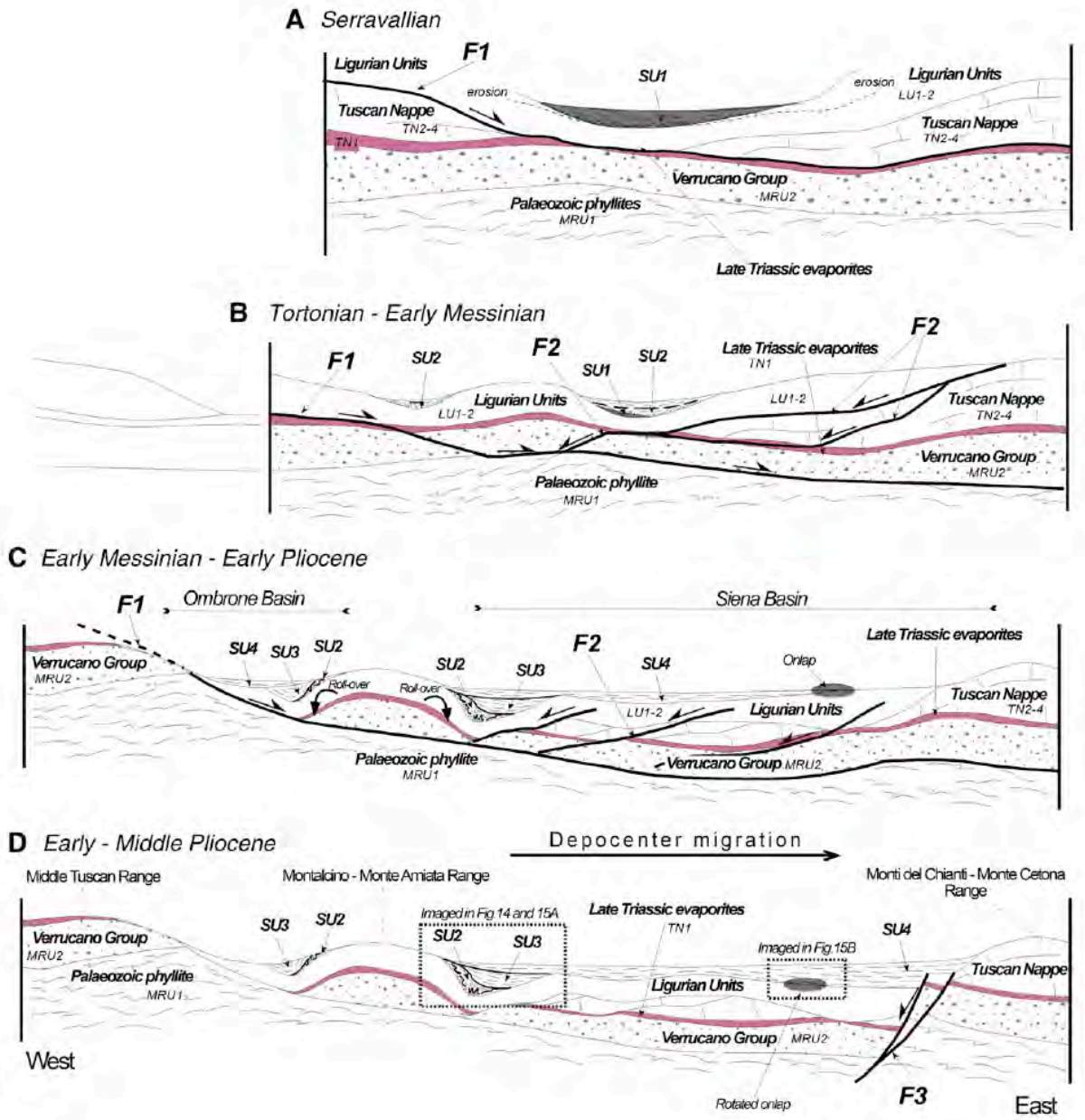

Fig. 18. Cartoon (not to scale) showing four stages illustrating the development of the Siena Basin. (A) The main east-dipping low-angle normal fault (F1) affected the stacked tectonic units after the collisional event; the main detachment level developed within the Late Triassic evaporite (TN1), producing the Tuscan Nappe lateral segmentation and a structural depression where the SU1 sediments deposited. B) Progressive faulting gave rise to the development of antithetic (west-dipping) low-angle normal faults (F2) contemporaneously with the deepening of the F1 fault accommodating at the top of the Palaeozoic phyllite (MRU1); the activity of the F2 faults produced the tectonic depression where the SU2 sediments deposited; C) the rotation of the hanging wall of the antithetic low-angle normal fault gave rise to the deformation of the SU2 deposits, and produced space accommodation for the SU3 sediments. SU4 sediments filled a broad structural depression and (D) were affected by west-dipping normal fault system (Rapolano Fault, F3) during Early–Pliocene times, mainly in the eastern side of the basin. Such a fault system dissected the previously developed low-angle normal faults.

Brogi et al 2011

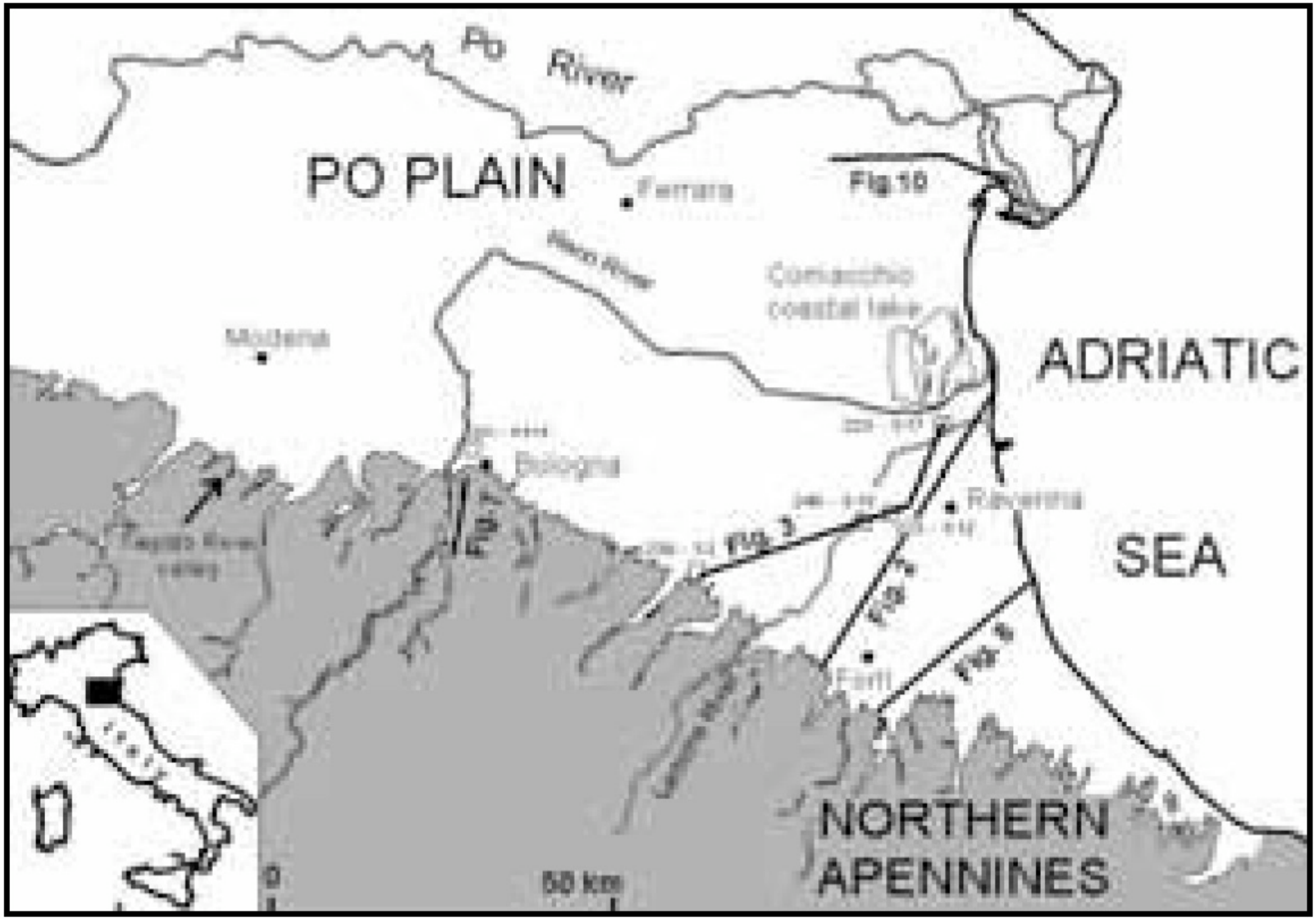

Figure 1 - Location map of the study area, showing section traces of Figures 2, 3, 7, 8 and 10.

Romagna and ENI AGI

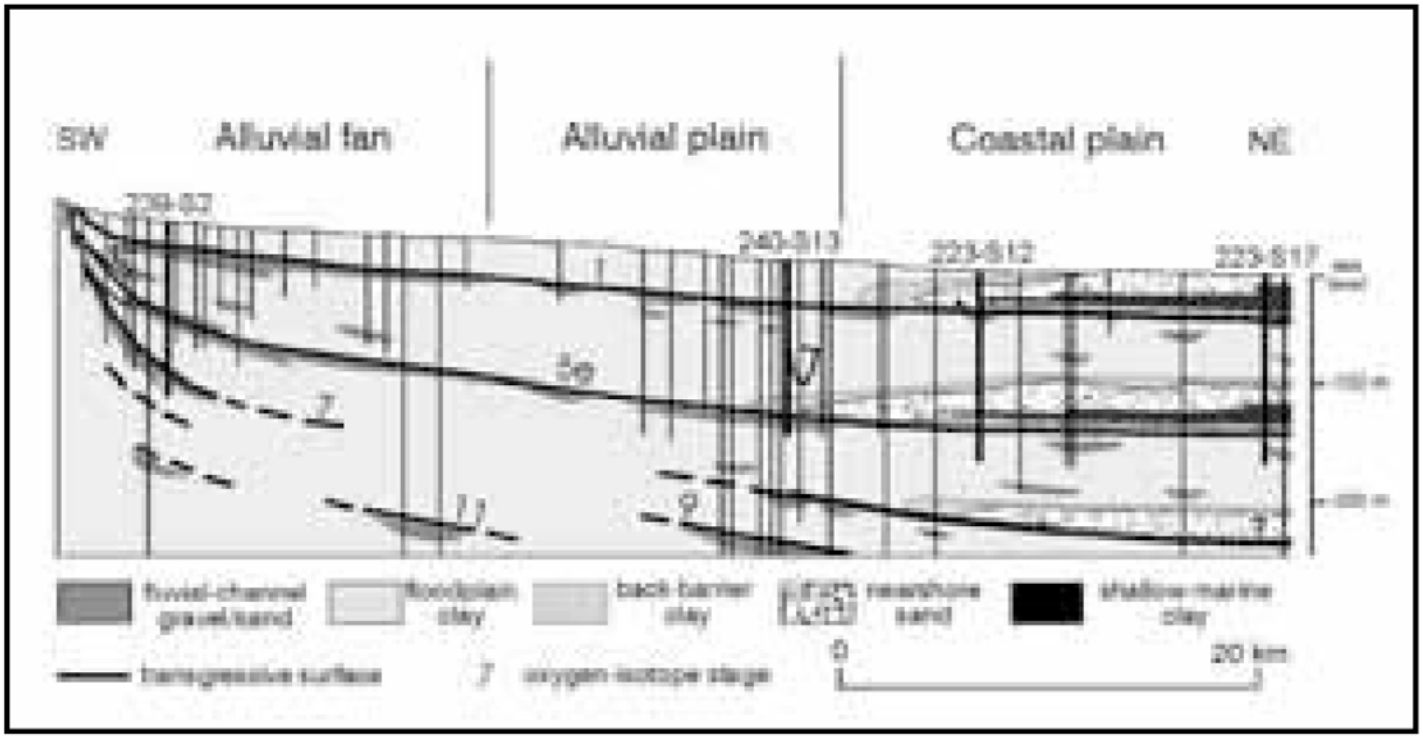

2004). The close rela
between stratigrap
architecture and pol
distribution sugge
that sedimentat
in the Po Basin v
predominantly dri
by combined eust
sea-level changes a
climatic variatic
Correlation with
marine oxygen-isot
record documents st
relationships betweer
R sequences and glac

Figure 3 - Stratigraphic overview of the Upper Emilia-Romagna Synthem (see section trace in Fig. 1), showing the subdivision into transgressive-regressive sequences (subsynthems) and the geometric linkage between updip fluvial strata and downdip deltaic and coastal-marine deposits. From Amorosi & Colalongo (in press).

Amorosi
et al 2005

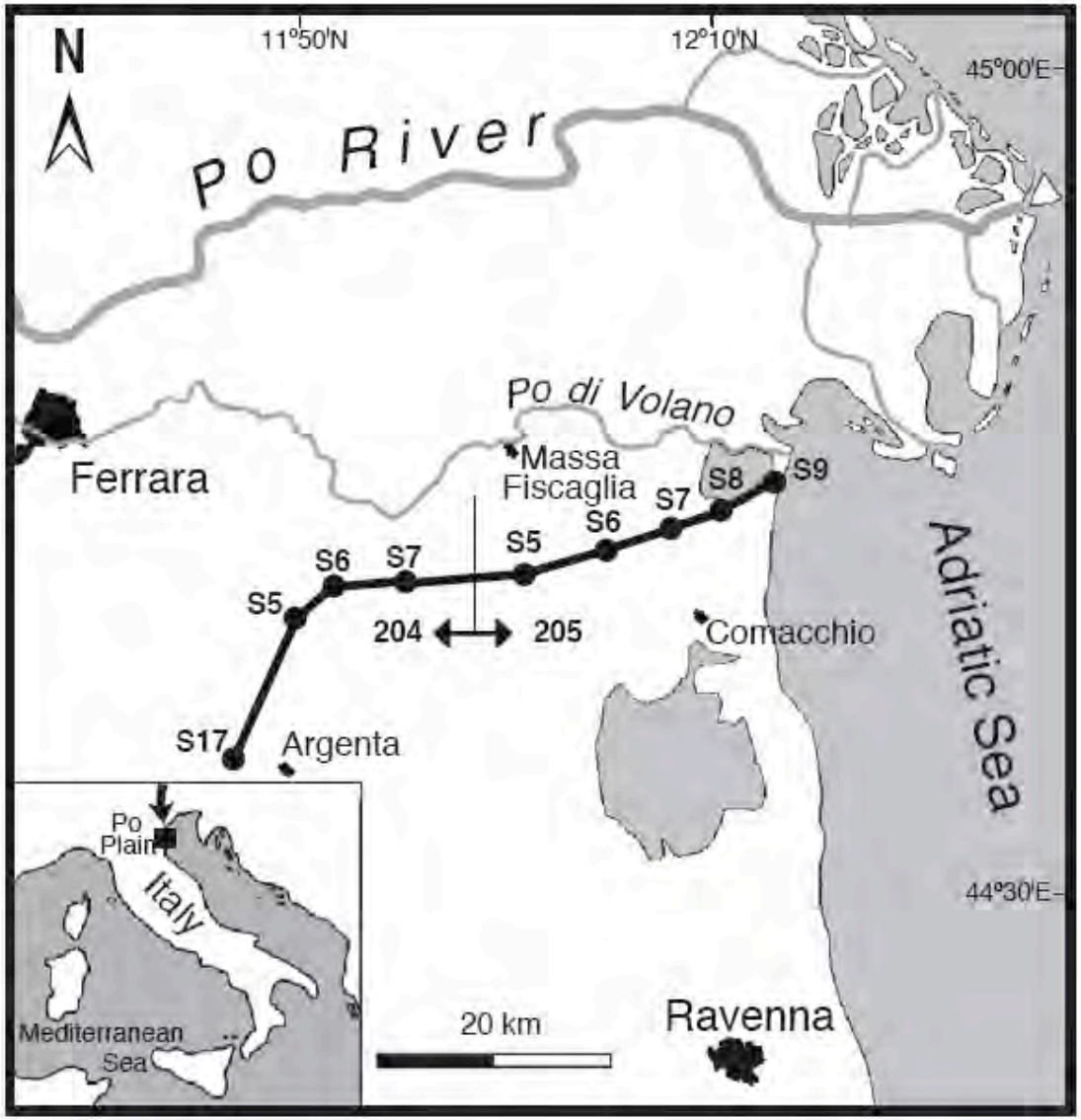

Fig. 1. Sampling sites of sediment cores in the study area and section traces of Figs. 3 and 4. The numbers (204 to the west and 205 to the east) refer to the sheets of the Geological Map of Italy to scale 1:50,000.

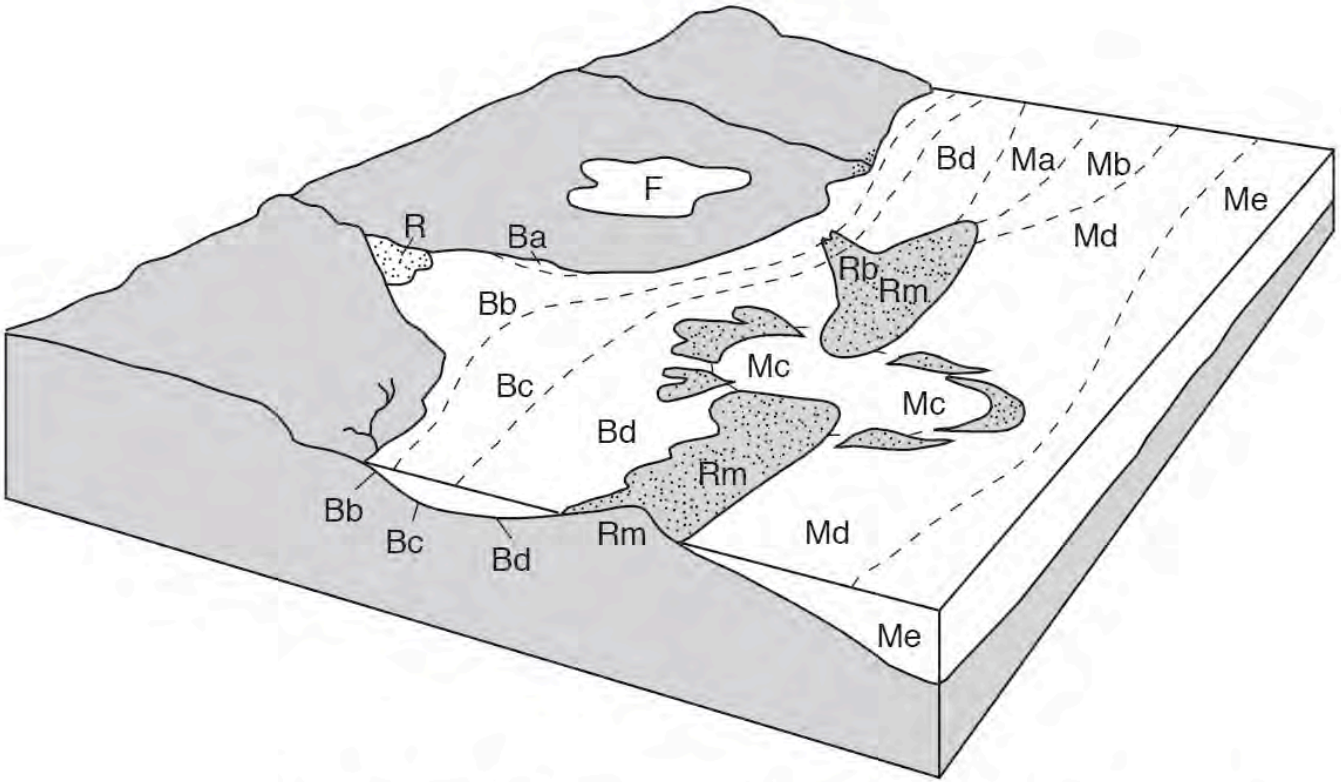

Fig. 2. Environmental zonation of the 12 microfossil associations identified in cores (see Fig. 3). See text for description.

Amorosi
et al 2005

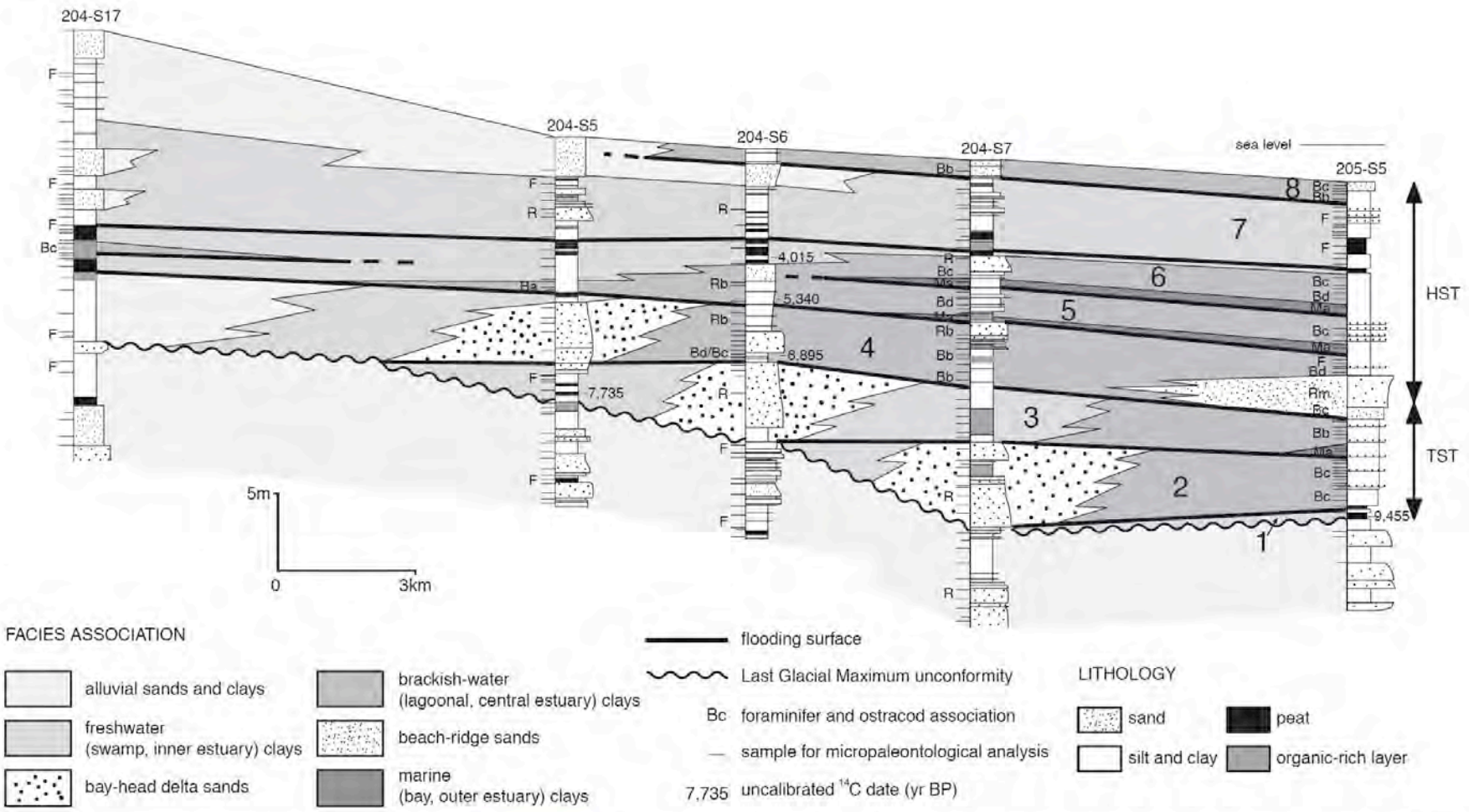

Fig. 3. Detailed stratigraphic cross-section (location is shown in Fig. 1), showing facies architecture, attribution of the study samples to the twelve microfossil associations, and subdivision in eight parasequences. TST: transgressive systems tract, HST: highstand systems tract.

Amorosi
et al 2005

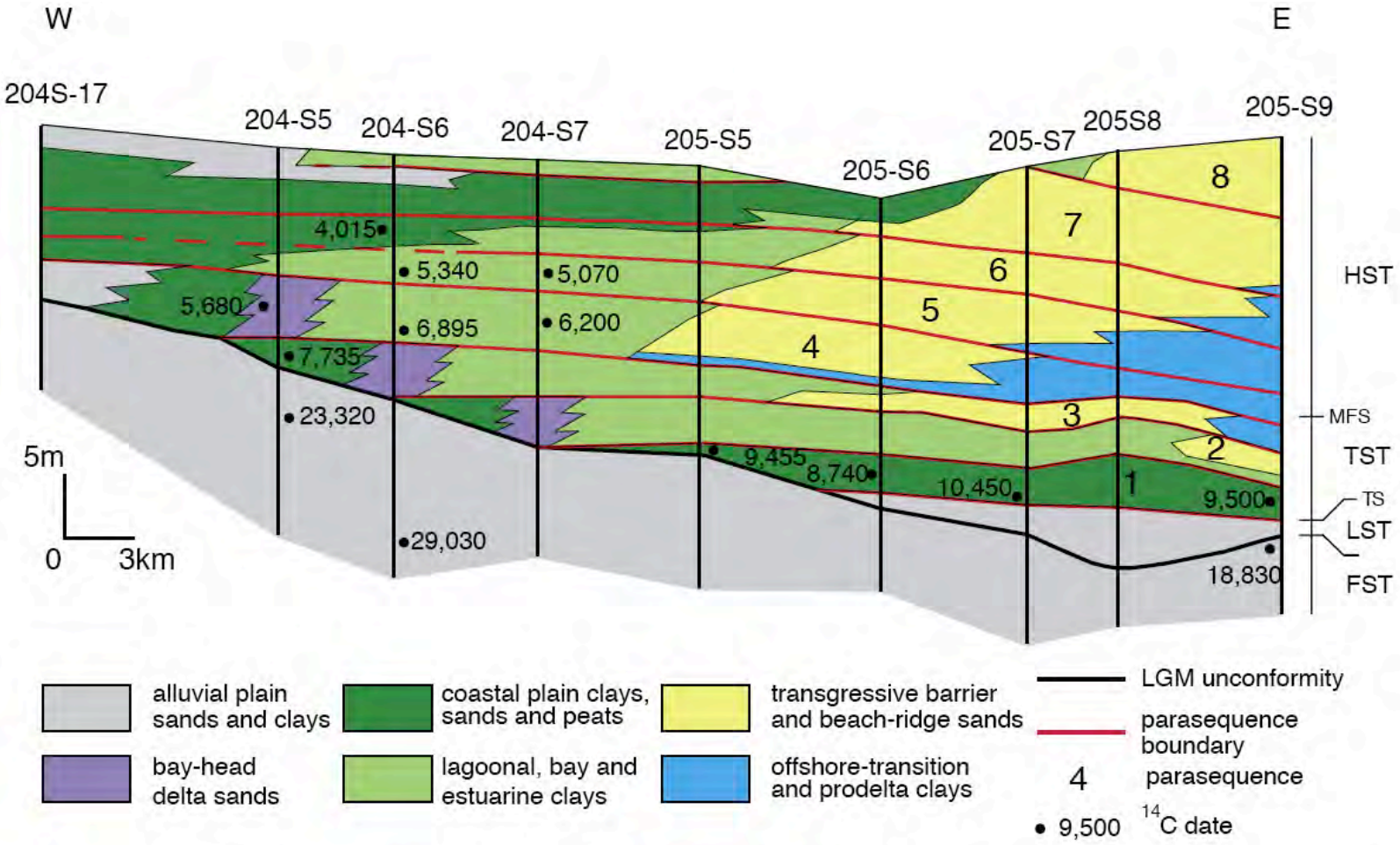

Fig. 4. Simplified stratigraphic cross-section (location is shown in Fig. 1), showing parasequence architecture of Holocene deposits beneath the modern Po coastal plain. FST: falling-stage systems tract, LST: lowstand systems tract, TST: transgressive systems tract, HST: highstand systems tract, TS: transgressive surface, MFS: maximum flooding surface The two dates reported for core 204-S7 are projected from Bondesan et al. (1999).

Amorosi
et al 2005

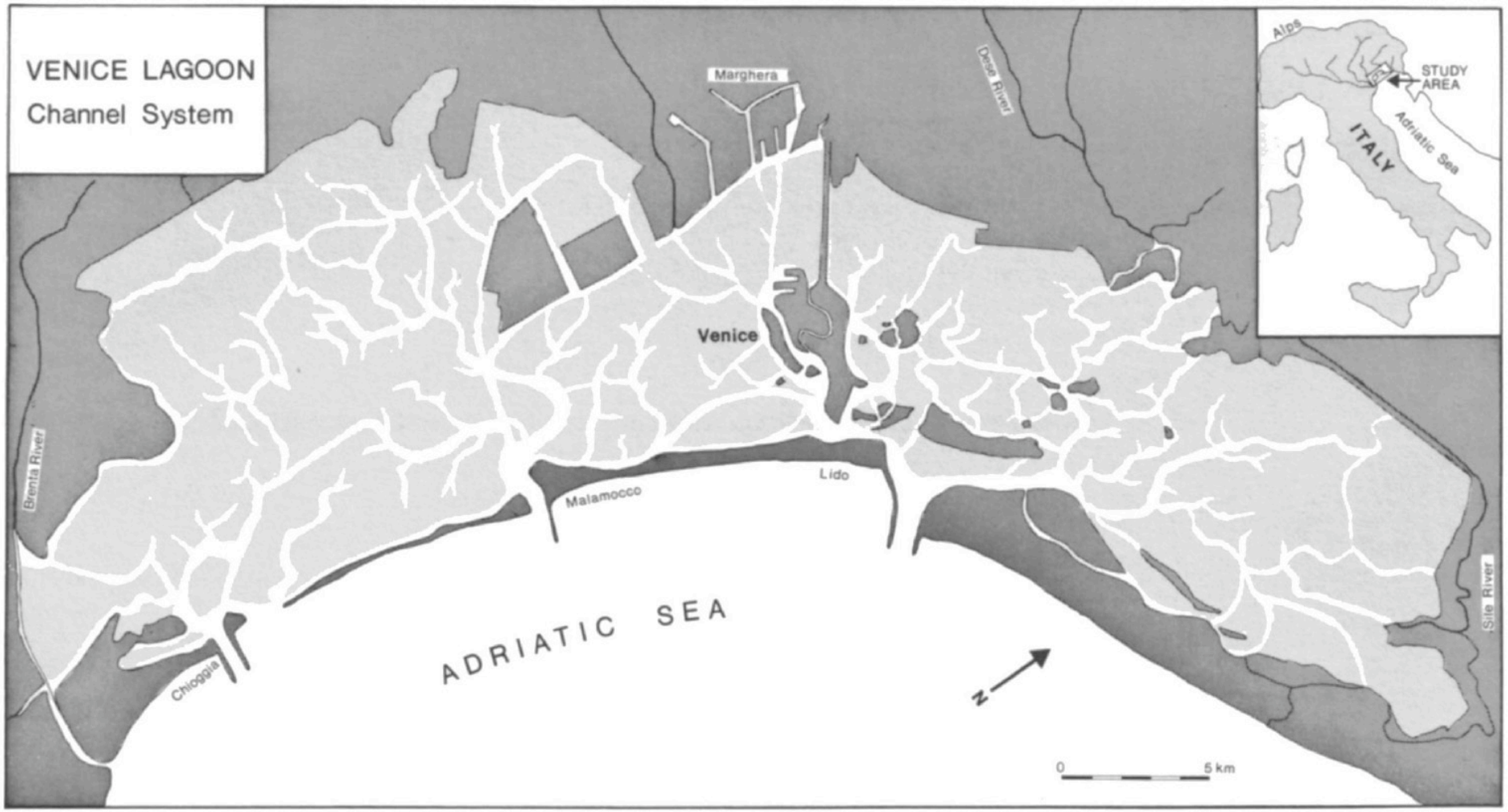

Figure 1. The natural and dredged channel system (white) is complex among the marshes and mudflats (both light grey) within the Lagoon of Venice. The three, jetty-stabilized tidal inlets which cut through the barrier beaches to the Adriatic Sea are named as are the cities of Maghera and Venice. Rivers are shown flowing into and around the lagoon, and on the inset map of Italy and the study area location.

MeClennon et al 1996

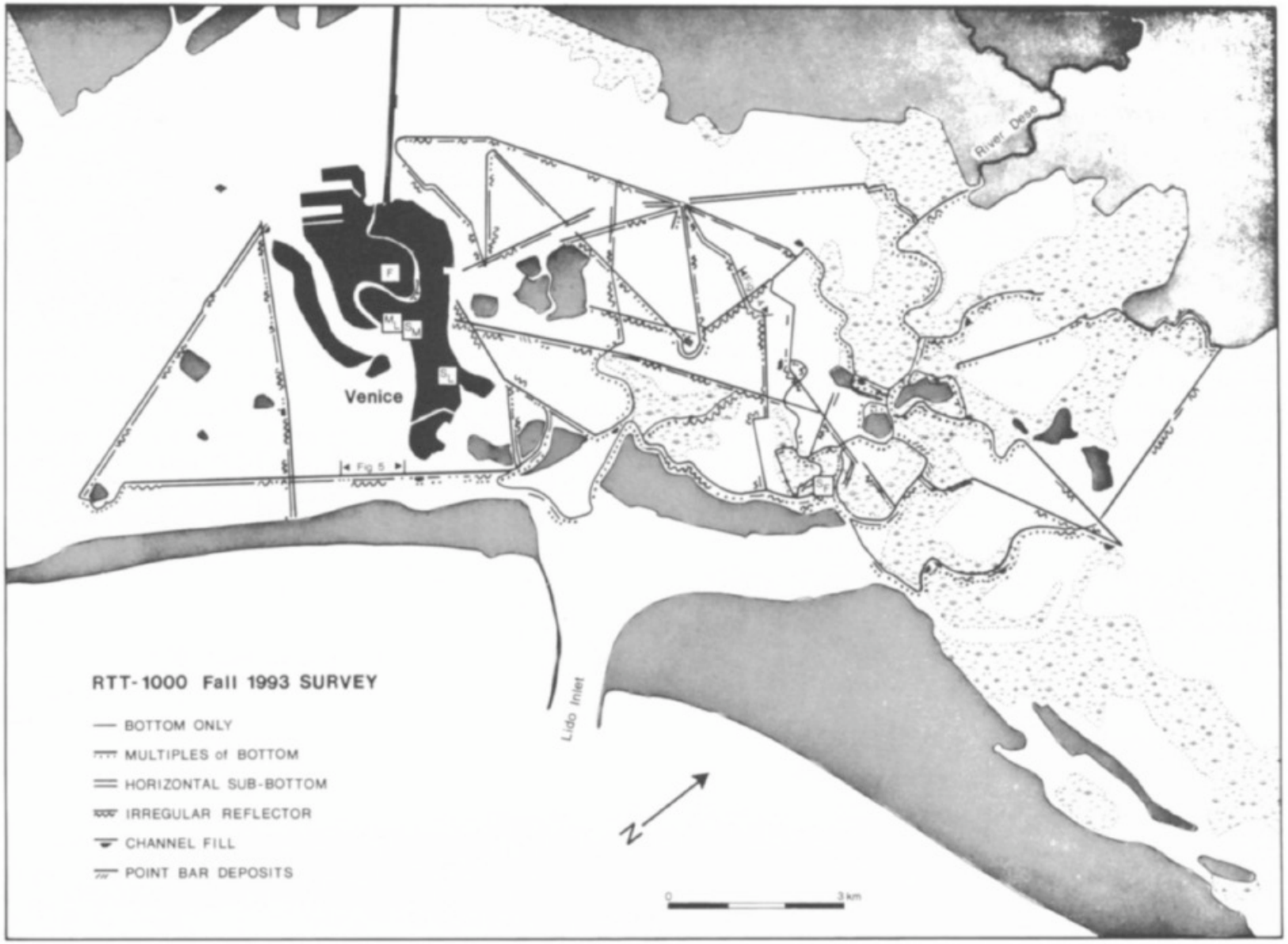

Figure 2. The six different observed types of acoustical reflection patterns are plotted along the RTT-1000 (7 kHz) survey tracklines, which are located both over sub-tidal mudflats and in marsh and open lagoonal channels. Archaeological site locations are symbolized: Frari (F), Marciana Library (ML), I. San Francesco del Deserto (SF), San Lorenzo (SL), and San Marco (SM) as are the location of records illustrated in Figures 4 and 5.

MeClennon et al 1996

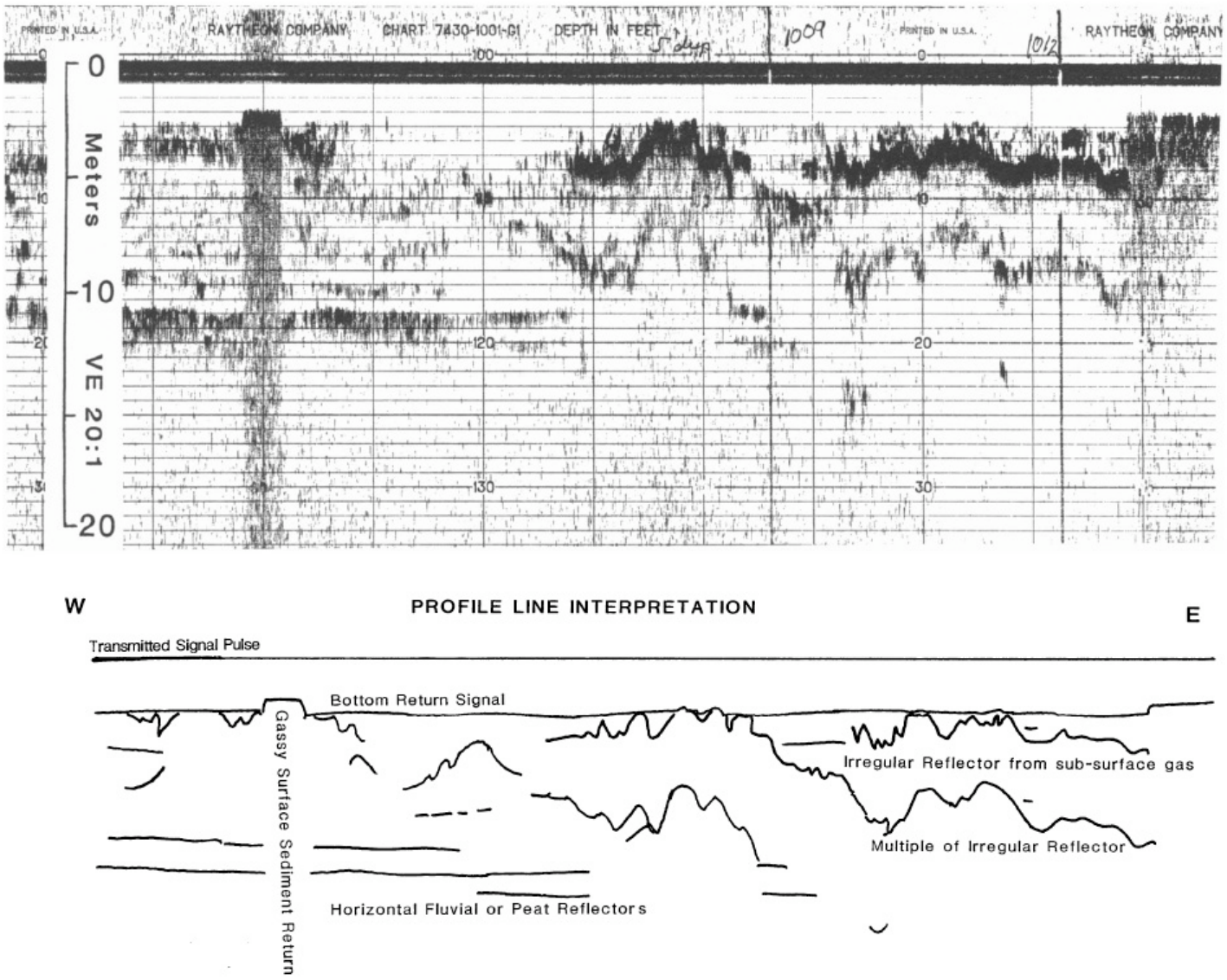

Figure 4. RTT-1000 record (above) collected over a section of the sub-tidal mudflats about 5 km northeast of Venice (see Fig. 2). The line interpretation (below) indicates the horizontal bedding, bold irregular reflection surface with a multiple and two short segments of dark bottom reflection which obscure sub-bottom stratigraphy (mid left side and extreme right). Note the depth below transducer (assuming a sound velocity of 1,500 m/sec.) scale on the left margin and the 20:1 vertical exaggeration as well as the W–E orientation.

MeClennon et al 1996

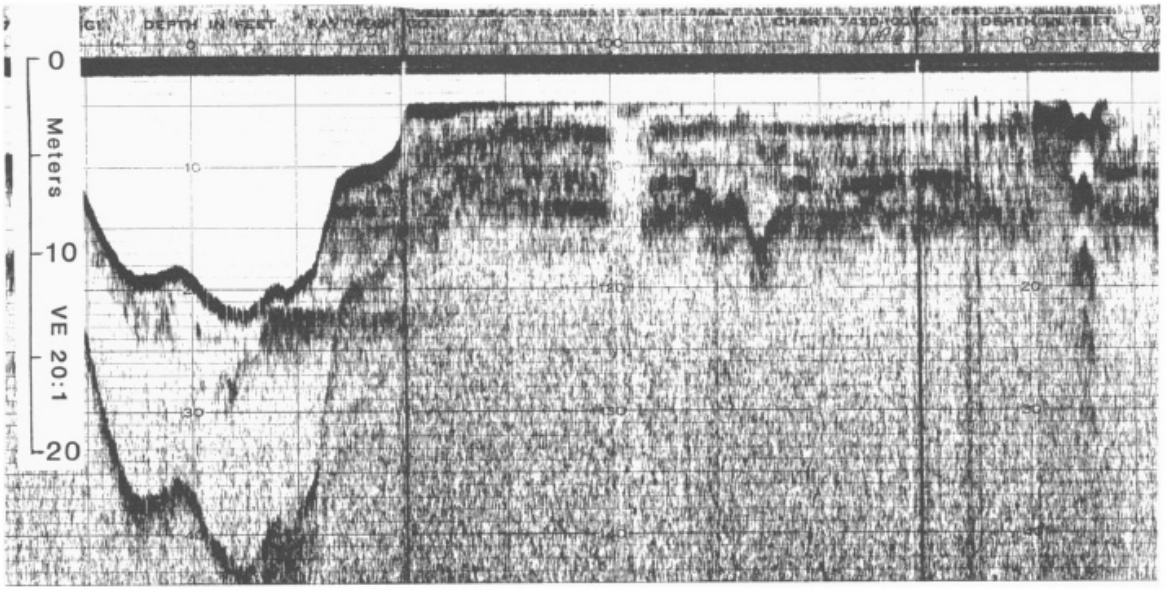

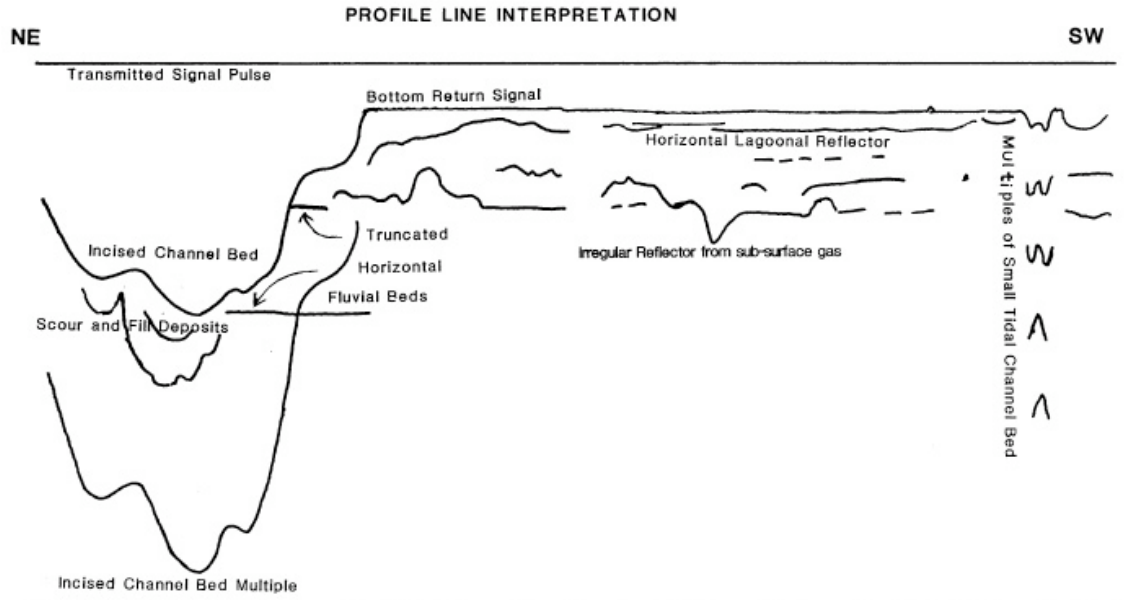

Figure 5. RTT-1000 record (above) collected over Can. di S. Nicolo and the adjacent mudflat between Venice and the Lido (NE-SW, see location in Fig. 2). The line interpretation (below) indicates the strong multiple of the main channel bottom as well as the truncated sub-channel horizontal reflectors and possible channel fill deposits (left side). Near the extreme right is a small channel marked by a bathymetric depression and several bottom multiples. Between the large and shallow channels are typical horizontal beds and irregular reflectors discussed in the text.

MeClennon et al 1996

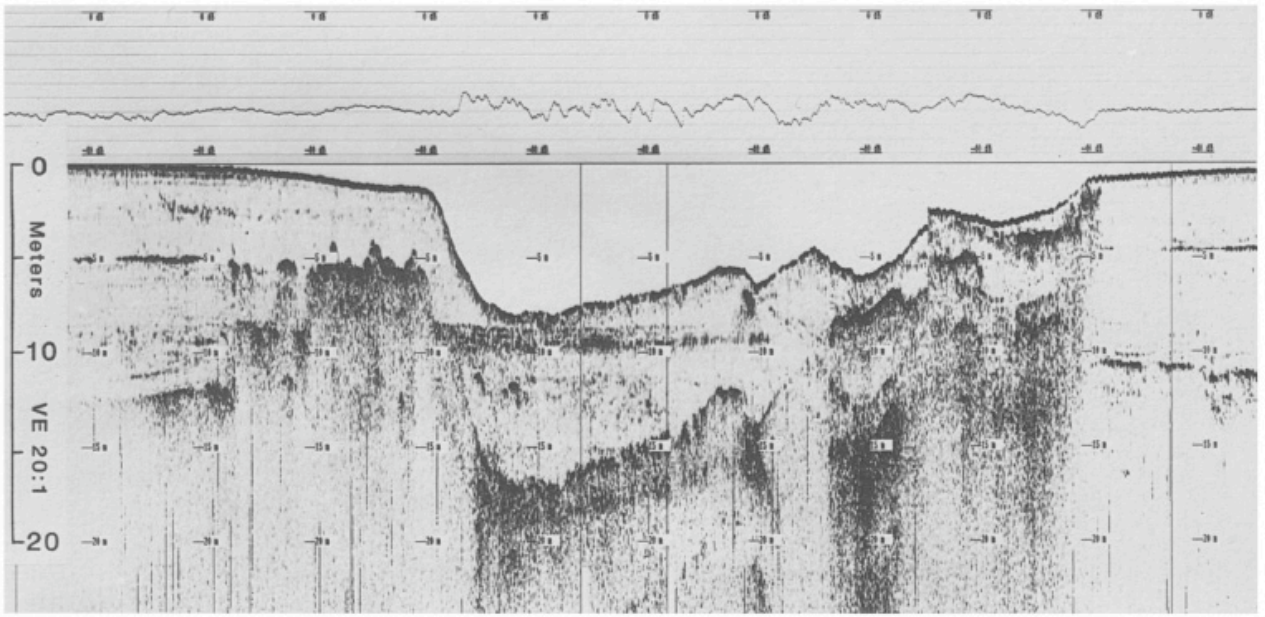

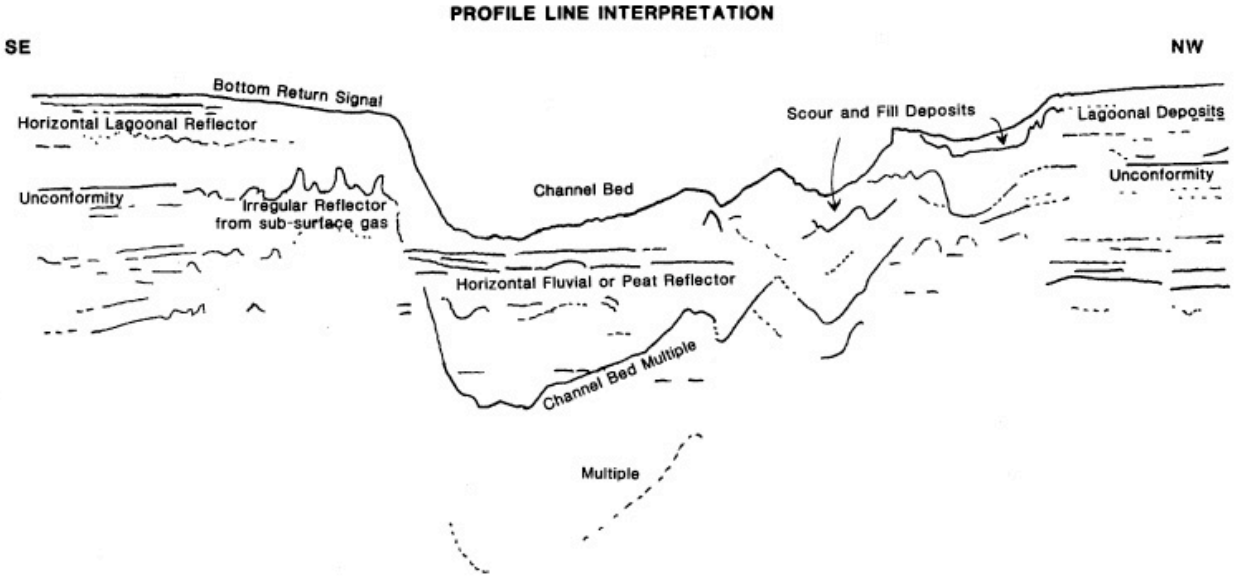

Figure 7. X-Star record with line interpretation of Can. d. Navi, just east of Venice (see Fig. 3 for location of SE-NW segment), showing clear sub-bottom reflectors, both horizontal and irregular under the main channel and adjacent mudflats. There is also channel fill indicated (right), which is distinct from the multiples of the channel bed. Note the more variable intensity of the bottom reflectivity graphed along the top of the profile over the channel as compared to the adjacent mudflats. The strong reflector at 5 m depth (left and right sides) is likely the unconformity between lagoonal and fluvial deposits.

MeClennon et al 1996

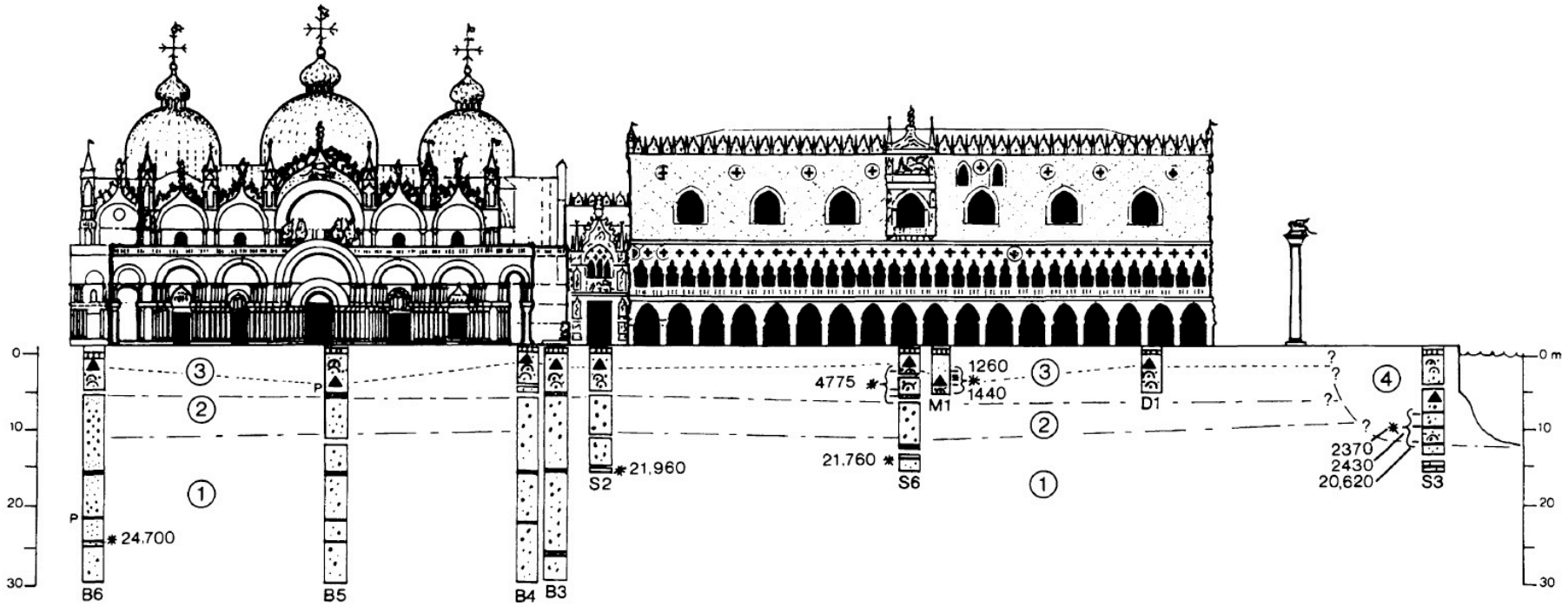

Figure 8. San Marco and Ducal Palace in Venice (see Fig. 3 for location) showing their relationship to the stratigraphic cross section seen in the underlying cores extending to near the water's edge (right, south). AMS ^{14}C dates are presented as years BP by the "*" along each core. Unit 1 is late-glacial, silty, fluvial-lacustrine deposit with ^{14}C dated (~21,000 to 25,000 BP) peat beds and sandy lenses within. Unit 2 is a sand rich sequence of similar fluvial outwash deposits. Unit 3 is the upper 5 meters; lagoonal deposits containing marine shells with the base of anthropic material indicated by triangles connected by a dotted line. A charcoal sample from near the base of Unit 3 (4.6 m depth below sealevel in cores S-6) has an AMS ^{14}C date of 4,775 BP. Unit 4 is the ~2,400 BP lagoonal channel fill sediment resting on and against the eroded section of late-glacial units (1 & 2) and subsequently capped with much younger artificial fill (AMMERMAN *et al.*, 1995).

MeClennon et al 1996

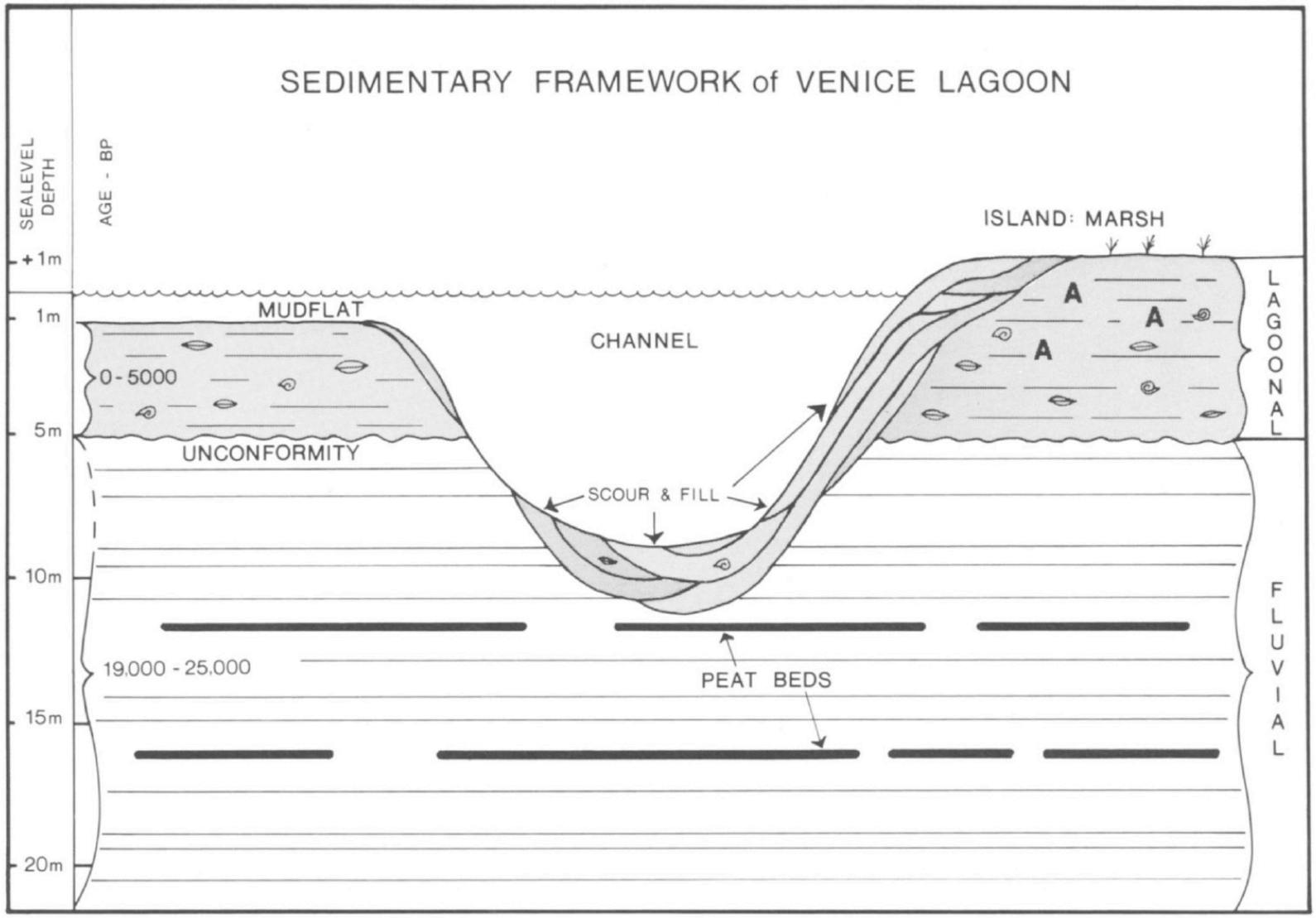

Figure 11. This cartoon of the sedimentary framework, constructed from seismic-reflection profiles and core data, emphasizes the relative ages, thicknesses and stratigraphic relationships typical of the Venetian Lagoon. Note that the tidal channel is incised into the underlying fluvial deposits and partially refilled with more recent deposits. Marine shells and anthropic (A) material are indicated within the mudflat and channel fill deposits.

MeClennon et al 1996

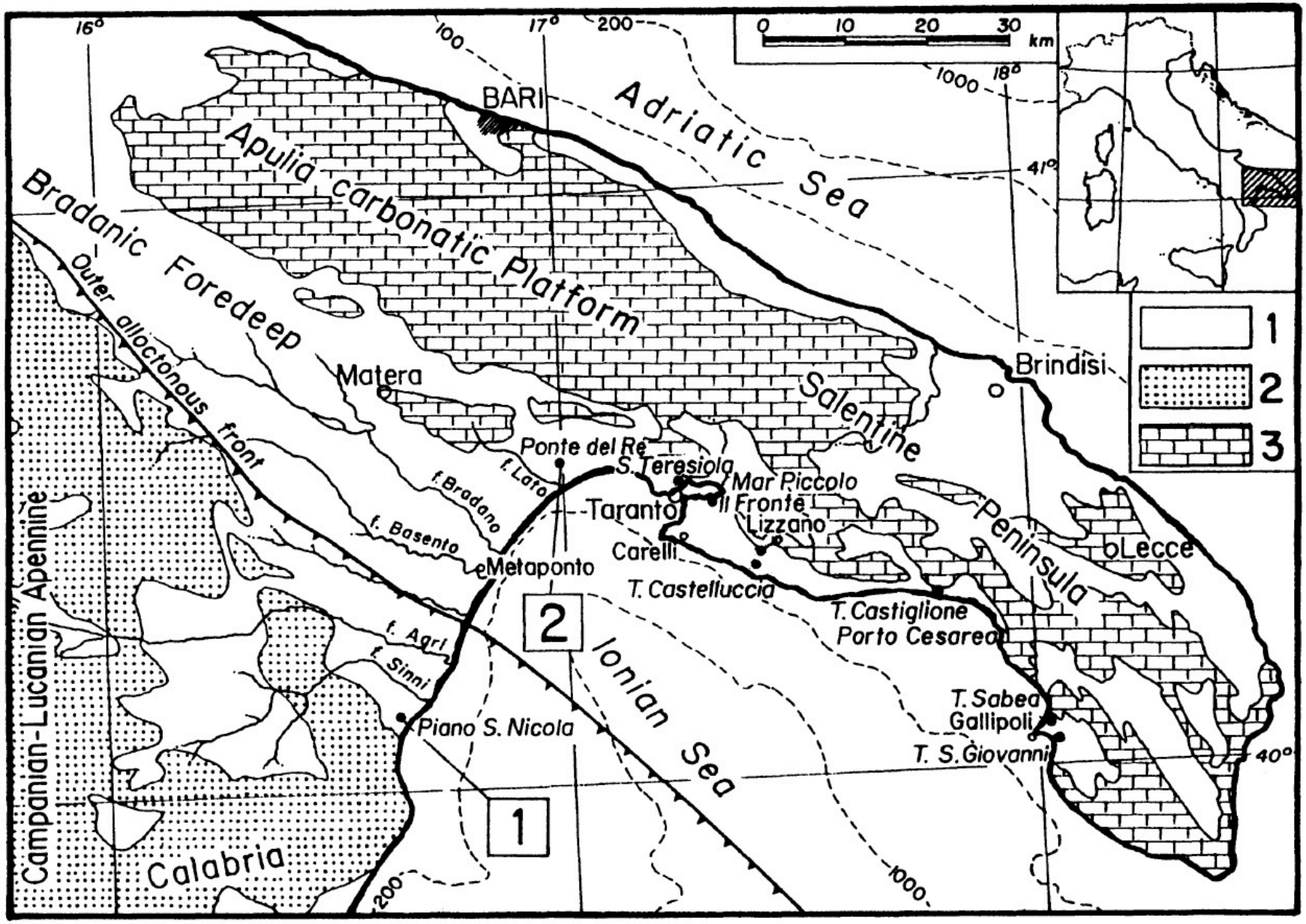

Figure 1. Structural scheme of the Gulf of Taranto. (1) Neogene sediments; (2) allochthonous Tertiary flysch deposits; (3) Cretaceous platform carbonates. Study sites 1 and 2 are identified in boxes. (Geology after OGNIBEN, 1973).

Hearty & Dai Pra 1992

Table 1. *Mean a/I ratios comprising aminogroups from the Mediterranean, Bermuda and the southeast U.S. coastal plain. Mean a/I is for* Glycymeris *(Gly) or* Glycymeris *equivalents [GE in square brackets] from marine deposits unless otherwise indicated (see below). Definitions, analytical and methodological information are provided in* Hearty et al. *(1986a).*

Region (T°C) Reference	Aminogroup	Mean A/I (Gly or GE)	(N=)	Radiometric*, Apparent+ or Estimated ~Age
ITALY—Toscana—North Lazio	C	0.31 ± 0.02	(7)	90 ± 15 KA~
(15.5–16.5) Hearty and Dai Pra, 1986a,b	E	0.39 ± 0.02	(39)	118–135 KA+
	F	0.50 ± 0.01	(18)	180–250 KA+
	G	0.58 ± 0.03	(35)	>300 KA+
	K	1.00–1.20	(15)	>1 MY?+
ITALY—So. Lazio, Latina, (~16) Hearty and	A	0.12 ± 0.02	(4)	4,630 YR BP*
Dai Pra, 1986b; Antonioli *et al.*, 1988	C	0.29 ± 0.02	(10)	90 ± 15 KA~
	E	0.39 ± 0.03	(25)	118–135 KA+
	G	0.60 ± 0.02	(19)	>300 KA~
	H	0.73 ± 0.05	(3)	>400 KA?~
ITALY—Puglia	C	0.28 ± 0.02	(5)	90 ± 15 KA~
(*ca.* 17), Hearty and Dai Pra, 1985;	E	0.41 ± 0.03	(42)	123 ± 4 KA*
Hearty *et al.*, 1986; Hearty, 1986	F	0.48 ± 0.02	(7)	290 ± 50 KA*
	G	[0.64]a	(3)	>300 KA*
ITALY—Puglia	At	0.12 ± 0.01	(17)h	5 ± 1 KA*
(16.9–17.2) (This study; includes 1985 data)	Cm	0.29 ± 0.02	(11)	*circa* 85 KA~
	Ct	0.28 ± 0.01	(18)h	<85 KA+
	Em	0.39 ± 0.03	(56)	*circa* 125 KA*
	Et	0.34 ± 0.01	(2)h	<125 KA+
ITALY—Calabria	C	0.29 ± 0.04	(3)	80–85 KA~
(17–17.5) Hearty *et al.*, 1986b; Dumas *et al.*, 1988	D?	0.37 ± 0.03	(3)	*circa* 105 KA+
	Et	0.39 ± 0.01	(3)h	≤125 ka+
	E	0.42 ± 0.03	(33)	118–135 KA*
	F	0.51 ± 0.07	(4)c	≥180 KA+

Hearty & Dai Pra 1992

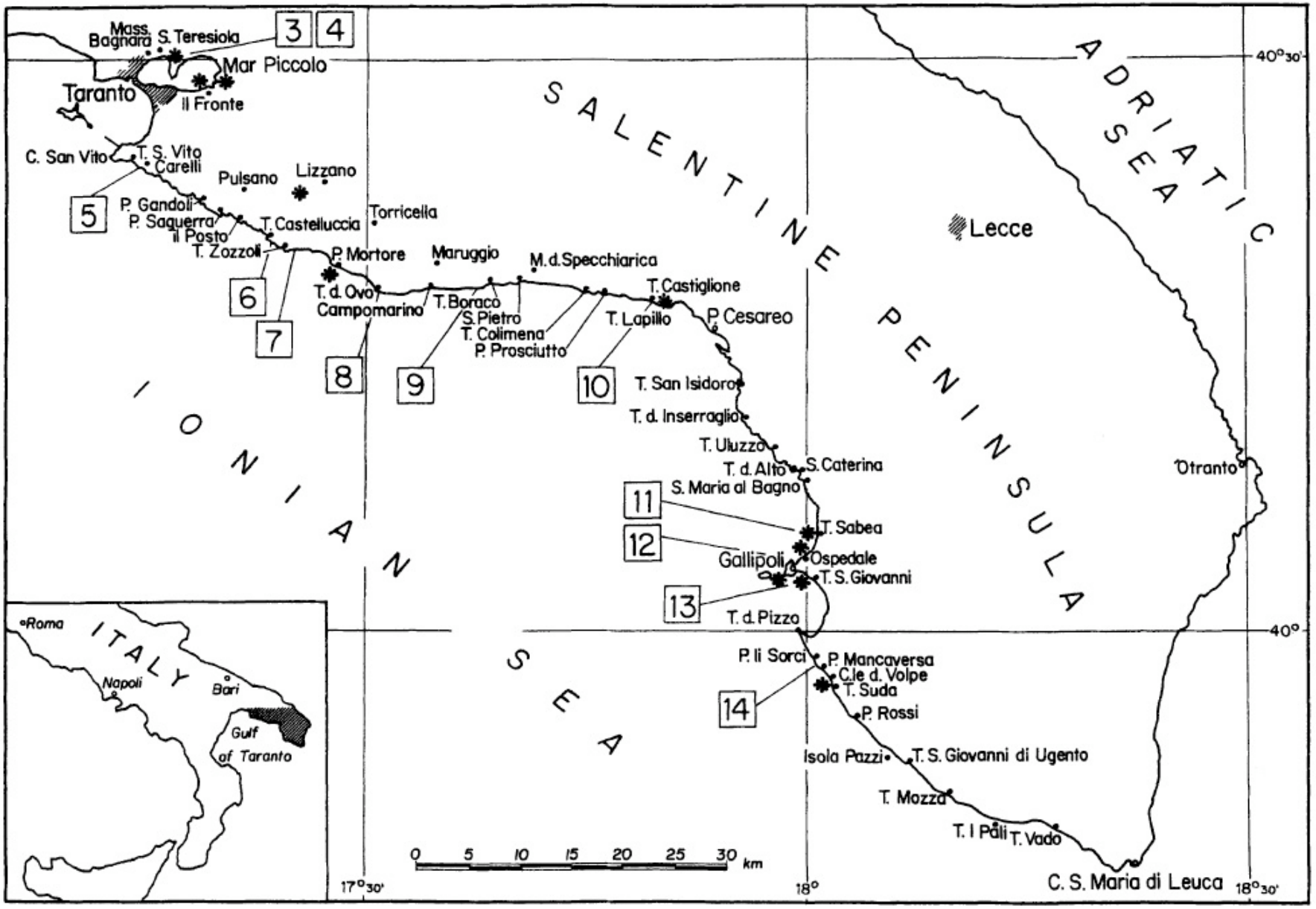

Figure 2. Location map of study sites 3 to 14 (boxes) along the Salentine Peninsula of southeast Italy.

Hearty & Dai Pra 1992

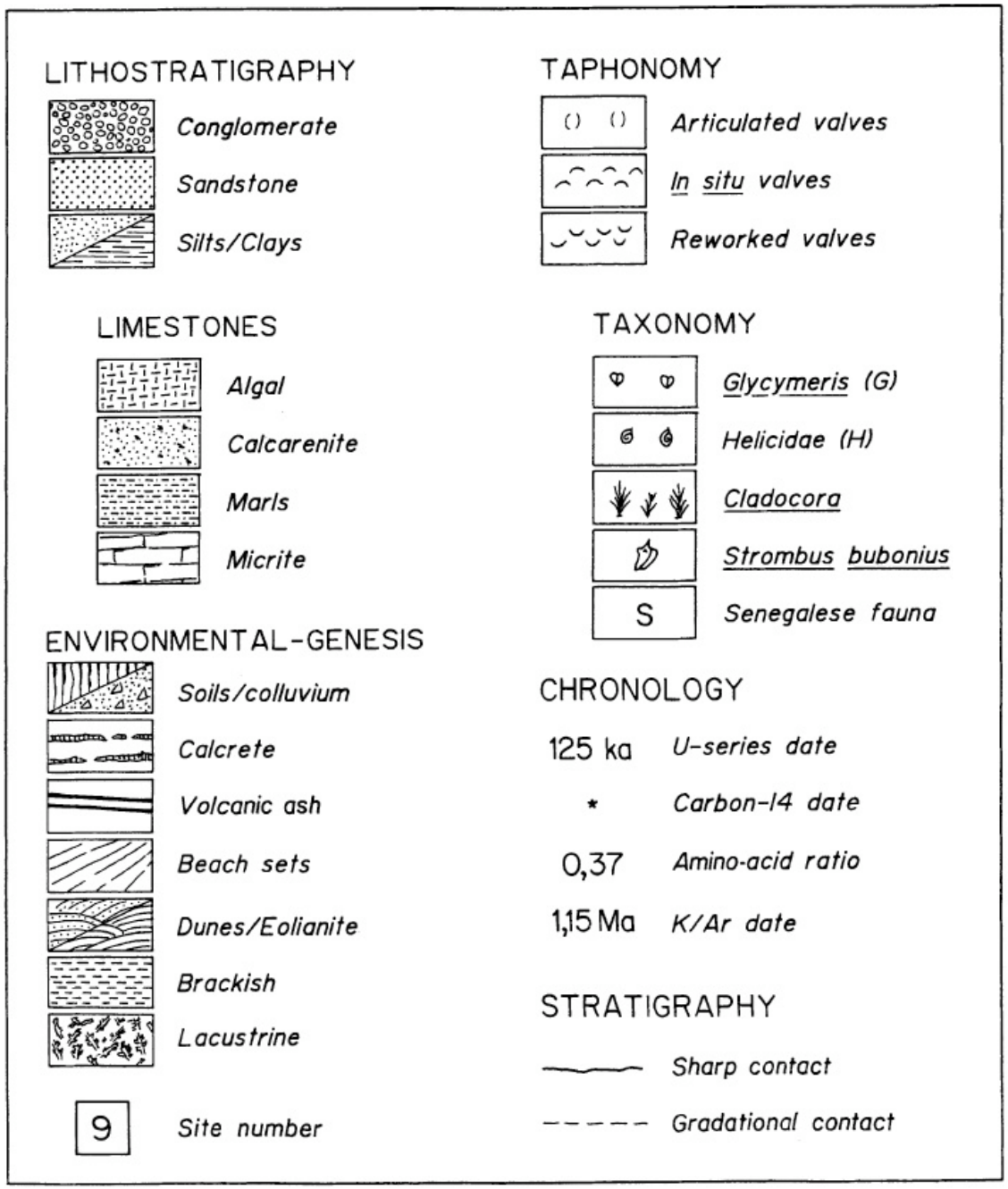

Figure 3. Legend for Figures 4 to 11. Stratigraphic complexes or sequences are identified by Roman numerals I (Holocene) to V (middle Pleistocene).

Hearty &
Dai Pra 1992

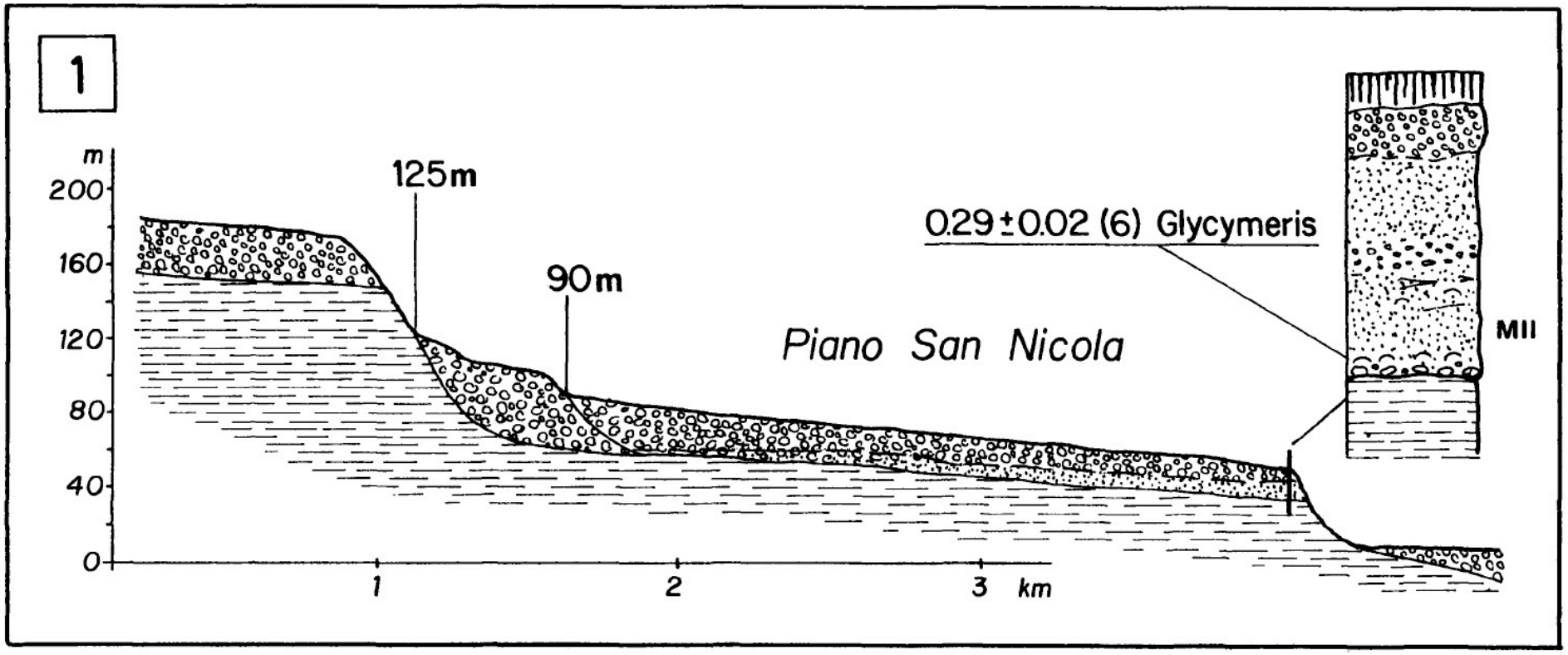

4. Site 1—The Piano San Nicola section.

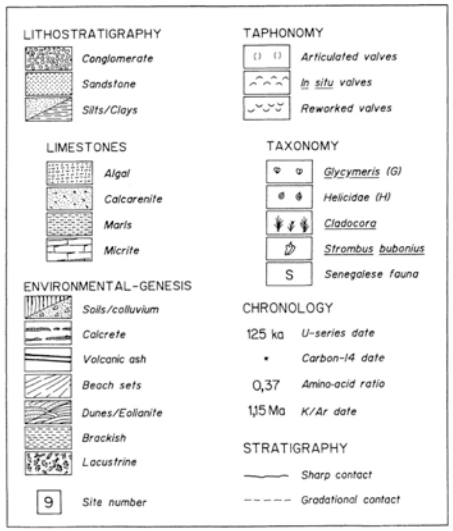

Figure 3. Legend for Figures 4 to 11. Stratigraphic complexes or sequences are identified by Roman numerals I (Holocene) to V (middle Pleistocene).

Hearty &
Dai Pra 1992

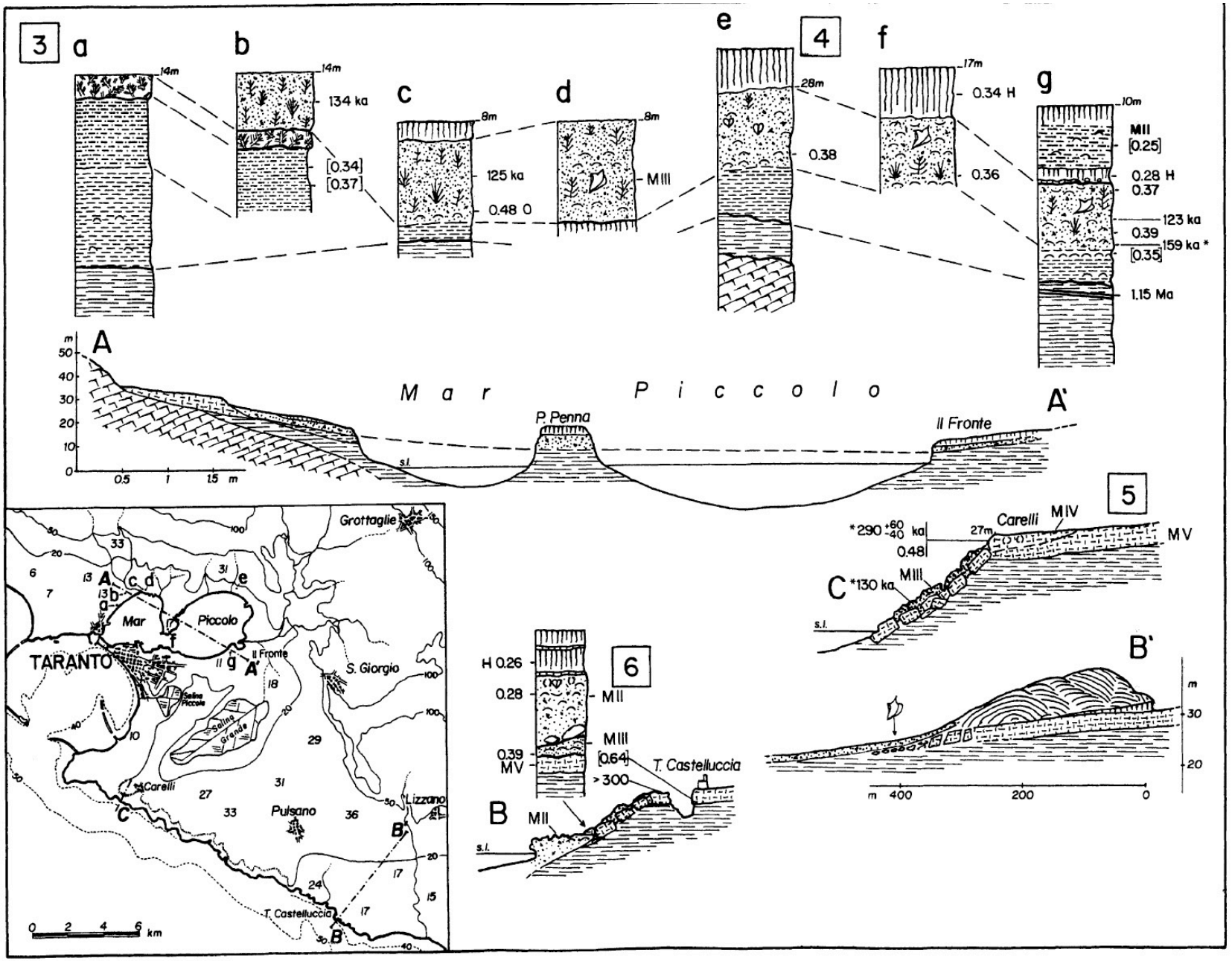

Figure 6. Study sites in the Mar Piccolo area: (Sites 3, 4, 5 and 6). Sections: a = Masseria Saracino; b = Masseria Bagnara; c = Santa Terisola; d = Santa Teresiola East; e = Masseria San Pietro; f = Punta Penna; g = Il Fronte. Correlations are indicated by the dashed line. Cross-sections A-A′, B-B′, and C-C′ are located in the inset.

Hearty & Dai Pra 1992

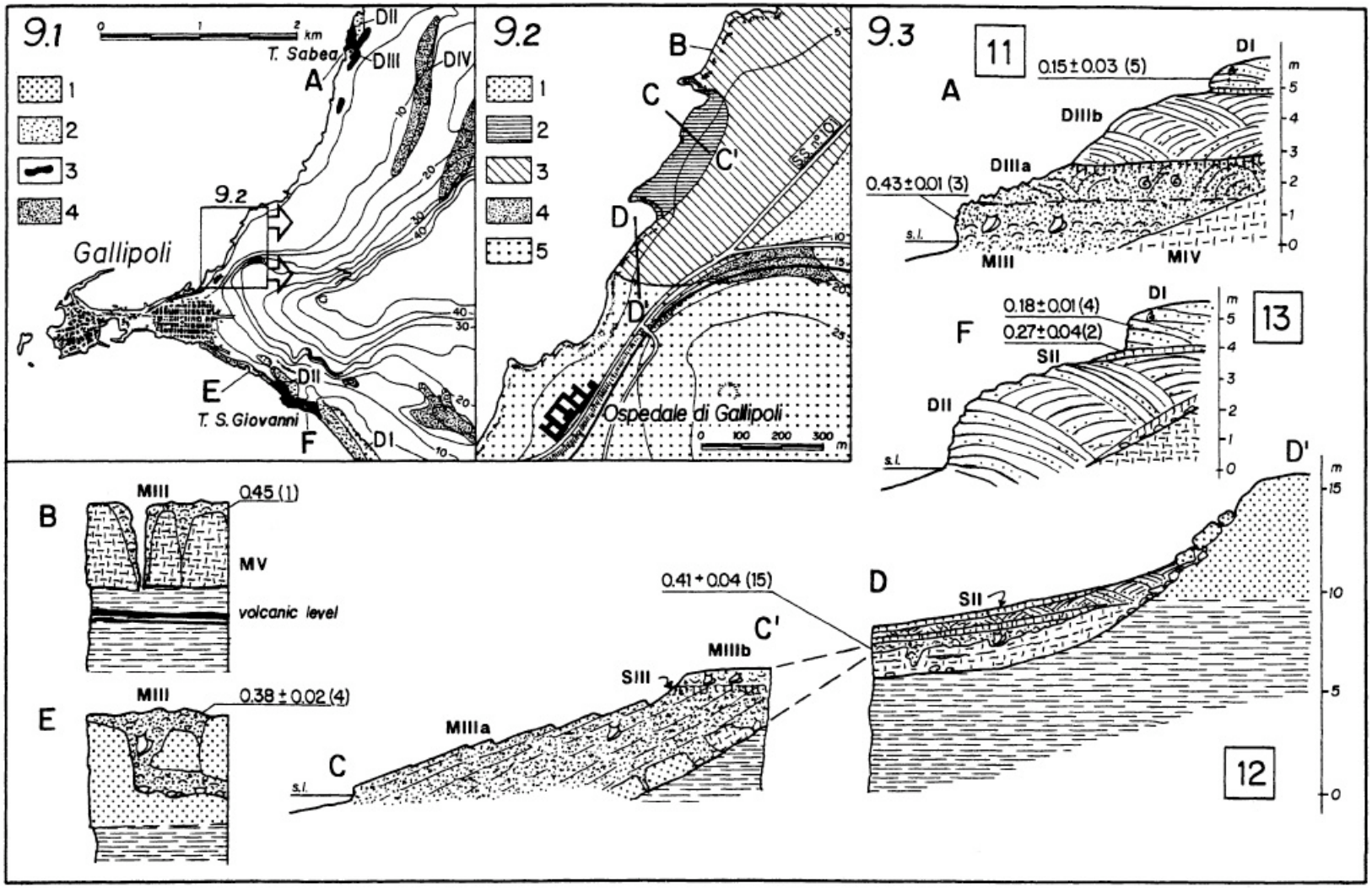

Figure 9. Stratigraphy of the Gallipoli area. Site 11 = Torre Sabea, Site 12B, 12C-C', and 12D-D' = Gallipoli (Ospedale), Site 13E and 13F = Torre San Giovanni. Legend for Figure 9.1 (Gallipoli Peninsula): (1) Historical dunes; (2) Holocene dunes; (3) post-*Strombus* dunes; (4) older dunes. Legend for Figure 9.2 (Ospedale di Gallipoli): (1) Holocene deposits; (2) beach deposits with *Strombus bubonius*; (3) bioclastic calcarenite; (4) eolianite; (5) "Sicilian" littoral sandstones with *Globorotalia truncatulinoides excelsa* (Coppa and Crovato, 1985; Rio *et al.*, 1991).

Hearty & Dai Pra 1992

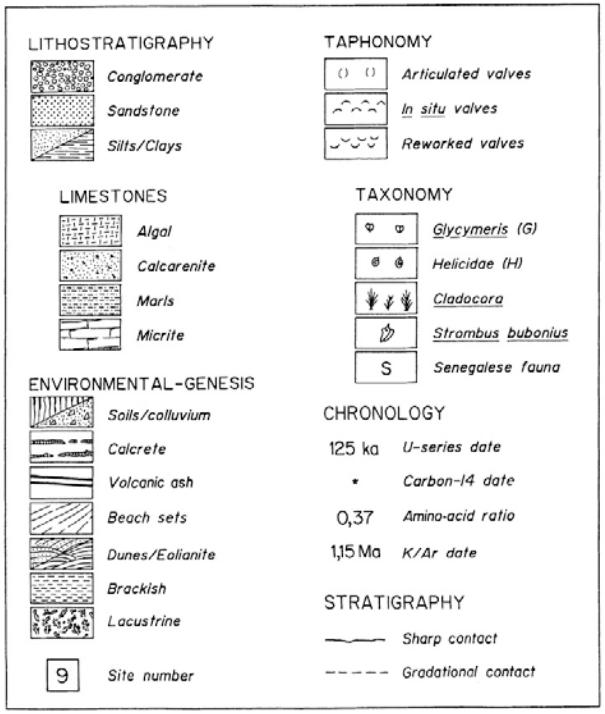

Figure 3. Legend for Figures 4 to 11. Stratigraphic complexes or sequences are identified by Roman numerals I (Holocene) to V (middle Pleistocene).

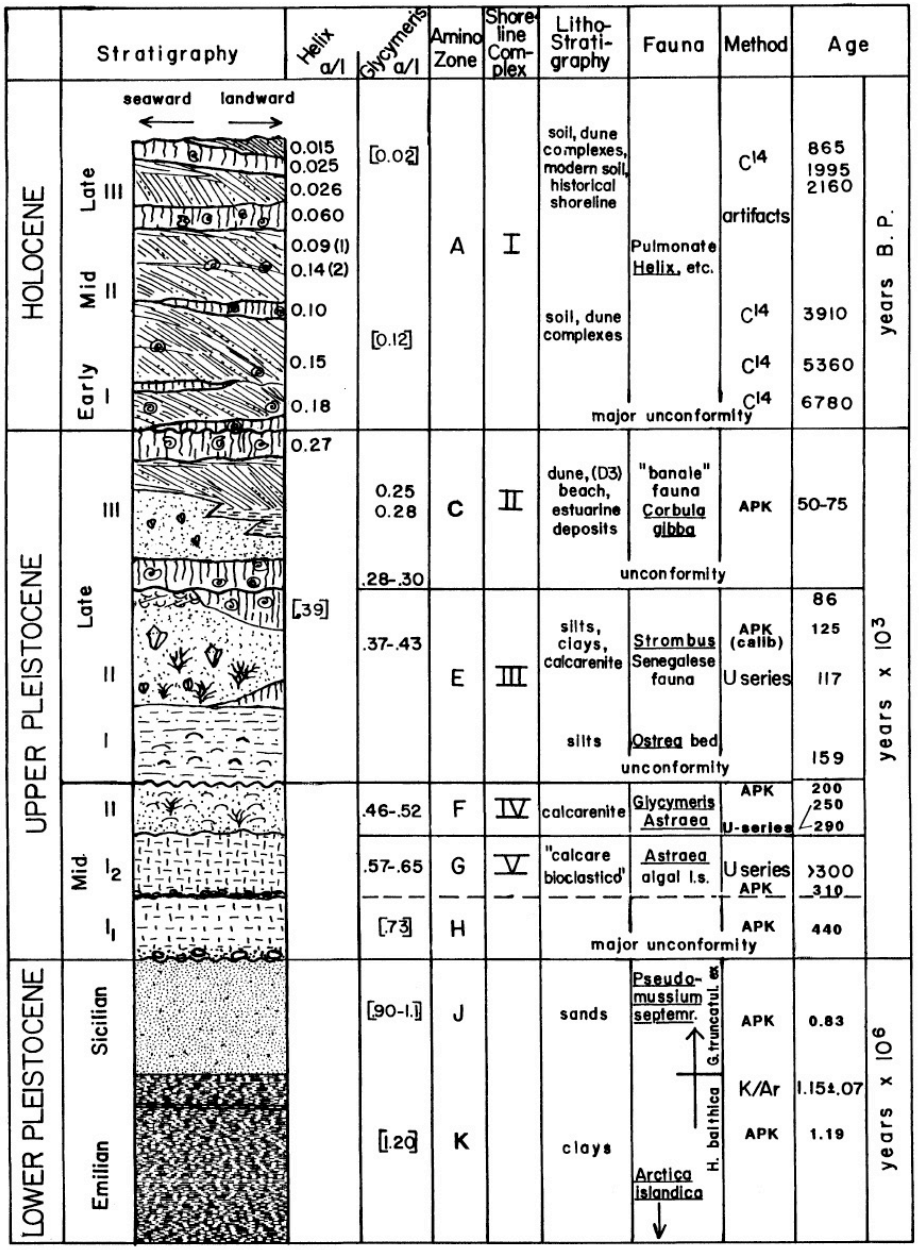

Figure 11. The composite stratigraphic section of southeast Italy includes rock sequences (I to V) bounded by unconformities, aminostratigraphy and aminozones, invertebrate biostratigraphy, and chronostratigraphy. The composite section reflects a multiple-systems approach to the geological evolution of the area. Legend as in Figure 3.

Hearty & Dai Pra 1992